Boundary effects in quantum spin chains and Finite Size Effects in the Toroidal Correlated Percolation model

Sebastian Grijalva

université PARIS-SACLAY

Boundary Effects in Quantum Spin Chains and Finite-Size Effects in the Toroidal Correlated Percolation Model

Effets de Bord dans les Chaînes de Spin Quantiques et Effets de Taille Finie dans le Modèle Toroïdal de Percolation Corrélé

Thèse de doctorat de l'université Paris-Saclay

École doctorale n° 564, Physique en Île-de-France (EDPIF)
Spécialité de doctorat : Physique
Unité de recherche : Université Paris-Saclay, CNRS, LPTMS, 91405, Orsay, France.
Référent : Faculté des Sciences d'Orsay

Thèse présentée et soutenue à Paris-Saclay, le 15/10/2020, par

Denis Sebastian GRIJALVA

Composition du Jury

Nikolai KITANINE Professeur, Institut de Mathématiques de Bourgogne. Dijon, France.	Président
Karol KOZLOWSKI Chargé de Recherche (HDR), Laboratoire de Physique Théorique, École Normale Supérieure de Lyon. Lyon, France.	Rapporteur & Examinateur
Pierre PUJOL Professeur, Laboratoire de Physique Théorique, IRSAMC, Université Paul Sabatier. Toulouse, France.	Rapporteur & Examinateur
Christian HAGENDORF Professeur, Institut de Recherche en Mathématique et Physique, Université catholique de Louvain. Louvain-la-Neuve, Belgique.	Examinateur
Vincent PASQUIER Directeur de Recherche, Institut de Physique Théorique CEA. Gif-sur-Yvette, France.	Examinateur

Direction de la thèse

Véronique TERRAS Directrice de Recherche, Laboratoire de Physique Théorique et Modèles Statistiques, (LPTMS). Orsay, France.	Directrice de thèse
Raoul SANTACHIARA Chargé de Recherche (HDR), Laboratoire de Physique Théorique et Modèles Statistiques, (LPTMS). Orsay, France.	Co-Directeur de thèse

Thèse de doctorat

NNT 2020UPASP093

Resumé en Français

Cette thèse est divisé en deux parties : d'un coté nous analisons des surfaces aléatoires avec corrélations à grande portée où l'on peut définir des surfaces de niveau *corrélés*. Soit $\Omega = [0, N-1] \times [0, M-1] \subset \mathbb{N}^2$ un réseau carré et Ω^* le réseau «réciproque»des vecteurs d'onde $\mathbf{k} = 2\pi(x_1/N, x_2/M)$, où $(x_1, x_2) \in \Omega$. Sur ce réseau l'on place les surfaces aléatoires suivantes :

$$u : \mathbf{x} \in \Omega \to \mathbb{R}$$
$$u(\mathbf{x}) = \frac{1}{norm}\frac{1}{NM}\sum_{\mathbf{k}\in\Omega^*} |\lambda_{\mathbf{k}}|^{\frac{(1+H)}{2}} w_{\mathbf{k}} e^{i\mathbf{k}\cdot\mathbf{x}}, \tag{1}$$

où $\lambda_{\mathbf{k}} = 2\cos(k_1) + 2\cos(k_2) - 4$ sont les valeurs propres du laplacien fractionnaire en deux dimensions, $\{w_{\mathbf{k}}\}_{\mathbf{k}\in\Omega^*}$ son des nombres aléatoires gaussiens et complèxes, et *norm* est une valeur de normalisation qui donne une variance unitaire en chaque point. L'exposant H, appéllé aussi *exposant de Hurst*, permet de classifier ce type de surfaces selon les propriétés statistiques dans la limite d'échelle.

On choisit alors une hauteur h et on «coupe»la surface à cette valeur, i.e. on définit

$$\theta(\mathbf{x}) = \begin{cases} 1, & \text{if } u(\mathbf{x}) > h \\ 0, & \text{else} \end{cases} \tag{2}$$

Avec cette définition, on obtient des ensembles de niveau (*level sets* en anglais) dont le nombre de points non nuls («actifs») nous permet de définir un problème de percolation qui garde les corrélations des surfaces originales. En effet, la rélation entre h et la probabilité d'avoir un point actif est donné (dans le cas non corrélé $H = -1$), par $p(h) = \frac{1}{2}\text{erfc}(h/\sqrt{2})$. On trouve numériquement, pour chaque valeur $-1 < H < 0$ qu'il existe un *niveau critique* h_c où on observe l'émergence d'un cluster «infinit». Dans ce point critique, on trouve évidence de l'invariance par échelle quand on passe à la limite $N \to \infty$ et en plus on observe les valeurs de l'exposant de longeur de corrélation ν et de la dimension fractale D_f, qui varient de façon inusuelle pour différents régions de H.

Nous allons ensuite étudier la *fonction de connectivité* :

$$p(\mathbf{r}) = \text{Prob}[\mathbf{x}, \mathbf{y} \text{ sont dans le même cluster, avec } |\mathbf{x} - \mathbf{y}| = |\mathbf{r}|] \tag{3}$$

Dans la Fig. 2 on montre la fonction de connectivité pour différentes valeurs de H, où on a multiplié par $|\mathbf{r}|^{2(2-D_f)}$ pour obtenir ainsi une fonction qui ne dépend que de $|\mathbf{r}/N$. En chaque cas, le passage à l'échelle diffère selon la valeur de H. En cette thèse, nous nous sommes intéressés à étudier les corrections de taille finie de cette loi, en particulier pour montrer qu'elles sont liées à l'existence de l'invariance *conforme* dans ces ensembles de niveau. L'évidence la plus significative c'est la présence d'un terme quadratique $(|\mathbf{r}|/N)^2$ liée à la brisure de la proportion N/M pour des réseaux rectangulaires, ainsi comme des termes $\propto \cos(2\vartheta)(r/N)^4$ où ϑ mésure l'orientation des points à comparer.

On arrive aux résultats suivants :

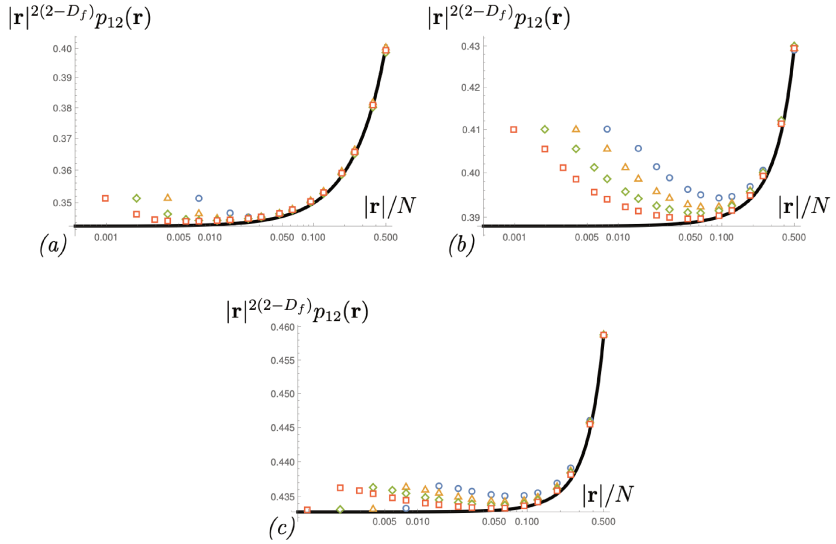

FIGURE 1 – Connectivité $|\mathbf{r}|^{2(2-D_f)}p(\mathbf{r})$ pour tailles $N = 2^8 - 2^{11}$. En noir, on dessine la loi attendue à la limit d'échelle. Ces résultats nous permettent de déterminer les corréctions de taille finie de la connectivité. Avec techniques numériques du même esprit, mais pour des réseaux de dimensions rectangulaires, on determine des corrections de ordre supérieur, montrant ainsi l'évidence de une théorie conforme qui explique ces exposants.

(i) Nous avons développé un protocole complet pour la construction de surfaces gaussiennes corrélées à longue portée, en utilisant des conditions aux bords doublement périodiques (toroïdales). Ces surfaces peuvent être associées à un modèle de percolation corrélée à longue portée en produisant un ensemble d'excursions à un niveau critique précis. Ce niveau a été trouvé par deux méthodes indépendantes : en recherchant l'apparence d'un cluster wrapping et en comparant les cumulants Binder des clusters. Les principales quantités que nous utilisons pour caractériser les propriétés universelles des ensembles d'excursions percolantes sont l'exposant de longueur de corrélation, nu et la dimension fractale D_f. Nous constatons que nos valeurs mesurées sont conformes à l'état de l'art des travaux récents. De plus, nous avons inclus un code numérique pour classer et extraire des statistiques des clusters dans nos surfaces. Ce code est inclus en annexe.

(ii) Nous avons étudié les corrections universelles de taille finie de la fonction de connectivité à deux points, qui sont un produit des conditions aux limites. Nous avons constaté que ces corrections peuvent être extraites en configurant correctement la géométrie du réseau et l'orientation du vecteur de rayon entre les points. Plus précisément, nous avons constaté que les corrections principales sont données par une loi de puissance d'exposant universel $2 - 1/\nu$, et qu'une correction sous dominante importante avec exposant 2 émerge lorsque nous construisons le réseau de taille rectangulaire. De plus, nous avons montré que le coefficient de la correction sous dominante dépend de l'orientation

du vecteur rayon. Ces aspects sont profondément liés à la symétrie conforme des clusters. De plus, nous avons trouvé un excellent accord entre notre modèle de percolation corrélée et les résultats analytiques de [15]. Nous avons terminé avec des commentaires sur la fonction de connectivité à trois points pour notre modèle.

La deuxième partie concerne l'étude d'un système quantique unidimensionelle, caracterisé par l'Hamiltonien suivant :

$$\mathcal{H} = \sum_{j=1}^{L-1} (\sigma_j^x \sigma_{j+1}^x + \sigma_j^y \sigma_{j+1}^y + \Delta \sigma_j^z \sigma_{j+1}^z) + h_- \sigma_1^z + h_+ \sigma_L^z \tag{4}$$

Ce système, appelé *chaîne de spin XXZ*, appartient à la familie des systèmes *Yang-Baxter intégrables*, dont plusieures propriétés statistiques (même à la limite thermodynamique) peuvent être calculés de façon *analitique*, en utilisant les techniques associées à la méthode de *l'Ansatz de Bethe Algébrique* (ABA).

L'Ansatz de Bethe Algébrique part d'une famille à un paramètre de opérateurs $B(\mu)$ qui forment une algèbre et qui fournisent un système couplé d'equations –*les Équations de Bethe*– dont les solutions λ_i, $i = 1, \dots N$ nous permettent de construir des états propres de l'Hamiltonien (4), avec l'ansatz

$$|\boldsymbol{\lambda}\rangle = \mathcal{B}(\lambda_N) \cdots \mathcal{B}(\lambda_1)|\mathbf{0}\rangle, \tag{5}$$

où $\boldsymbol{\lambda} = (\lambda_1, \dots, \lambda_N)$. En plus, l'état fondamental peut être representé par ces ensembles de racines à la limite $L \to \infty$, sur la forme d'une densité de racines $\rho(\lambda)$, qui est la solution d'un ensemble équations intégrales. La chaîne (4) possèdant des conditions de bord *ouvertes*, présente une structure différente au modèle périodique. Par exemple, son système de racines decrivant l'état fondamental dans la limite thermodynamique est complementé, pour certaines valeurs des champs aux bords h_-, h_+, par des solutions *complèxes*.

Dans cette thèse, nous nous intéressons exclusivement à la version ouverte de ce modèle. Cette dernière est toujours intégrable [84], et l'hamiltonien peut être diagonalisé dans le cadre de la théorie des représentations de l'algèbre de réflexion [85], sous la forme d'une version «avec bords»du ABA, qui a été introduite par Sklyanin dans [86]. Le système d'équations de Bethe pour la chaîne ouverte est plus complèxe, ainsi que la méthode pour y arriver, car les opérateurs $\mathcal{B}$ pour l'ansatz sont construits avec une matrice de transfert qui appartient à l'algèbre de Reflection. Ces méthodes sont appélés par le nom de *Ansatz de Bethe Algebrique avec Bords* ('Boundary Algebraic Bethe Ansatz').

Il y a des aspects importants qui différencient le cas aux frontières ouvertes de son homologue périodique. Les paramètres agissant sur le premier et le dernier site (représentant un champ magnétique aux frontières de la chaîne de spin) engendrent un diagramme de phase plus élaboré et, comme nous le verrons, permettent l'existence des 'boundary modes'. Ceux-ci ont été activement étudiées dans le contexte de

la chaîne de Kitaev (liée à la chaîne XY à champ transverse via une transformation Jordan-Wigner), qui présente des fermions de Majorana localisées [87] aux bords du système, formant ainsi des états dégénérés qui combinent les deux modes avec bords. Plus récemment, dans [88], il a été montré que la chaîne XYZ espacée contient ce qu'on appelle des modes zéro fort, qui sont des opérateurs définis aux bords de la chaîne et qui commutent avec l'hamiltonien jusqu'à des opérateurs de correction de taille finie dont les valeurs moyennes disparaissent de façon exponentielle avec la taille du système. Ces 'Strong Zero Modes' agissent sur un état dans un secteur de la symétrie discrète et donnent un état propre de secteur différent de l'hamiltonien avec la même énergie, jusqu'à corrections d'order $O(L^{-\infty})$. Ces quasi-dégénérescences sont remarquablement une caractéristique non limitée à l'état fondamental mais à une famille d'états dans tout le spectre.

Ces proprétés peuvent être observés par le comportament de la fonction d'autocorrélation au bord de la chaîne semi-infinite. À temperature nulle et à la limite thermodynamique, elle est donné par la contribution à la magnetisation au bord de la racine de Bethe complèxe (aussi appélé 'boundary root' (BR)) :

$$\lim_{t\to\infty}\lim_{L\to\infty}\lim_{h_-\to h_+}\langle\sigma_1^z(t)\sigma_1^z\rangle^c\big|_{T=0} = \left|\langle\sigma_1^z\rangle_{\mathrm{BR}}\Big|_{\xi_-=\xi_+}\right|^2 \tag{6}$$

où dans l'expression, $\xi_\pm$ sont une parametrisation pour les champs aux bords $h_\pm$. Même si on perturbe le modèle loin du point intégrable, le temps de cohérence doit rester long -comme l'était montré dans [89–91] -, donc cette quantité présente un intérêt physique en raison de son plateau de longue durée à des moments intermédiaires. Dans un premier temps pour étudier cette question, nous profiterons du cadre du Boundary ABA pour obtenir une expression exacte et explicite de la fonction d'autocorrélation à température nulle, à la limite thermodynamique et à long temps. En effet, la structure intégrable du modèle permet d'expliquer l'émergence de la quasi-dégénérescence de l'état fondamental et la gamme de valeurs des paramètres du système pour lesquelles ce phénomène est possible. On arrive aux résultats suivants :

(i) La description de l'état fondamental en termes de racines de Bethe dépend fortement des paramètres aux bords de la chaîne, ainsi que la parité de la longueur de la chaîne. Contrairement à la chaîne périodique, l'ensemble des racines de Bethe décrivant l'état fondamental peut inclure des solutions complexes isolées, liées aux facteurs aux limites apparaissant dans les équations de Bethe. Nous avons déterminé les valeurs des champs aux bords pour lesquels ces racines limites sont présentes pour l'état fondamental - pour un nombre pair et impair de spins - ainsi que comparé l'énergie des états d'énergie les plus faibles. Pour la chaîne de longueur paire, nous avons constaté que, lorsque les champs frontières sont dans l'intervalle $|h_\pm| < \Delta - 1$ et qu'ils coïncident, le spectre est 'gapped' et il y a deux états fondamentaux quasi-dégénérés dans la limite de grande L.

(ii) Nous avons recalculé l'aimantation au bord dans la limite de chaîne semi-infinie. Bien qu'il existent des résultats précédents sur cette quantité, ils

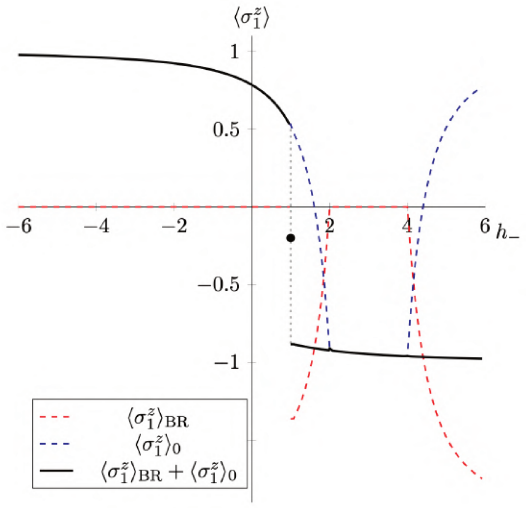

FIGURE 2 – Magnétisation au bord de la chaine XXZ ouverte quand le champ à droite est fixé à $h_+ = 1$. La contribution de la 'boundary root' est donné par la ligne rouge, qui compense donc la contribution du reste en bleu. Le saut dans la magnétisation. peut être calculé de façon exacte grâce au Boundary ABA, et ça nous permet aussi de lier (toujours de façon exacte) cette discontinuité a la limite a temps long de la fonction de autocorrelation du spin au bord.

n'étaient que pour un champ limite nul à l'infini $h_+ = 0$. Grâce à notre étude de l'état fondamental, nous sommes capables de calculer cette quantité dans le cas plus général $h_+ \neq 0$. On voit que l'aimantation au bord de la chaîne demi-infinie dépend toujours du champ au bord h_+ à l'infini, c'est à dire, quand on fait varier h_- il existe une discontinuité de cette quantité à $h_- = h_+$ dans le cas de longueur paire. Cela est dû au fait que la description de l'état fondamental en termes de 'boundary root' est différente lorsque $h_- < h_+$ (la 'boundary root' est localisée dans le bord droit et ne contribue pas à la valeur de l'aimantation) et quand $h_- > h_+$ (la 'boundary root' est localisée dans le bord gauche et contribue à la valeur de l'aimantation). Dans le cas de longueur impaire, la discontinuité est à $h_- = -h_+$ et est due au fait que l'état fondamental n'est pas dans le même secteur d'aimantation quand $h_- < -h_+$ et quand $h_- > -h_+$.

(iii) Nous avons obtenu la limite longue de la fonction d'autocorrélation de l'opérateur σ_1^z, pour L pair. Ce dernier n'est non nul que quand $h_+ = h_-$, en raison de la quasi-dégénérescence de l'état fondamental, et est lié à la discontinuité mentionnée de l'aimantation aux bords.

Preface

In this thesis we present original results on two topics, one concerning the critical behaviour of two-dimensional classical percolation models, the other about the boundary effects of an interacting quantum spin chain. For two-dimensional classical systems or one-dimensional (1+1) quantum models, mean-field approaches or perturbative techniques generally fail, as the effects of the (classical or quantum) fluctuations are enhanced at low-dimension. On the other hand, at this dimension, non-perturbative approach to critical phenomena and exact methods are possible. We are referring in particular to the conformal field and to the quantum integrability theories, that represent, nowadays, central objects of study in modern theoretical physics. These two theories are very different in their scope and points of view: one, the conformal field theory, aims to provide an effective field theory that captures the universal behaviour of (1+1) quantum critical systems or two-dimensional critical classical system. The other aims to solve exactly particular (1+1) quantum models or two-dimensional lattice statistical models, for instance by computing respectively the ground-state energy or the free energy in the critical and non-critical phase, and then also calculate their correlation functions. However, it turns out that there are strong relations between these two theories, mainly because they are both built from the representation of certain symmetry algebras. In the case of conformal field theory, these algebras originate from the invariance of the statistical observables under angle-preserving transformations. In the context of quantum mechanics, the existence of integrable models exemplifies the power of symmetry through the presence of quantum groups and the exactly solvable spin chains that emerge from them.

The thesis is divided in two parts and we shall introduce both in more detail below. The first part deals with connectivity in a toroidal correlated percolation model, a classical critical model at the scaling limit. The model is created from discrete random fractal surfaces, whose correlations are parametrized by the so-called Hurst exponent, $H < 0$. Excursion sets are then defined by selecting the sites above a certain level h and define a family of percolation models with long-range correlations. The resulting clusters percolate at a finite critical value $h = h_c$ and for $H \leq -\frac{3}{4}$ the phase transition is expected to remain in the same universality class of

uncorrelated percolation. However, for $-\frac{3}{4} < H < 0$, there is a line of critical points with continuously varying critical exponents. We focus on the connectivity function, defined as the probability that two sites belong to the same level cluster. Extending the results of CFT for pure percolation to the correlated case, we show numerically that the finite-size corrections to the connectivity function —which are determined by the topology of the lattice— make manifest the conformal invariance for all the critical line $H < 0$. In particular, exploiting the anisotropy of the rectangular torus ($M \neq N$), we directly test the behaviour of subleading corrections, as predicted by CFT.

The second part is dedicated to the study of the open-boundary XXZ spin-$\frac{1}{2}$ Heisenberg spin chain. We study the model in the anti-ferromagnetic regime, for even and odd number of sites, and for generic longitudinal magnetic fields at the edges. We discuss the ground state via the Algebraic Bethe Ansatz and detail the regime where the spectrum is gapped. Moreover we find under which conditions the ground state is doubly degenerate and, in the L even case and under specified conditions, we find this degeneracy holds up to exponentially small corrections in the number of sites L for the even case. The quasi-degeneracy is linked to the presence of a boundary root, namely an excitation localized at a boundary. We compute the local magnetization at the left edge of the chain and we show that, due to the existence of a boundary root, the magnetization depends also on the value of the field at the opposite edge, even in the half-infinite chain limit. Moreover we give an exact expression for the large time limit of the spin autocorrelation at the boundary, which we explicitly compute in terms of the form factor between the two (quasi)degenerate ground states. The latter is shown to be equal to the contribution of the boundary root to the local magnetization.

Throughout the chapters, there appear mentions to common themes: periodic and open boundary conditions, two-point correlation functions, thermodynamic limits and the collaboration between numerical algorithms and analytical calculations. These are all signatures from the field of statistical physics to which my doctoral project was devoted, and whose richness will hopefully be appreciated in the following pages.

Acknowledgements

This doctoral project was possible thanks to the kind efforts of my two supervisors, Véronique Terras and Raoul Santachiara. I gladly also acknowledge my collaborators during the creation of the work presented here, Nina Javerzat and Jacopo De Nardis. I feel fortunate to have shared the trade with all of them.

I am also thankful for the support given by the Ecuadorian Government by means of the SENESCYT Scholarship Program and crucially to CNRS and the Laboratoire de Physique Théorique et Modèles Statistiques during the last months of my studies. I am happy to have been a part of LPTMS and to have witnessed the efforts and joys of its (post)doctoral and permanent members. I remain in awe of the efficiency and humane qualities of Emmanuel Trizac as director of the laboratory and Claudine Le Vaou and Karolina Kolodziej as administrative staff.

A final word of gratitude goes to Alexandra Elbakyan for her bibliographic support and to Sofía Jijón for her resoluteness, loving spirit and typesetting help.

Contents

I Long-Range Correlated Percolation on a Torus

Chapter 1

Introduction

In this part, we study two-dimensional lattice percolation models focusing, in particular, on the emergence of conformal symmetry at their critical phases. Percolation models are in general defined by a random bi-partition of the lattice, obtained by activating the sites (site percolation) or the edges (bond percolation) with a certain probability [1, 2]. The percolation models focus on the statistical properties of the clusters, that are connected sets of activated sites or edges. A set is said to be connected when any two of its points can be joined by a path of points belonging to the set. By varying the fraction of active sites/bonds, the percolation models undergo a continuous phase transition separating two phases where the probability to find an infinite cluster jumps from 0 to 1.

The simplest example of percolation models are the ones where the sites (or bonds) are activated independently to one another. We will refer to these models as pure percolation models. Pure percolation models represent a paradigm of second order phase transitions and are certainly among the most studied statistical models. In Figure 1.1, instances of pure site and bond percolation are shown.

At the critical point $p = p_c$, the system is scale-invariant and the critical clusters represents an example of random fractals. One of the main questions we address here is whether the critical clusters of the percolation model under investigation enjoy a larger symmetry than the scale one, the conformal symmetry. A conformal transformation f is an angle-preserving transformation between two domains, $f : \mathcal{D} \to \mathcal{D}'$. If a system is conformally invariant (or more precisely, covariant), by knowing the expectation values in one domain $\mathcal{D}$, one can determine these in any other domain $\mathcal{D}'$ obtained by conformal transformation, $\mathcal{D}' = f(\mathcal{D})$. In two dimensions, any holomorphic function is a conformal transformation and this makes conformal invariance particularly powerful, as it imposes several restrictions on the expectation values. We will show this on a particular observable: the probability that two points belong to the same cluster, which is known also as two-point connectivity.

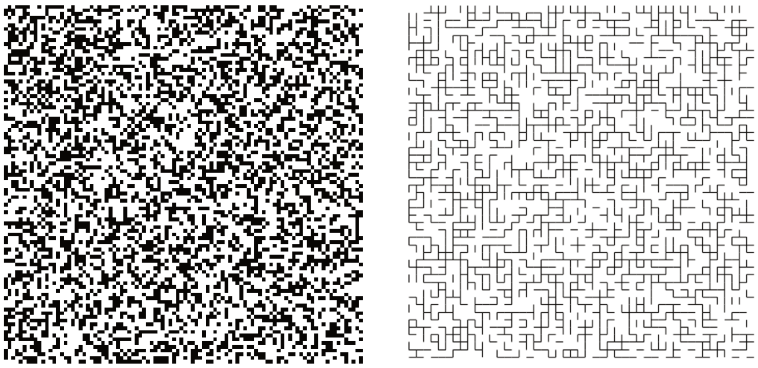

Figure 1.1 – Site and Bond Percolation. Two bi-partitions of a finite square lattice where sites (on the left) or bonds (on the right) are activated independently at the corresponding critical probability $p_c^{\text{site}} = 0.5927\ldots$ and $p_c^{\text{bond}} = 0.5$. While the value of the critical probability differs between the two models, the exponents determing the scaling behavior of the clusters are the same. This equivalence is an example of universality.

Some time ago, physicists argued that, for models defined by Hamiltonians with short-ranged interactions, scale invariance implies conformal invariance [3]. Their arguments were based on the interplay between the local nature of the interactions and renormalization group ideas. A few rigorous results supported these insights: for instance a there is a theorem that states that, in an unitary and local two-dimensional quantum field theory, scale invariance implies conformal one [4]. However, rigourous proofs of conformal invariance in lattice models are in general a very hard problem, which attracted great interest from the mathematical community [5, 6].

For non-local (and non-unitary) models, such as the percolation models, the occurence of conformal invariance is much less granted. A very important family of percolation models where conformal invariance is nevertheless well established is the Q-Potts random cluster model [7]. This is a one parameter (Q) family of integrable bond percolation models that contains the pure percolation ($Q = 1$) as a special case. Only very recently [8–13], it has been understood how to use conformal invariance to predict the connectivity properties of Potts clusters and, in particular, of pure percolation clusters.

In this thesis, we investigate the excursion sets of random surfaces with negative Hurst exponent H (see (2.28)). As we detail later, the study of these sets define a percolation model where the probability of activating two distant sites decays algebraically with respect to their distance and with exponent $-2H$. This is a one-parameter (H) family of percolation models that, unlike the Potts one, is not integrable. The behavior of these models strongly depends on H. For $H < -3/4$, the correlations decay sufficiently quick for the model to remain in the universality class of pure (uncorrelated) percolation. For $-3/4 < H < 0$ this is not anymore true

and the models present a new line of critical points whose critical exponents differ from those of pure percolation. The universality classes of these points is by far less understood than those of the Q-Potts clusters. Even the occurence of conformal invariance is debated. We refer the reader to the introduction of our paper [14] for a detailed summary of the state of the art of this problem.

The following chapters present our contribution to this problem: by using a combination of numerical and Conformal Field Theory (CFT) approaches, we will show the emergence of conformal invariance in these models. We attack the problem by assuming conformal invariance and other broad conditions inspired by recent results on pure percolation [15], to predict the behavior of the two-point connectivity. In particular, we study the universal finite size effects associated to the toroidal geometry where the manifestations of conformal invariance becomes evident. We will also extract some information of the CFT describing these points.

This part of the thesis is divided in two chapters: Chapter 2 defines random surfaces and the associated percolation model that is pertinent to our study. We also describe several methods to extract statistical properties from the emerging clusters. Then, in Chapter 3 we consider the two-point connectivity function as a probe for the universality class of the model. A numerical code to reproduce the observations is included as an appendix, in Chapter 5.

Chapter 2

Percolation in Fractional Gaussian Surfaces

As we mentioned in the introduction, we shall study percolation models defined by the excursion set of random surfaces. We considered a special family of random functions: the discrete fractional Gaussian surfaces. Below, we will explain in detail how to generate these random functions and how the study of their excursion set defines a percolation model with algebraically decaying correlations. We show in particular how we can determine the critical percolation point and the corresponding critical exponents: the correlation length ν and the order parameter β exponents.

It is important to stress that there are many ways to generate random surfaces whose percolative properties fall in the same universality class of those studied here. For instance, in the framework of the Filtering method explained below, one can choose non-Gaussian distribution functions for the initial set of independent random variables (see (2.7)) and/or a different convolution kernel than the one chosen here (see (2.19) and (2.21)). Our choices are different from those of the previous works and are mainly motivated by the fact that we are particularly focused on generating doubly-periodic random surfaces. The results presented in this chapter provide therefore an independent verification of several conjectures concerning ν and β [16–19].

2.1 From uncorrelated to correlated Gaussian Surfaces

Let us consider a square lattice $\Omega \subset \mathbb{Z}^2$ of size $N \times M$:

$$\Omega = [0, N-1] \times [0, M-1], \tag{2.1}$$

where the sites of Ω will be written in bold notation:

$$\mathbf{x} = (x_1, x_2), \quad x_1 \in \{0, \cdots, N-1\}, \quad x_2 \in \{0, \cdots, M-1\}. \tag{2.2}$$

We shall assume doubly periodic boundary conditions,

$$(x_1, x_2) = (x_1 + N, x_2 + M), \quad \forall\, (x_1, x_2) \in \Omega, \tag{2.3}$$

thus giving the lattice the topology of a flat torus, $\Omega \sim \mathbb{Z}^2/(N\mathbb{Z} + M\mathbb{Z})$. Consider also the reciprocal lattice Ω^*

$$\Omega^* = \left\{ \frac{2\pi}{N}\big[0, N-1\big] \times \frac{2\pi}{M}\big[0, M-1\big] \right\}, \tag{2.4}$$

of sites

$$\mathbf{k} = (k_1, k_2), \quad k_1 \in \left\{0, \frac{2\pi}{N}, \cdots, \frac{2\pi(N-1)}{N}\right\}, \quad k_2 \in \left\{0, \frac{2\pi}{M}, \cdots, \frac{2\pi(M-1)}{M}\right\}. \tag{2.5}$$

We will define functions $f : \Omega \to \mathbb{R}$, that can also be expressed in terms of its Fourier series with the following conventions:

$$f(\mathbf{x}) = \frac{1}{NM} \sum_{\mathbf{k}\in\Omega^*} f_{\mathbf{k}}\, e^{i\mathbf{k}\cdot\mathbf{x}}, \quad f_{\mathbf{k}} = \sum_{\mathbf{x}\in\Omega} f(\mathbf{x})\, e^{-i\mathbf{k}\cdot\mathbf{x}}. \tag{2.6}$$

We now show how to generate a correlated Gaussian random surface $u(\mathbf{x})$ living on Ω. By correlated we mean that for different $\mathbf{x}, \mathbf{y} \in \Omega$, a function $u(\mathbf{x})$ will have a nonzero covariance $\mathbb{E}[u(\mathbf{x})u(\mathbf{y})]$, with $\mathbb{E}[\cdot]$ the average over all instances of u.

Consider first an uncorrelated Gaussian surface $w(\mathbf{x})$, also known as white noise. This is a function whose Fourier coefficients $\{\omega_{\mathbf{k}} \in \mathbb{C}\}_{\mathbf{k}\in\Omega^*}$ are independent complex Gaussian random variables satisfying:

$$\begin{aligned} w(\mathbf{x}) &= \frac{1}{NM} \sum_{\mathbf{k}\in\Omega^*} w_{\mathbf{k}} e^{i\mathbf{k}\cdot\mathbf{x}}. \\ \mathbb{E}[w_{\mathbf{k}}] &= 0 \\ \mathbb{E}[w^*_{\mathbf{k}} w_{\mathbf{q}}] &= NM\delta_{\mathbf{k},\mathbf{q}}. \end{aligned} \tag{2.7}$$

($\delta_{\mathbf{k},\mathbf{q}}$ indicates the Kronecker symbol). With this definition the surfaces w will be centered and of unit variance:

$$\begin{aligned} \mathbb{E}[w(\mathbf{x})] &= 0, \\ \mathbb{E}[w(\mathbf{x})w(\mathbf{y})] &= \delta_{\mathbf{x},\mathbf{y}}, \end{aligned} \tag{2.8}$$

To ensure $w(\mathbf{x})$ is real, we must impose

$$w^*_{(k_1,k_2)} = w_{(2\pi-k_1,2\pi-k_2)}. \tag{2.9}$$

Starting with $w(\mathbf{x})$, one can construct random surfaces with built-in correlations via linear combinations:

$$u(\mathbf{x}) = \sum_{\mathbf{y}\in\Omega} S(\mathbf{x}-\mathbf{y})w(\mathbf{y}), \tag{2.10}$$

where the convolution kernel S is a deterministic function. This method goes by the name of Fourier Filtering Method in the literature [20]. Then, the Fourier coefficients (2.6) $u_{\mathbf{k}}$ are given by:

$$u_{\mathbf{k}} = S_{\mathbf{k}} w_{\mathbf{k}}. \tag{2.11}$$

The condition $S^*_{(k_1,k_2)} = S_{(2\pi-k_1,2\pi-k_2)}$ ensures that $u(\mathbf{x})$ is real. The correlations of the surface (2.10) are now given by:

$$\begin{aligned}\mathbb{E}[u(\mathbf{x})u(\mathbf{y})] &= \mathbb{E}\left[\sum_{\mathbf{z},\mathbf{z}'\in\Omega^2} S(\mathbf{x}-\mathbf{z})w(\mathbf{z})S(\mathbf{y}-\mathbf{z}')w(\mathbf{z}')\right] \\ &= \sum_{\mathbf{z},\mathbf{z}'\in\Omega^2} S(\mathbf{x}-\mathbf{z})S(\mathbf{y}-\mathbf{z}')\mathbb{E}[w(\mathbf{z})w(\mathbf{z}')] \\ &= \sum_{\mathbf{z}\in\Omega} S(\mathbf{x}-\mathbf{z})S(\mathbf{y}-\mathbf{z}),\end{aligned} \tag{2.12}$$

which shows that the correlations are fixed by the convolution kernel. This becomes evident in Fourier space, where:

$$\Big(\mathbb{E}[u(\mathbf{x})u(\mathbf{y})]\Big)_{\mathbf{k}} = S^*_{\mathbf{k}} S_{\mathbf{k}} = S^2_{\mathbf{k}}. \tag{2.13}$$

Let us now focus on the case where the covariance (2.12) decays asymptotically with a power law:

$$\mathbb{E}[u(\mathbf{x})u(\mathbf{y})] \sim |\mathbf{x}-\mathbf{y}|^{2H}, \quad |\mathbf{x}-\mathbf{y}| \gg 1, \tag{2.14}$$

where H is known as the Hurst exponent [20]. Using Fourier theory, according to which the large distance behavior of a function is determined by the small distance asymptotics in the dual space, from (2.13) the function $S_{\mathbf{k}}$ should behave as:

$$S_{\mathbf{k}} \sim |\mathbf{k}|^{-(H+1)}, \quad |\mathbf{k}| \ll 1 \tag{2.15}$$

Note that we have a lot of freedom to choose the kernel $S_{\mathbf{k}}$. A natural choice comes from generalizing the discrete free Gaussian field $u^{\mathrm{GFF}}(\mathbf{x})$ on a flat torus. This field is defined as:

$$u^{\mathrm{GFF}}(\mathbf{x}) = \sum_{\mathbf{k}} |\lambda_{\mathbf{k}}|^{\frac{1}{2}} \ \omega_{\mathbf{k}} \, e^{i\mathbf{k}\mathbf{x}}, \tag{2.16}$$

where the plane wave $e^{i\mathbf{k}\mathbf{x}}$ and $\lambda_{\mathbf{k}}$ are respectively the eigenfunctions and the eigenvalues of the discrete Laplace operator $\nabla^2\big|_{\mathrm{discr.}}$. This operator is defined as:

$$\begin{aligned} \nabla^2\big|_{\mathrm{discr.}} f(x_1, x_2) = f(x_1+1, x_2) + f(x_1-1, x_2) - 4f(x_1, x_2) \\ + f(x_1, x_2+1) + f(x_1, x_2-1) \end{aligned} \tag{2.17}$$

and the eigenvalue equation $\nabla^2 f^{(\lambda)} = \lambda_{\mathbf{k}} f^{(\lambda)}$ is solved in Fourier space by:

$$\begin{aligned} \lambda_{\mathbf{k}} &= \big(2\cos(k_1) + 2\cos(k_2) - 4\big) = -|\mathbf{k}|^2, \text{ for } |\mathbf{k}| \ll 1 \\ f^{(\lambda)} &= e^{i\mathbf{k}\cdot\mathbf{x}}. \end{aligned} \tag{2.18}$$

Defining the convolution kernel as:

$$S_{\mathbf{k}} = |\lambda_{\mathbf{k}}|^{-\frac{H+1}{2}}, \quad \mathbf{k} \neq (0,0) \tag{2.19}$$

provides a natural generalization of $u^{\mathrm{GFF}(\mathbf{x})}$, with the asymptotic behavior (2.15) satisfied. Two further adjustments are needed:

(i) We have to fix the divergence of the zero mode $u_{\mathbf{k}=\mathbf{0}}$:

$$u_{\mathbf{k}=\mathbf{0}} = S_{\mathbf{0}}\omega_{\mathbf{0}} \ = \sum_{\mathbf{x}\in\Omega} u(\mathbf{x}). \tag{2.20}$$

Setting $S_{\mathbf{0}} = 0$ would introduce long-distance correlations as it would imply that we generate only surfaces with vanishing volume. A better choice is to set

$$S_{\mathbf{0}} = 1, \tag{2.21}$$

which results in the weaker condition $\mathbb{E}\left[\sum_{\mathbf{x}\in\Omega} u(\mathbf{x})\right] = 0$. This way, while some surfaces may be higher than others, in average they remain at the zero level. This is a weak enforcement of boundedness in the surfaces.

(ii) We normalize the surfaces to have unit variance at each point $\mathbf{x}$. The normalization factor can be obtained from:

$$\mathrm{norm}^2 = \mathbb{E}[u(\mathbf{x})^2] = \frac{1}{NM}\sum_{\mathbf{k}} S_{\mathbf{k}}^2. \tag{2.22}$$

With these elements, we can give the complete definition of the fractional Gaussian surfaces:

$$u(\mathbf{x}) = \frac{1}{\text{norm}} \frac{1}{NM} \sum_{\mathbf{k}} S_{\mathbf{k}} w_{\mathbf{k}} e^{i\mathbf{k}\cdot\mathbf{x}}, \tag{2.23}$$

where $S_{\mathbf{k}}$ is given by (2.19), and we include the conventions (2.20) and (2.22).

Instances of $u(\mathbf{x})$ are shown in Figure 2.1. In order to generate them, we implemented a code reported as an in Chapter 5.

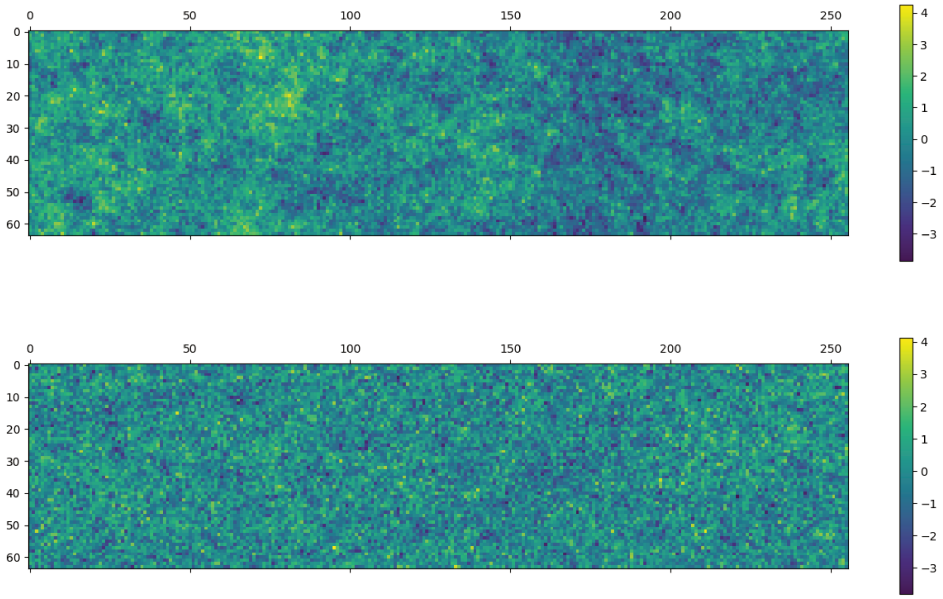

Figure 2.1 – Instances of fractional Gaussian surfaces, $u(\mathbf{x})$, for $N = 256$, $M = 64$, and $H \in \{-0.25, -0.625\}$. Higher values of H create more correlated surfaces, lower values will produce noisy surfaces.

2.2 Percolation model

We show now how to define a percolation model from the study of $u(\mathbf{x})$. We say that a site is active whenever $u(\mathbf{x}) > h$ for $h \in \mathbb{R}$. More formally, we introduce the following bipartition map θ on the lattice Ω:

$$\begin{aligned} \theta_h &: \Omega \to \{0, 1\} \\ \theta_h(\mathbf{x}) &\equiv \begin{cases} 1 & \text{if} \quad u(\mathbf{x}) \geq h \\ 0 & \text{if} \quad u(\mathbf{x}) < h. \end{cases} \end{aligned} \tag{2.24}$$

The set of active points is called the level-h excursion set. The probability of activating a site is given by:

$$p(h) = \mathbb{E}[\theta_h(\mathbf{x})]. \tag{2.25}$$

Note that since for any vector $\mathbf{a} \in \Omega$, $\mathbb{E}[\theta_h(\mathbf{x}+\mathbf{a})] = \mathbb{E}[\theta_h(\mathbf{x})]$ (translation invariance) and $\mathbb{E}[\theta_h(\mathbf{x} + (nN, mM))] = \mathbb{E}[\theta_h(\mathbf{x})]$, for n, m integers (double periodicity, inherited from u), the activation probability only depends on the level h.

Being a linear combination, (2.23), the surface at each point $\mathbf{x}$ is again a centered Gaussian variable of unit variance. This implies that:

$$p(h) = \frac{1}{\sqrt{2\pi}} \int_h^\infty \exp(-t^2/2)dt = \frac{1}{2}\text{erfc}\left(\frac{h}{\sqrt{2}}\right) \tag{2.26}$$

$$p(h)(1-p(h)) = \mathbb{E}[(\theta_h(\mathbf{x}) - p(h))^2]. \tag{2.27}$$

In this way one ensures that the correlations of θ_h inherit the algebraic correlation of the random surface:

$$\mathbb{E}\left[\frac{1}{NM}\sum_{\mathbf{x}\in\Omega}\Big(\theta_h(\mathbf{x}) - p(h)\Big)\Big(\theta_h(\mathbf{x}+\mathbf{r}) - p(h)\Big)\right] \sim |\mathbf{r}|^{2H}, \tag{2.28}$$

We verified numerically this dependence and show the correlations in Fig. 2.2. Notice that as H grows, i.e., as the correlations have longer range, the algebraic scaling is obeyed more closely. As a consequence, on can see that the clusters become more compact (or have less "holes"). We didn't try to push the number of samples above $O(10^5)$ since the connectivities that we will study on the next chapter were only sampled up to this number.

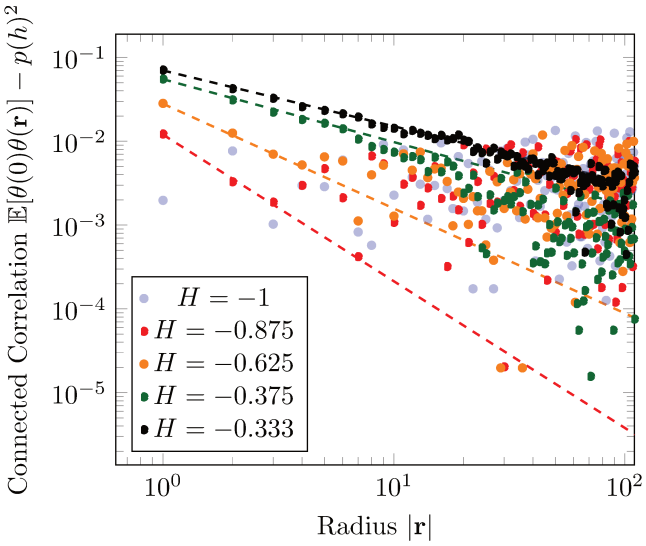

Figure 2.2 – Correlations of excursion sets for several values of H. Numerical results for the scaling of $\mathbb{E}[\theta(0)\theta(r)] - p(h)^2$. $H \in \{-1, -0.875, -0.625, -0.375, -0.333\}$, $N = 2^9$ and $\mathrm{O}(10^5)$ samples. The dashed lines indicate the scaling $\sim r^{2H}$. We have included the uncorrelated case $H = -1$ as a reference.

2.3 Finding the critical level and the properties of the clusters

With the excursion sets θ_h defined, we will now find the critical level h_c in which the emerging clusters will show fractal geometrical properties. We shall write only $\theta(\mathbf{x})$ whenever $h = h_c$.

2.3.1 Critical Level

As mentioned in the introduction, the percolation model defined above undergoes a second order phase transition at the critical level h_c. We will now find h_c for different values of H. Note that h_c can be precisely determined for $H = -1$. In this case indeed the convolution kernel (2.19) is just the unit constant and the surface u is a white noise, $u(\mathbf{x}) = w(\mathbf{x})$. The sites are activated therefore in an independent way and we recover the site pure percolation. Even if in this case p_c^{pure} is not known exactly, extensive numerical studies [21] have determined the value of with high accuracy: $p_c^{\text{pure}} \approx 0.59274\ldots$. Using (2.26), the corresponding level is:

$$h_c = \sqrt{2}\,\mathrm{erfc}^{-1}(2p_c) \approx -0.23461\ldots \tag{2.29}$$

For $H > -1$, we will follow two strategies to find h_c. One is based on the probability of finding a percolating cluster. The second one is based on the calculation of the Binder cumulants of the clusters. These two methods provide independent

methos not only to define h_c but to test the correlation length exponent ν and the order parameter exponent β. We proceed to explain both approaches

Detection of Percolating Clusters

The protocol is the following: For each H, we generate a sample on a square lattice $M = N$. We increase the value of h until the first cluster connecting two opposite boundaries appears. The level h is then stored and the procedure is restarted. The average of these levels, $h_c(N)$ will converge to the critical level up to finite size corrections. One expects the following scaling law [1]:

$$|h_c(N) - h_c| \sim N^{-1/\nu}, \tag{2.30}$$

As mentioned in the Introduction, for $H \leq -3/4$, the correlations are decay quickly enough to not influence the large distance behavior of the system. In other words, the universality class at the transition point (charecterized by the critical exponents) is the same of the pure percolation model. Above this value a renormalization group calculaton predicted [22] that $\nu = -1/H$. In summary, the correlation length is given by [17–19]:

$$\nu = \begin{cases} \nu_{\text{pure}} = 4/3, & -1 < H < 3/4 \\ -1/H, & H \geq -3/4 \end{cases} \tag{2.31}$$

Notice that $\nu \to \infty$ as $H \to 0^-$. The divergence of the correlation length exponents implies that the scaling formula (2.30) depends more weakly on the size. One is forced to generate larger and larger sizes to find some convergence. Our numerical method thus becomes inneffective close to $H = 0$. As shown in [23], the fluctuation of the critical level remains finite even when $N \to \infty$. This is a manifestation of the breaking of self-averaging, and this is why we always consider $H < 0$.

By plotting the observed $h(N)$ with respect to $N^{1/\nu}$, where ν is given by (2.31), one can extrapolate the intersection of the lines with the y-axis to obtain an estimate for the critical level. Figure 2.3, where we compare the scaling of $h_c(N)$ with the expected result (2.30), provides a good verification of the theoretical prediction (2.31). Also, Table 2.1 shows the extrapolation values $h_c(\infty)$. We remind that these values are not universal quantities but expected to depend on the details of how we generate the random surface. Nevertheless, it is interesting, by transforming them to percolation probabilities via (2.26), to compare our results with to the ones of [16],

where the random surfaces are quite similar to ours, although a slightly different convolution kernel was used.

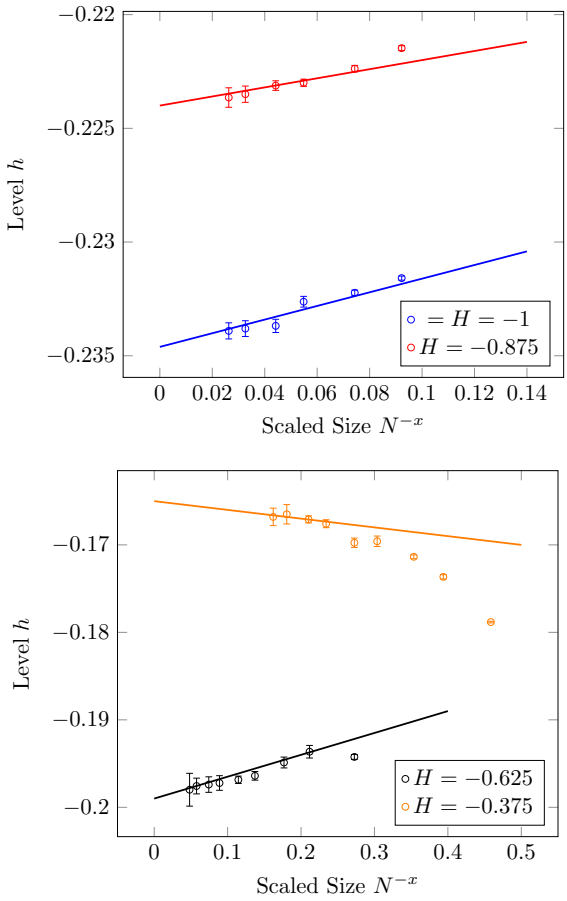

Figure 2.3 – Scaling of $\mathbb{E}[h(N)]$ with system size N for different H. $O(10^6)$ samples. *Top*: scaling as $N^{-1/\nu_{\text{pure}}}$. *Bottom*: scaling as N^H (see (2.31)). For larger values of H, the scaling law converges more weakly on system size, so $h(N)$ becomes difficult to probe.

H	h_c	p_c	p_c ([16])
-1	-0.234(6)	0.592(7)	0.59(3)
-0.875	-0.224(0)	0.588(6)	0.59(0)
-0.625	-0.198(5)	0.578(6)	0.58(0)
-0.375	-0.166(7)	0.566(1)	0.56(0)

Table 2.1 – Extrapolated values of the critical level h_c for each value of H by the detection of percolating clusters. We also show the corresponding percolation threshold values and those of [16] for comparison.

Binder cumulant method

The other method [24] is based on the moments of the distribution of clusters. Define the average of the i-th moment of a cluster, $\mathbb{E}[M_i]$:

$$\mathbb{E}[M_i] = \mathbb{E}\left[\sum_{s=1}^{NM} s^i \, \mathsf{n}_s\right] \tag{2.32}$$

where n_s is the number of clusters composed by s sites. We will be in particular interested in $\mathbb{E}[M_2]$ and $\mathbb{E}[M_4]$ as a function of the level h. The finite size scaling form can be given when $|p - p_c| \ll 1$ and N large [25] :

$$\begin{aligned} \mathbb{E}[M_2](N) &\sim N^{2+\gamma/\nu} F_2(N^{1/\nu}(p - p_c)) \\ \mathbb{E}[M_4](N) &\sim N^{4+2\gamma/\nu} F_4(N^{1/\nu}(p - p_c)), \end{aligned} \tag{2.33}$$

where γ is another critical exponent related to ν and β and where $F_{2,4}$ are scaling functions that relate N and p. The method then consists in comparing, for each H and for several N, the Binder cumulant, defined as the following ratio:

$$B(N) = \frac{\mathbb{E}[M_4]}{\big(\mathbb{E}[M_2]\big)^2} \sim f(N^{1/\nu}(p - p_c)), \tag{2.34}$$

for $f = F_4/(F_2)^2$. Since (2.33) is valid for every N, the curves should all intersect at the critical level h_c when $N \to \infty$. Close to the critical point p_c, we can expand the Binder coefficient to first order:

$$B(N) \approx f(0) + (p - p_c) N^{1/\nu} f'(0) + a N^{-\omega} \tag{2.35}$$

where the term $aN^{-\omega}$ is a correction to the finite-size scaling when N is still small. Then, for two different sizes $N, 2N$, we must have equal Binder coefficients close to p_c:

$$(p - p_c) N^{1/\nu} f'(0) + a N^{-\omega} = (p - p_c)(2N)^{1/\nu} f'(0) + a(2N)^{-\omega} \tag{2.36}$$

which implies $p - p_c \sim N^{-\frac{1}{\nu} - \omega}$. As we have seen in (2.26), there is a monotonic relationship between p and the crossing level h, and thus our first order approximation is still valid for h close to the critical level, h_c:

$$h(N) - h_c \sim N^{-\frac{1}{\nu}-\omega}. \tag{2.37}$$

We fit the resulting values via a univariate spline method [26] to obtain curves for $B(N)$ with respect to h for each N. While for smaller N the curves do not intersect in the chosen interval, the next intersections come closer to the expected value h_c. Error bars are obtained by calculating the combined errors in M_4 and M_2:

$$B(N) = \frac{\mathbb{E}[M_4]}{\mathbb{E}[M_2]^2} \pm \left(\frac{\sigma[M_4]}{\mathbb{E}[M_2]^2} + 2\frac{\mathbb{E}[M_4]\sigma[M_2]}{\mathbb{E}[M_2]^3} \right) \frac{1}{\sqrt{\text{samples}}} \tag{2.38}$$

where $\sigma[\cdot] = \sqrt{\text{Var}[\cdot]}$ is the standard deviation. In the figure below, we show the obtained curves and the crossing points.

H	h_c	p_c
-1	-0.234(6)	0.592(7)
-0.875	-0.224(0)	0.588(6)
-0.625	-0.198(7)	0.578(7)
-0.375	-0.167(0)	0.566(3)

Table 2.2 – Extrapolated values for h_c from the Binder cumulant scaling, (2.37).

Using the derivative at the critical level of each Binder cumulant line, one can also obtain an estimate of ν [24], with the following scaling:

$$\left.\frac{\mathrm{d}B(N)}{\mathrm{d}h}\right|_{h=h_c} \sim N^{1/\nu} \tag{2.39}$$

This test provides a strong verification of (2.31), as can be seen in Figure 2.6, where we have plotted in logarithmic scale the derivatives of the curves at the extrapolated critical level h_c. The points land on the expected scaling line first with rather small sizes (up to $N = 256$ is good enough, as mentioned in [24]), but as we increase H above $-3/4$ one sees again how smaller sizes are not in the scaling region.

H	ν	$\nu_{\text{predicted}}$
-1	1.3(4)	$4/3$
-0.875	1.3(6)	$4/3$
-0.625	1.6(1)	$8/5$
-0.375	2.6(3)	$8/3$

Table 2.3 – Extrapolated values for ν from the scaling of the slopes of the Binder cumulants, (2.39).

Order Parameter exponent and Fractal Dimension

The order parameter of the percolation model is defined as the probability that a site belongs to an infinite cluster [1]. Close to the critical point, this quantity decays as $\sim (p - p_c)^\beta$ for $p > p_c$ and is zero for $p \leq p_c$ (at $N \to \infty$). This exponent is directly related to the Fractal Dimension, D_f, by the relation $D_f = 2 - \beta/\nu$. We will choose to concentrate on the fractal dimension D_f of the level percolation clusters. We estimate the value of D_f by measuring the mean area of the largest cluster A_{largest}. This quantity scales as [1]:

$$\mathbb{E}[A_{\text{largest}}](N) \sim N^{D_f}, \tag{2.40}$$

To obtain estimates for this quantity, we control the best fit parameter by removing succesively the smaller sizes in our samples, as shown in Figure 2.7. In the case of pure site percolation, the value of D_f is known to be exactly $91/48$. This corresponds well to our estimates for $H < -1/2$. Note however that once we move past $H > -1/2$, the value of D_f deviates from the value of pure site percolation. In fact, the precise threshold at which this value begins to change is unknown [17],

and numerical experiments to measure D_f present different results [17–19]. We have verified that our surfaces –which we remark are defined with a different convolution kernel (defined in equations (2.18) and (2.19))– indeed show an increase in the fractal dimension for $-1/2 < H < 0$, which is in the zone where [27] also found this increment, see Table 2.7.

Both methods, by percolating clusters and by Binder cumulants, expose the scaling features of the correlated surfaces that we generate, in particular by veryfing both the prediction (2.31) and by sitting in values of fractal dimension that other studies report for the cases $H > -1$. Our surfaces can be thus considered numerically consistent with those in the literature.

H	D_f
-1	1.895(8)
-0.875	1.896(0)
-0.625	1.896(6)
-0.375	1.90(7)

Table 2.4 – Extrapolated values for h_c from the scaling of the largest cluster, (2.40).

2.4 Numerical Implementation

2.4.1 Generating fractional surfaces on a computer

The following procedure was used to create fractional gaussian surfaces : Begin with $N \times M$ real random gaussian numbers $\{w_{\mathbf{x}}\}$ each one $\mathcal{N}(0,1)$. Then use a Fast Fourier Transform algorithm (FFT) to get the associated complex set of gaussian numbers $\{w_{\mathbf{k}}\}$, which will already be arranged in such a way $w^*_{(k_1,k_2)} = w_{(N-k_1,M-k_2)}$.

Some different choices can be made: one can begin with a desired correlation function $C(\mathbf{r})$, take its discrete Fourier transform and adapt the resulting coefficients (e.g. by cutting off the negative values), before finally multiplying by a complex gaussian random variable and taking the inverse DFT. This produces a real and imaginary part that will have the desired correlations, although the direct relationship with the Hurst exponent is lost because now the scaling relation $C(\mathbf{r}) \sim f(a)|\mathbf{r}|^a$ is not zero for $a = -2$.

Finally, some authors [17] consider instead the correlation function $(1 + |\mathbf{r}|^2)^{\gamma/2}$ which will have the same long-range behavior and whose Fourier Transform avoids the zero-mode singularity, again at the expense of losing contact with the Hurst exponent. Nevertheless, all these choices show good agreement with the Extended Harris Criterion.

For a chosen a Hurst exponent H, we set the convolution kernel entries (2.19) $\{S_{\mathbf{k}}\}$ and with them the norm factor (2.22). Finally multiply site by site the convolution kernel with the set $\{w_{\mathbf{k}}\}$ and do an inverse FFT in order to get the fractional surface, dividing by norm to ensure unit variance.

With this procedure we are able to generate large surfaces ($N \sim 2^{13}$) although the memory requirements grow exponentially with size. One has to keep in mind the cost of generating the surfaces with two applications of the FFT algorithm, then properly labelling the cluster structure and then, as we develop in the next chapter, sample the two-point connectivity function on these clusters.

When finding the critical level, it is sometimes useful to add a small-size correction to the scaling of the critical level, given by

$$|h_c(N) - h_c\infty| \sim N^{-1/\nu}\big(A + BN^{-\omega} + CN^{-1/\nu} + \dots\big), \tag{2.41}$$

where B and C may indeed be very small for certain values of H. We've also found that ω is usually some value ≤ 2.

2.4.2 Hoshen - Kopelman Algorithm for determining Clusters

In order to study cluster properties of surfaces of large size, we will need a fast algorithm to classify and count them once excursion sets have been obtained. The idea of the *Hoshen-Kopelman algorithm* is to traverse the array one time, looking for nearest neighbors that may be connected and renaming the sites with cluster representatives along the way. Instead of editing the contents of the entire cluster every time there is a fusion, one simply matches the representatives of each, called *seeds*.

Crucial to the algorithm keeping track in parallel of a "label" array that stores the address of each seed, and whose first slot counts the number of clusters.

After the equivalence classes have been all identified, one makes an additional sweep to assign the seed label to all clusters (instead of only pointers to the seed). It is during this sweep when one can also keep track of the masses of the clusters, thus improving greatly the calculation time. Boundary conditions can be easily implemented by identifying the seed at the corresponding edges of the lattice.

The correlated nature of the excursion sets implies that a standard Monte Carlo scheme (as is usually the state of the art in pure percolation [21]) would need to be modified non-trivially, since populating the lattice is not independent of a given configuration. This is the main reason why we implemented the numerical protocol, as was noticed previously in [27].

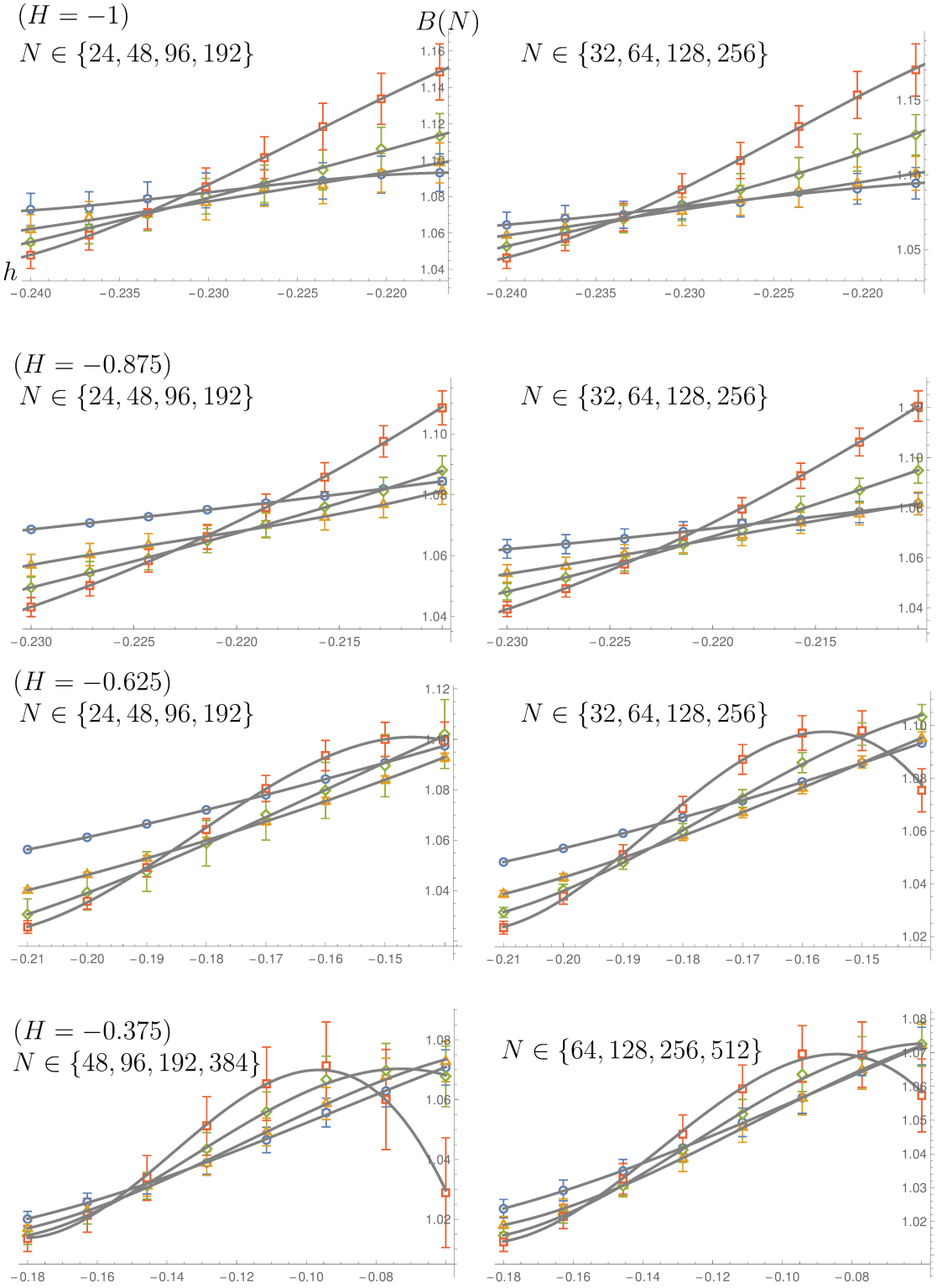

Figure 2.4 – Crossing of Binder cumulants, defined in (2.34) for $H \in \{-1, -0.875, -0.675, -0.375\}$, for sizes $24, 48, 96, 192$ (left) $32, 64, 128, 256$ (right). The crossings scale as N^{-x} with $1 < x < 3$, while the slopes at the extrapolated critical level scale as $\sim N^{1/\nu(H)}$. The fitting curves were obtained by a univariate smoothing spline method with 3 to 5 knots and the error bars are obtained from $\mathrm{O}(10^5)$ samples. Note how as we increase H above $-3/4$, larger sizes N are needed since the scaling becomes less strong.

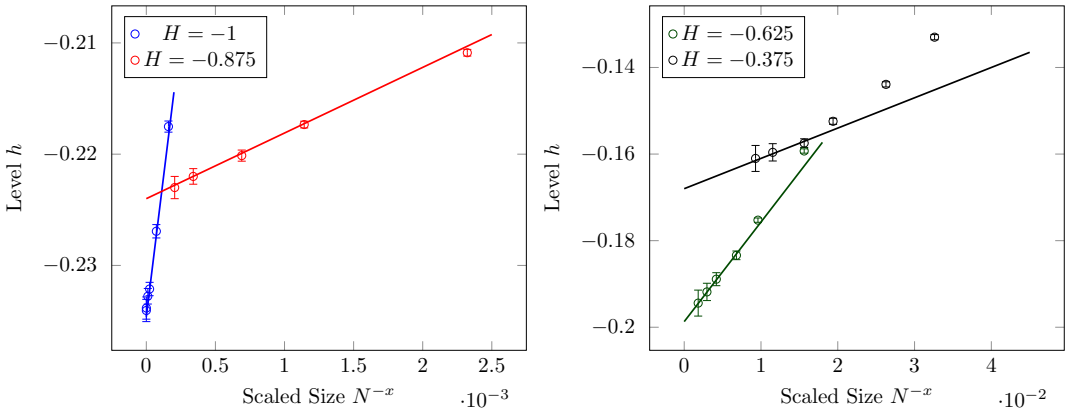

Figure 2.5 – Results from the Binder Cumulant method. Crossing points of $(N, 2N)$ Binder cumulant curves for $H \in \{-1, -0.875\}$ (left) and $H \in \{-0.625, -0.375\}$ (right). The sizes have been rescaled to N^{-x}, where $x = 1/\nu + \omega$, with $1 \leq x \leq 3$ in order to compare to a straight line. Notice that for $H < -3/4$ there is good agreement with the scaling (2.37), but for $H > -3/4$, where ν now increases, the scaling is weaker.

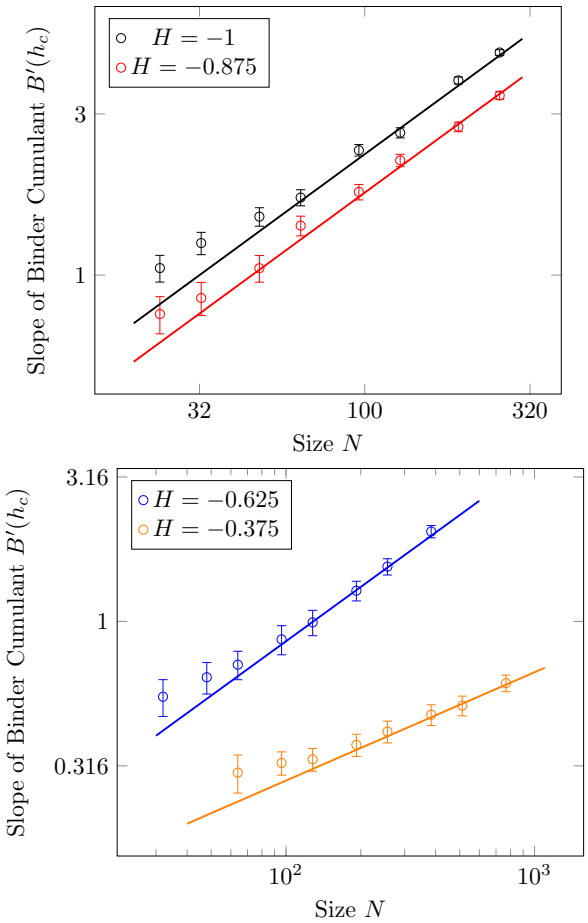

Figure 2.6 – Estimation of ν using the slopes of the Binder cumulants at the extrapolated critical level. *Above*: For $H < -3/4$. *Below*: For $H > -3/4$. To estimate ν, we calculated a linear fit over the last points in the data set. In all cases there is good agreement with (2.31)

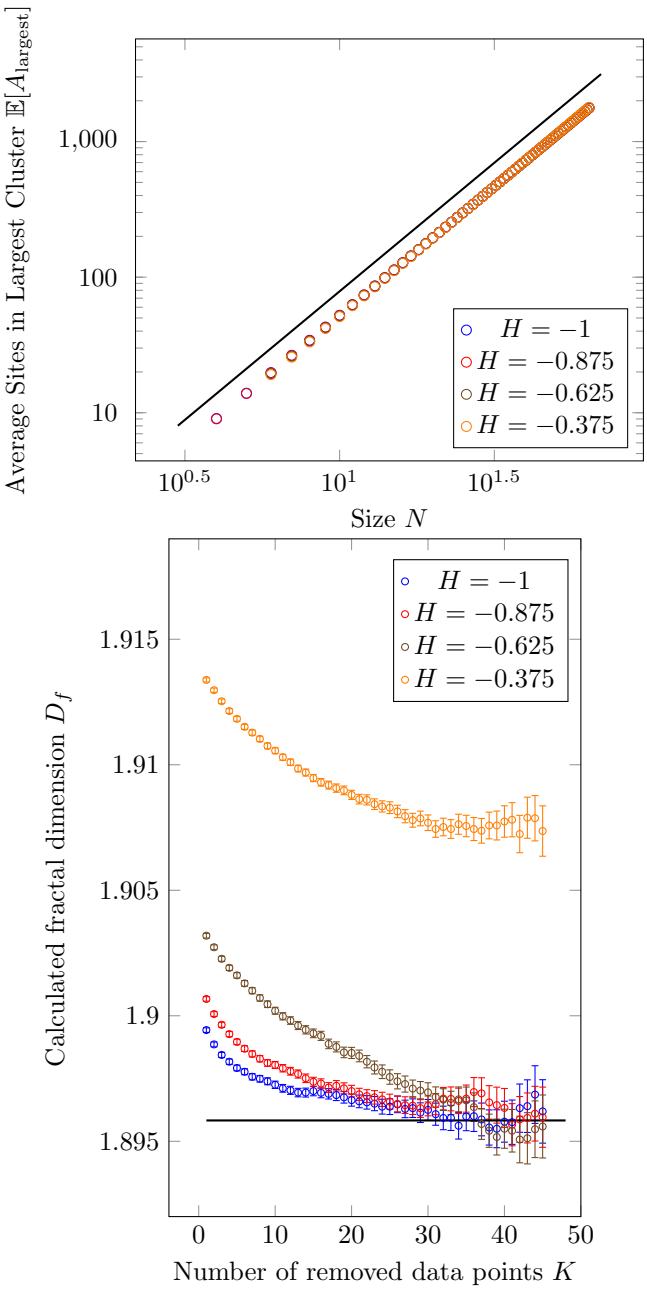

Figure 2.7 – Estimation of the Fractal Dimension. *Above*: Average number of sites of the largest cluster with respect to the lattice size N. For every value of H, the slopes are very close to each other. *Below*: Best fit parameter for the scaling exponent of the largest cluster ($H \in \{-1, -0.875, -0.675, -0.375\}$), where the K lowest sizes are removed. The black line is drawn at the value 91/48. Notice that while the first three values all converge to the expected $D_{\mathsf{F}} = 91/48 \approx 1.8959$, once we choose $H > -0.5$, the estimated fractal dimension is higher.

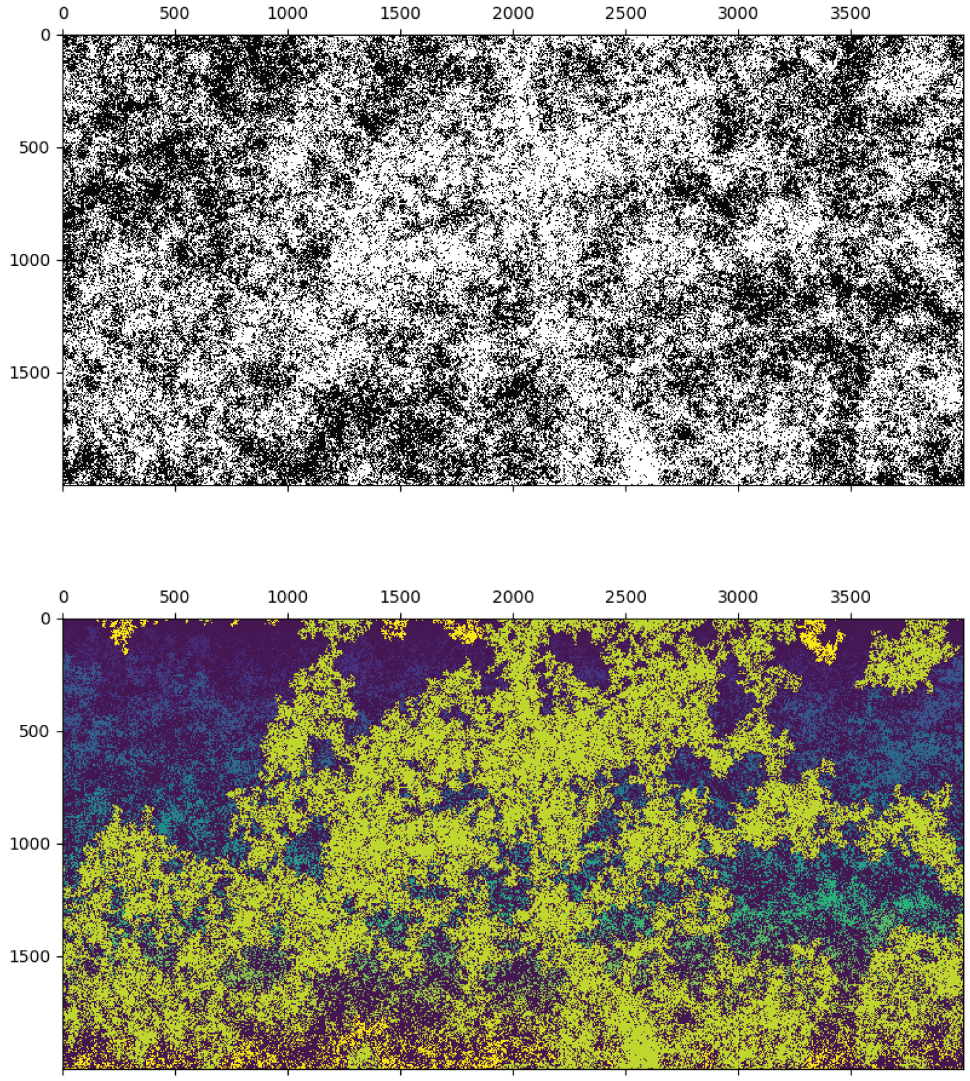

Figure 2.8 – Clustering using the Hoshen-Kopelman algorithm. *Above*: Example of an excursion set of a 2000×4000 fractal surface ($H = -0.125$) at the extrapolated critical level. *Below*: Cluster detection after running the Hoshen-Kopelman algorithm, where each cluster is assigned succesive integer numbers and then a color.

Chapter 3

Cluster connectivities

In the previous chapter we have seen that the excursion sets of fractional random Gaussian surfaces define a problem of long-range percolation. We have located in Tables 2.1 and 2.2 the critical point of these percolation models and determined numerically the two main exponents, the correlation lenght exponent ν (Table 2.3) and the fractal dimension D_f (Table 2.4). As we explained above, these results confirmed previous conjuctures and numerical results, and support the precision of our estimation of the critical point. We present now the more original part of our work, mainly concerning the two-point connectivity, p_{12}. This is a very natural observable in percolation theory [1] and it is defined as:

$$p_{12}(\mathbf{x}, \mathbf{y}) = p_{12}(\mathbf{x} - \mathbf{y}) = \text{Prob}\Big[\mathbf{x} \text{ is connected to } \mathbf{y}\Big] \tag{3.1}$$

Due to the translation invariance of the surface measure, $p_{12} = p_{12}(\mathbf{r})$ depends only on the vector

$$\mathbf{r} = \mathbf{x} - \mathbf{y} = r\,(\cos\theta, \sin\theta). \tag{3.2}$$

where $r = |\mathbf{r}|$ is the distance between the two points and θ is the angle formed with the vertical axis. p_{12} is expected to depend in general on r and on the orientation θ. In the scaling limit, the angle dependence enters in the finite size corrections when the lattice Ω has a rectangular shape ($N \neq M$) and therefore the rotational symmetry is (weakly) broken. We will see that θ-dependence of p_{12} is the crucial ingredient to test conformal invariance at the critical point.

Before entering in some detail, let us gain familiarity with the behavior of the above quantity. In Figure (3.1), we show some measures of p_{12} for square lattices Ω with $N = M$. The measures have been taken for pure percolation but the features that emerge are the same for all $-1 < H < 0$:

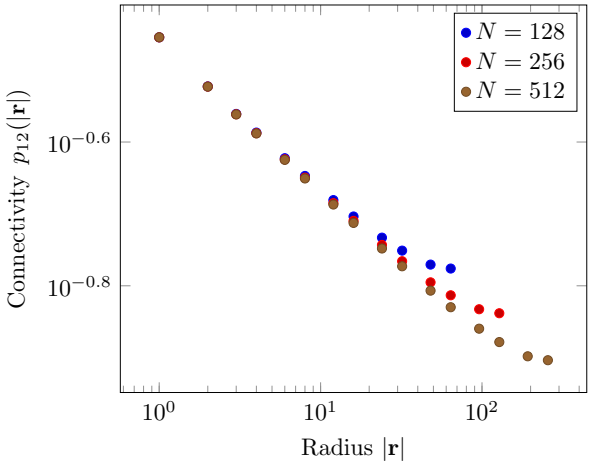

Figure 3.1 – Two-point connectivity function p_{12}. We show different N for a square torus ($N = M$) and for pure percolation ($H = -1$). The error bars are of the size of the points after taking $O(10^5)$ samples.

(i) Neighbouring sites ($r = 1$) are connected if they are both activated, and therefore $p_{12} = p_c^2$, where p_c is given in (2.29) in terms of the critical level h_c. For pure percolation, $p_c = 0.59274\ldots$ [21], and as we calculated in the previous chapter, p_c will decrease for $H > -1$. As $r > 1$, one has $p_{12} < p_c^2$.

(ii) There is a region $1 \ll r \ll N/2$ in which the connectivity behaves as a power law $p_{12} \sim r^{-\eta}$. The exponent η [1] is expressed as a function of D_f in (3.5).

(iii) The p_{12} decreases with the distance $1 \leq r \leq N/2$. However, close to $r = N/2$, one observes deviations from the algebraic decay $r^{-\eta}$. These deviations have an universal nature and understanding these for general value of H is the object of our study. For pure percolation, analytical results have been given in [15]

Let us focus on the toroidal finite size corrections, that explain the deviations from the single power law behavior observed in Figure (3.1). The torus topology of Ω is parametrized by the nome:

$$q = e^{-2\pi \frac{M}{N}}, \tag{3.3}$$

where the aspect ratio is usually written as $\tau = iM/N$. In the scaling limit, p_{12} takes the form:

$$p_{12}(\mathbf{r}) = \frac{d_0}{r^\eta}\, f_q\left(\frac{\mathbf{r}}{N}\right), \tag{3.4}$$

where d_0 is a non-unversal constant, and the exponent η has been determined to

be[1]

$$\eta = 2(2 - D_f). \tag{3.5}$$

The function $f_q(\frac{\mathbf{r}}{N})$ encodes the toroidal finite size corrections. They are expected to depend on the geometry of the torus, parametrized by q and on the ratio between the remaining two lenghts of the problem, the distance r and the size N. As we could have equivalentely chosen the other axis, of size M, this function has to obey: $f_{-\tau^{-1}}(\mathbf{r}/M) = f_\tau(\mathbf{r}/N)$. Equation (3.4) can be readily verified by the collapse of all lattice sizes into a single curve, as shown in Figure 3.1:

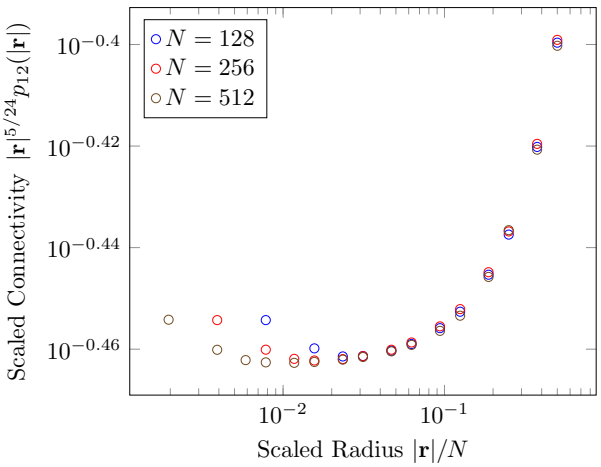

Figure 3.2 – Emergence of the scaling limit in the two-point connectivity. Rescaled connectivity function with the same data as 3.1. Notice how the different lattice sizes have now collapsing points for $r/N \gg 1$. The scaling region is characterized by the plateau that emerges with larger system sizes and which in the planar limit is given by the non universal value d_0 in (3.4)

In the regime where $r/N \ll 1$, one could try to find the small $1/N$ expansion of (3.4). The most general form is:

$$f_q\left(\frac{\mathbf{r}}{N}\right) = \sum_{i \in \mathbb{N} \cup \{0\}} \left(\frac{r}{N}\right)^{\beta^{(i)}} \left(\sum_{j \in \mathbb{N} \cup \{0\}} \alpha_{(i)}^{(j)}(q, \theta) \left(\frac{r}{N}\right)^j \right) \tag{3.6}$$

where the exponents β_i are an ordered set of non-negative real numbers, $\beta^{(i)} \in \mathbb{R}^+$, $\beta^{(i)} > \beta^{(i-1)}$. Note that in order to recover, in the infinite plane limit:

$$p_{12}(\mathbf{r}) = \frac{d_0}{r^{2(2-D_f)}}, \quad \left(\frac{r}{N} \to 0\right), \tag{3.7}$$

one has $\beta^{(0)} = \alpha^{(0)}_{(0)} = 1$. Thus:

$$f_q\left(\frac{\mathbf{r}}{N}\right) = 1 + \alpha^{(0)}_{(1)}(q,\theta)\ \left(\frac{r}{N}\right)^{\beta^{(1)}} + \cdots \tag{3.8}$$

The evaluation of the exponents $\beta^{(i)}$ and of the coefficients $\alpha^{(j)}_{(i)}$, that we recall are universal quantities, is a particularly hard problem. On the other hand, if a system is conformal, the CFT approach is particularly powerful to fix these quantities. Actually, the way the terms in the expansion (3.6) are organized is reminiscent of the typical structure of a CFT result: in CFT jargon, the $\beta^{(i)}$ are related to the dimension of the primary fields appearing in the expansion, while the coefficients $\alpha^{(j)}_{(i)}$ are related to the contribution of the j-th descendants. The CFT approach has been used in [15] for pure percolation($H = -1$) where conformal symmetry is well established. Assuming that for general $-1 < H < 0$, the critical point is described by a CFT theory, we predict that:

$$\begin{aligned}
&\beta^{(0)} = 0, \quad \alpha^{(0)}_{(0)} = 1, \quad \alpha^{(1)}_{(0)} = 0,\ \alpha^{(2)}_{0} = 2\cos 2\theta\ c_T(q) \\
&\beta^{(1)} = 2 - \frac{1}{\nu}, \quad \alpha^{(0)}_{(1)}(\theta,\tau) = c_\nu(q) && (3.9)\\
&\beta^{(2)} > 2. && (3.10)
\end{aligned}$$

The coefficients $c_T(q)$ and $c_\nu(q)$ are related to CFT torus one-point functions, as explained in detail our paper (Cf. Equation (19) of [14]), to which we refer the reader for more information about how the above coefficients have been found. In summary we have:

$$p_{12}(\mathbf{r}) = \frac{d_0}{|\mathbf{r}|^{2(2-D_f)}}\left[1 + c_\nu(q)\left(\frac{r}{N}\right)^{2-1/\nu} + \ 2c_T(q)\cos(2\theta)\left(\frac{r}{N}\right)^2 + o\left(\left(\frac{r}{N}\right)^2\right)\right]. \tag{3.11}$$

In the following we focus our attention on the meaning of the power-law exponents and on the θ dependence of the above formula. We will put aside the comments on the coefficients $c_\nu(q)$ and $c_T(q)$, whose interpretation would require advanced CFT notions.

3.1 Infinite plane limit

Let us begin with the dominant term in (3.11), given by (3.7). As shown in Figure (3.3), we exploit this relationship to find the non-universal coefficient d_0 as well as an independent measure of the fractal dimension D_f. The results are shown in Table (2.1) where a good agreement with the ones computed in the previous chapter can

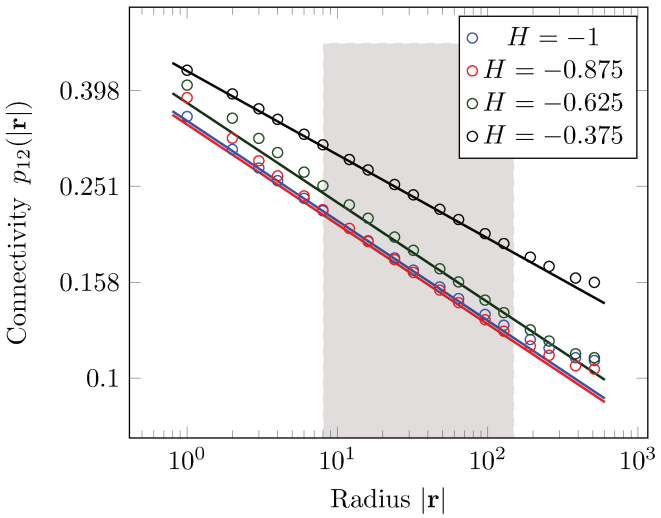

Figure 3.3 – Two-point connectivity for different values of H. Here $N = 1024$ and $O(10^5)$ samples in log-scale. A reference for scaling region is shown in gray. In this region, one expects the algebraic decay of (3.7). The corresponding best fit lines have been drawn below each data set. The intersection with the y axis gives the non-universal coefficient d_0. The slope is given by $2(2 - D_f)$, from which the fractal dimension can be estimated. Notice that at each value of H the scaling region may vary, as well as the short and large r behavior.

be verified.

H	d_0	D_f	$D_f^{(\text{Largest Cluster})}$
-1	0.344(3)	1.895(6)	1.895(8)
-0.875	0.338(4)	1.895(9)	1.896(0)
-0.625	0.375(6)	1.896(2)	1.896(6)
-0.375	0.437(2)	1.909(0)	1.90(7)

Table 3.1 – Observed values for the main components of the scaling limit algebraic law, the non-universal coefficient d_0, and the fractal dimension D_f. The values estimated by the scaling of the largest cluster, Table 2.4

3.2 Toroidal finite-size corrections

We discuss now how to measure and interpret the leading ($\sim (r/N)^{2-1/\nu}$) and sub-leading corrections ($\sim (r/N)^2$) in (3.11)

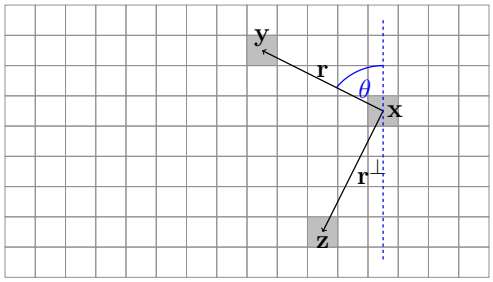

Figure 3.4 – Points and vectors in the lattice. The sites of the lattice (shaded gray) correspond to vectors $\mathbf{x}, \mathbf{y}, \mathbf{z}$. They are connected by the radius vectors $\mathbf{r}$ and $\mathbf{r}^{\perp}$. The latter will be taken to be perpendicular to $\mathbf{r}$ as in Equation (3.2). The value of the angle of $\mathbf{r}$ with respect to the vertical axis will be measured by θ.

3.2.1 Leading Correction

To isolate to leading correction we consider the lattice Ω with square shape, $N = M$ and $q = e^{-2\pi}$. Indeed, in this case, one can show that [14]:

$$c_T(q) = 0, \quad \left(q = e^{-2\pi}\right) \tag{3.12}$$

We obtain then:

$$p_{12}(\mathbf{r}, N) = \frac{d_0}{r^{2(2-D_f)}} \left[1 + c_\nu(q) \left(\frac{r}{N}\right)^{2-1/\nu} + o\left(\left(\frac{r}{N}\right)^2\right)\right], \tag{3.13}$$

In this way, by rescaling the connectivity function as

$$\frac{|\mathbf{r}|^{2(D_f-2)} p_{12}(\mathbf{r}, N)}{d_0} - 1 \longrightarrow c_\nu(q) \left(\frac{|\mathbf{r}|}{N}\right)^{2-1/\nu}, \tag{3.14}$$

we can access $c_\nu(q)$. This coefficient can be sampled for accessible sizes ($N < 2^{12}$) especially for values of $H < -1/2$. Notice that the collapse towards the expected scaling shows strong dependence on the type of convolution kernel and on the distribution of the uncorrelated random variables that define the surfaces. We included

surfaces generated with the method by [17] as well as our proposed protocol (reported in [14], where in addition a uniform distribution was used for (2.7)). In different ways, all of these support the proposed behavior (3.14)

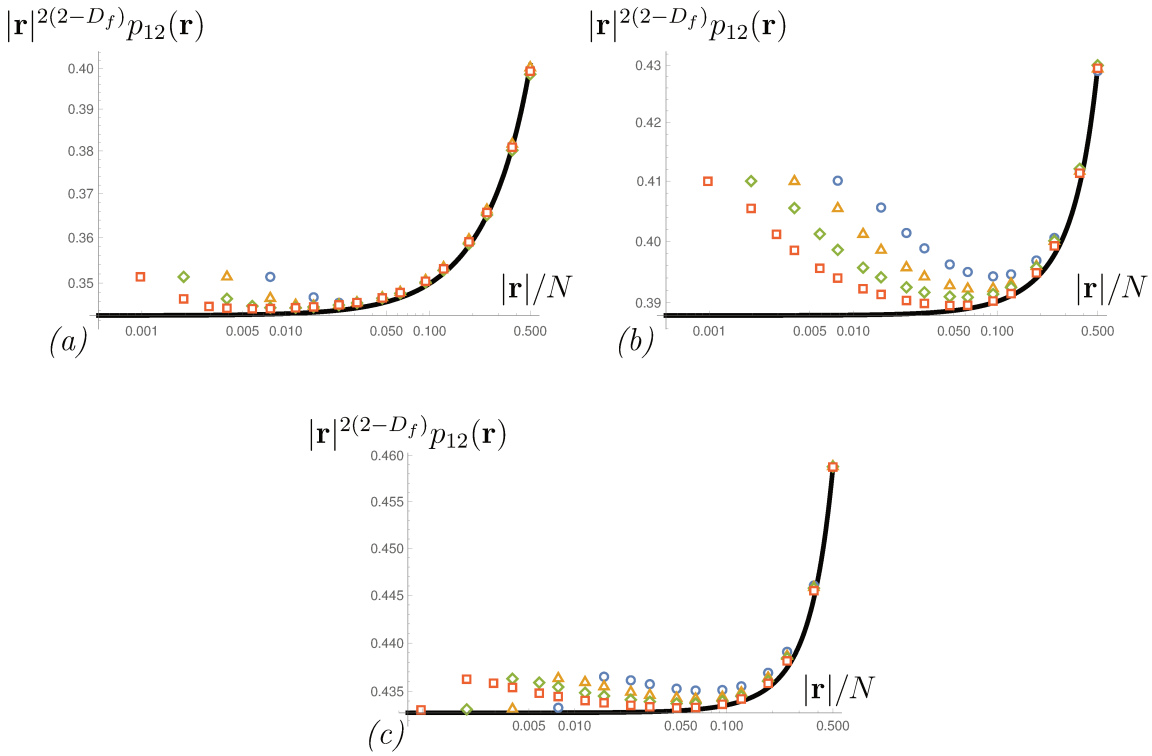

Figure 3.5 – Rescaled two-point connectivities showing the predicted scaling behavior for different values of H. Scaled two-point connectivities $|\mathbf{r}|^{2(2-D_f)}p_{12}(\mathbf{r})$, with the method proposed by [17] (different convolution kernel but with equivalent form at large $|\mathbf{r}|$) for increasing sizes at three different correlations: *(a)* Pure percolation, $\nu = 4/3$ and $D_f = 91/48$ *(b)* Clusters with higher correlation length exponent ($\nu > 4/3$), but still ordinary fractal dimension $D_f = 91/48$. *(c)* Clusters with both higher correlation length exponent and higher fractal fimension: $\nu > 4/3$ and $D_f > 91/48$. Each case was studied with $\mathrm{O}(10^5)$ samples and includes the best fit whose leading contribution is $\sim (|\mathbf{r}|/N)^{2-1/\nu}$

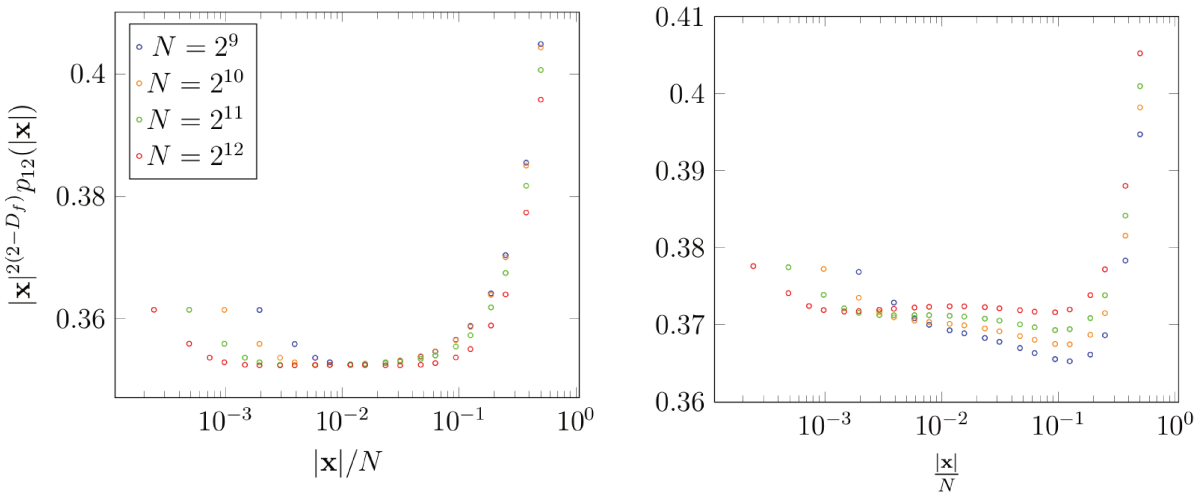

(a) $H = -5/8$

(b) $H = -3/8$

Figure 3.6 – Scaling behavior of the scaled two-point connectivity for two values of H. Two-point correlation function for $N = 2^9, 2^{10}, 2^{11}, 2^{12}$ multiplied by $r^{2(2-D_f)}$, by the protocol introduced in Chapter 2. While for small r different sizes are separated, for large r the (scaled) correlation function becomes a function of the ratio r/N. Notice the different behavior before scaling to a plateau.

3.2.2 Subleading Correction

We have stated that the presence of conformal invariance was crucial to fix the form of the exponents and coefficients in the expansion (3.6). Moreover, we predicted the presence of a subleading $\mathrm{O}\big((r/N)^2\big)$ term. In fact, this term is linked to the Noether current associated to the conformal symmetry: the stress-energy tensor. The corresponding subleading corrections can be then obtained by choosing a rectangular torus $M \neq N$ (such that we avoid (3.12)). To extract only the desired term, one additionally takes the combination $p_{12}(\mathbf{r}) - p_{12}(\mathbf{r}^{\perp})$, giving [14]:

$$p_{12}(\mathbf{r}, N) - p_{12}(\mathbf{r}^{\perp}, N) = \frac{d_0}{|\mathbf{r}|^{2(2-D_f)}} \left[4c_T(q) \cos(2\theta) \left(\frac{|\mathbf{r}|}{N}\right)^2 + o\left(\left(\frac{|\mathbf{r}|}{N}\right)^2\right)\right]. \tag{3.15}$$

The subleading correction (note how it depends on both modulus and orientation of the vector $\mathbf{r}$) will be:

$$\sim \cos(2\theta)\, |\mathbf{r}|^{2(D_f-2)} \left(\frac{|\mathbf{r}|}{N}\right)^2. \tag{3.16}$$

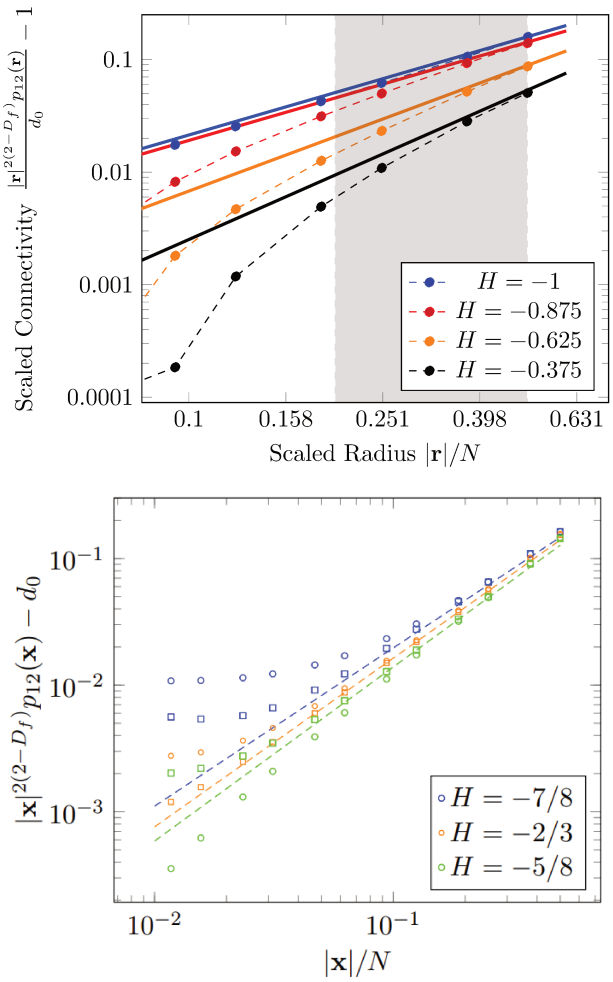

Figure 3.7 – Leading corrections (3.14) for different values of H. *Above*: Size $N = 2048$ and the convolution kernel in [17], with a Gaussian distribution. One can see the convergence of the (rescaled) connectivity towards the expected line $\sim (|\mathbf{r}|/N)^{2-1/\nu}$, ν from (2.31), in the referential shaded region. This convergence needs, as seen before, very large sizes for $H > 3/4$. *Below*: Results of [14] where a uniform distribution was used to generate the uncorrelated random variables and then compared to the gaussian distribution. Here we used larger sizes $N = 4096$ and the y-axis crossing of the reference line is $d_0 c_\nu$. The $|\mathbf{x}|$ in the labels is equivalent to $|\mathbf{r}|$.

This means we can exploit the orientation of $\mathbf{r}$ to reveal a remarkable result predicted by the CFT calculation: the subleading correction depends on the angle between $\mathbf{r} = \mathbf{x} - \mathbf{y}$ and the axes of the lattice (for a lattice of rectangular shape, $M \neq N$). The results at fixed ($\theta = 0$) angle at different values of H are shown in Figure 3.8, where the difference of the connectivity in both directions shows the emergence of the $(|\mathbf{r}|/N)^2$ scaling with excellent precision. We then vary θ at two values of H, revealing the angular dependence of the subleading correction term. This is shown in Figure 3.9.

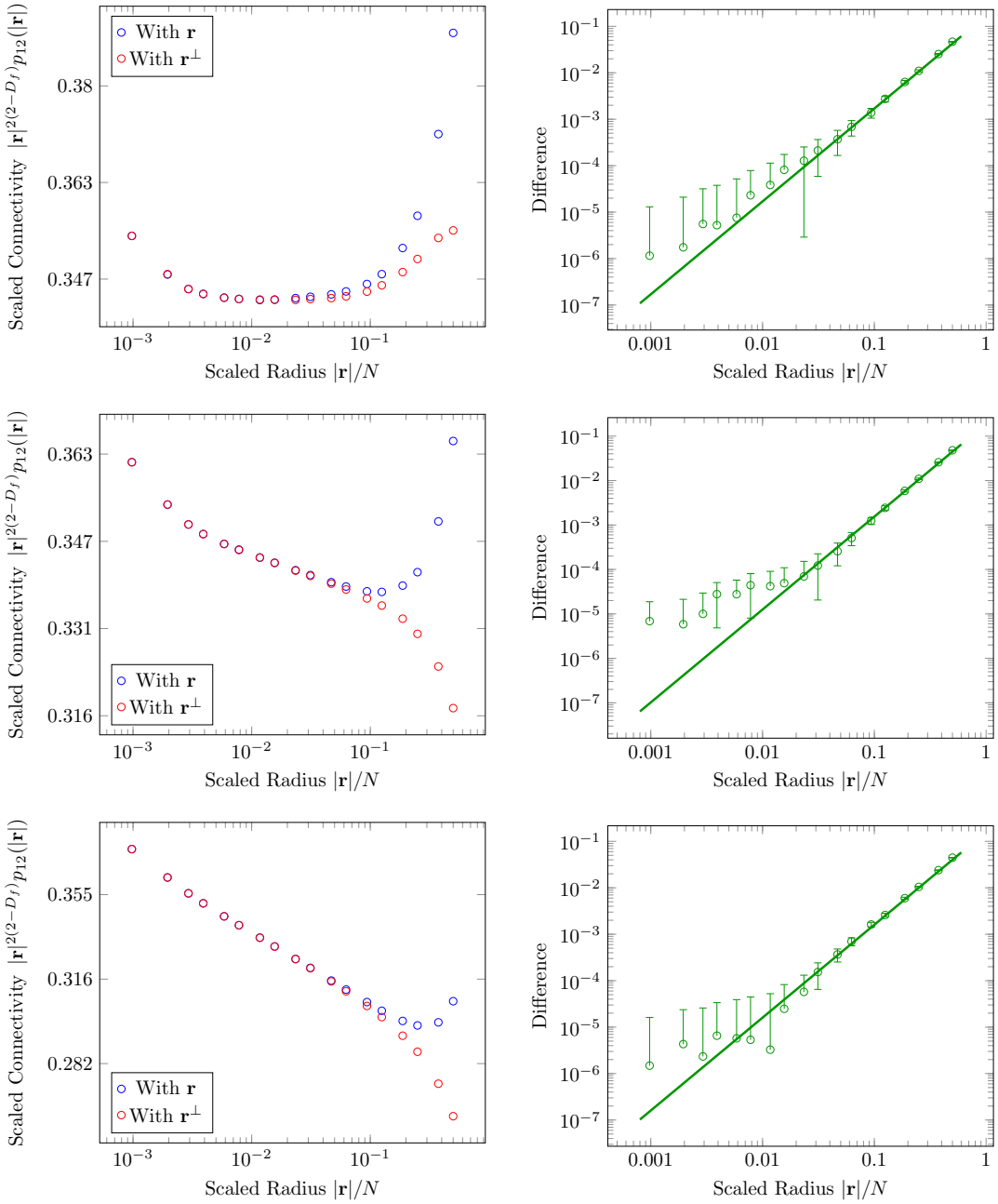

Figure 3.8 – Subleading corrections at $\theta = 0$ for $M/N = 3$. Each row corresponds to $H \in \{-0.875, -0.625, -0.375\}$. *Left*: Connectivities measured along the horizontal ($\mathbf{r}^\perp$) and vertical ($\mathbf{r}$) direction (they are aligned with the axes at $\theta = n\pi/2$, for n an integer). Notice the two-point correlation function along the longer cycle of the torus is smaller than that of the shorter cycle. *Right*: The difference between the connectivities of the long and short cycle (horizontal and vertical directions respectively) reveals the contribution of a geometric term in the corrections to the connectivity. This term is related to the stress-energy tensor of the related CFT. A reference line of $\sim (\mathbf{r}/N)^2$ has been added.

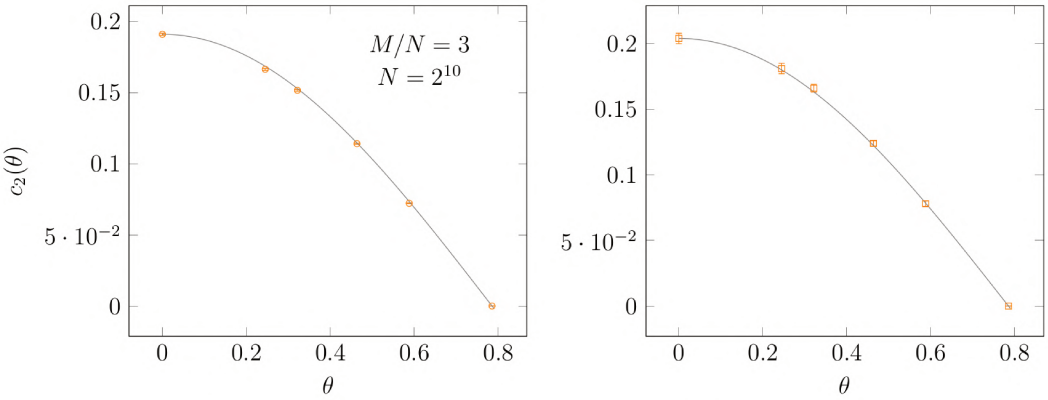

(a) $H = -2/3$ (b) $H = -3/10$

Figure 3.9 – Dependence of the subleading corrections on the angle θ. Difference of connectivities $|\mathbf{r}|^{2(2-D_f)}(p(\mathbf{r}) - p(\mathbf{r}^{\perp}))$ with rotated axis by different angles θ. Note that for $\theta = \pi/4$ there is a reflection symmetry between $\mathbf{r}^{\perp}$ and $\mathbf{r}$ along the horizontal axis, so the correction term should indeed vanish. A least-squares analysis shows that the points follow quite well the scaling $\sim \cos(2\theta)|\mathbf{r}|^2$

3.3 Three-Point Connectivity

We finish this chapter with some comments about the three-point connectivity function, defined similarly as in (3.1):

$$p_{123}(\mathbf{x},\mathbf{y},\mathbf{z}) = \text{Prob}\Big[\mathbf{x},\mathbf{y} \text{ and } \mathbf{z} \text{ are connected}\Big]. \tag{3.17}$$

We shall work with the radius vectors $\mathbf{r}_{ij} = \mathbf{i} - \mathbf{j}$, for $i, j \in \{\mathbf{x},\mathbf{y},\mathbf{z}\}$. The planar-limit form of three-point functions is also constrained by covariance under translations, rotations and global scale transformations to a sum of the following terms:

$$p_{123}(\mathbf{x},\mathbf{y},\mathbf{z}) \underset{N\to+\infty}{\longrightarrow} \sum_i \frac{D_0^{(i)}}{|\mathbf{r}_{xy}|^a |\mathbf{r}_{yz}|^b |\mathbf{r}_{zx}|^c}, \tag{3.18}$$

where each term satisfies $a + b + c = 3\eta$, and η is the scaling dimension of the connectivity function. If in addition the hypothesis of spectial conformal invariance is included, one obtains an expression in terms of a single term and exponent:

$$p_{123}(\mathbf{x},\mathbf{y},\mathbf{z}) \underset{N\to+\infty}{\longrightarrow} \frac{D_0}{(|\mathbf{r}_{xy}||\mathbf{r}_{yz}||\mathbf{r}_{zx}|)^{\eta/2}}. \tag{3.19}$$

It was argued in [28] that the ratio

$$R = \frac{p_{123}}{\sqrt{p_{12}p_{13}p_{23}}}, \tag{3.20}$$

should exhibit universal scaling. One way to picture this is to notice that $p_{123} \to p_{12}$ as two of the points approach each other, so the three-point function should factorize into a product of two-point functions. Indeed, this was shown to be the case for the Q-Potts model, which as we mentioned in the Introduction, includes pure percolation when $Q = 1$. This ratio was also investigated in [29, 30]. In Figure 3.10, we show the results we obtain for our correlated clusters. While we observe an emerging plateau at the expected value for pure percolation ($H = -1$), it is interesting to notice that the ratio deviates from the value proposed in [28] as we increase H. This may imply that the mechanism by which the non-universal term D_0 splits into that of the two-point functions is different from what was expected. We leave this remark as a motivation for future studies on these surfaces.

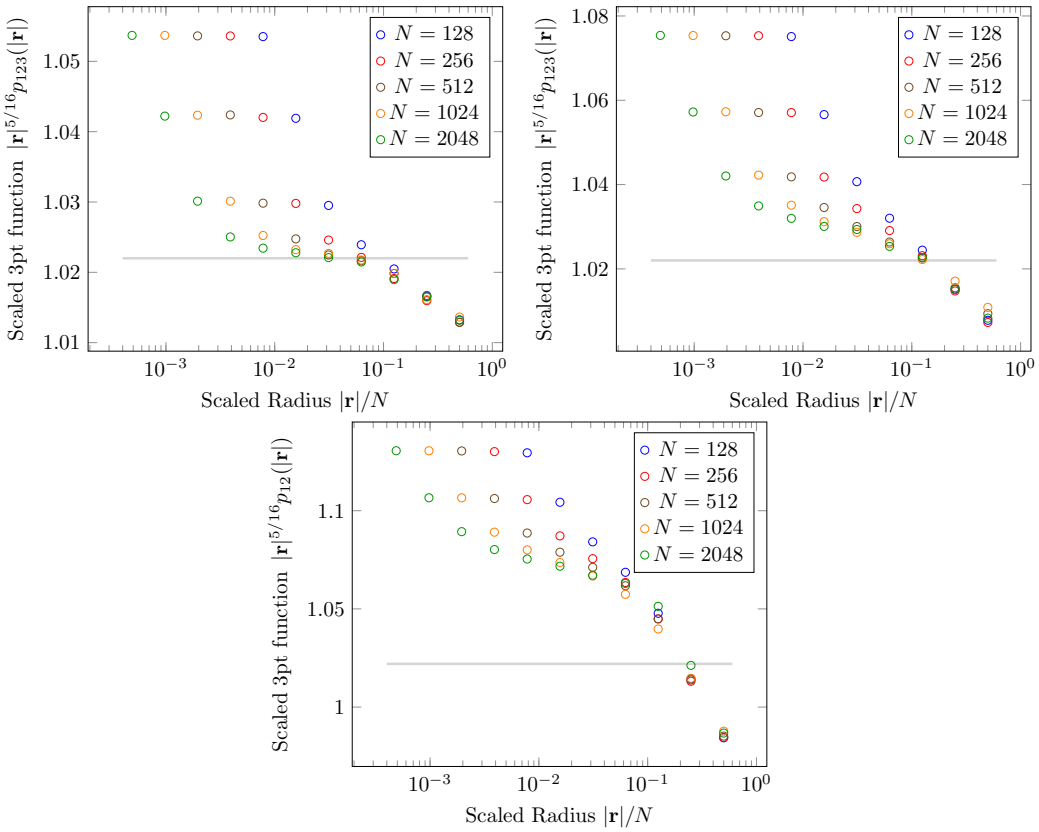

Figure 3.10 – Factorization ratio (3.20) **for increasing values of** H. We consider $H = \{-1, -7/8, -5/8\}$. The emerging plateau deviates from the calculation in [28], in which $R \approx 1.022$ (shown as a gray line) was predicted.

Chapter 4

Conclusion and perspectives

In this part, we have developed and studied several aspects of connectivity in a long-range correlated percolation model on a toroidal lattice. We summarize the most important results:

(i) We have developed a complete protocol for constructing long-range correlated Gaussian surfaces, using doubly-periodic (toroidal) boundary conditions. These surfaces can be associated to a long-range correlated percolation model by producing an excursion set at a precise critical level. This level was found by two independent methods: by searching for the appearance of a wrapping cluster and by comparing the Binder cumulants of the clusters. The main quantities that we use to characterize the universal properties of the percolating excursion sets are the correlation length exponent, ν and the fractal dimension D_f. We find that our measured values are consistent with the state-of-the-art in recent works. Moreover, we have included a numerical code to classify and extract statistics from the clusters in our surfaces. This code is included as an appendix.

(ii) We have investigated the universal finite-size corrections to the two-point connectivity function, which are a product of the boundary conditions. We found that these corrections can be extracted by properly setting up the lattice geometry and the orientation of the radius vector between points. More precisely, we found that the leading corrections are given by a power law of universal exponent $2 - 1/\nu$, and that an important subleading correction of exponent 2 emerges when we construct the lattice with a rectangular size. In addition, we showed that the coefficient of the subleading correction depends on the orientation of the radius vector. These aspects are profoundly related to the conformal symmetry of the clusters. Moreover, we have found excellent agreement between our correlated percolation model and the analytical results

of [15]. We finished by commenting on the three-point connectivity function for our model.

With the model presented in this thesis, one can explore many different points in the parameter space of the Hurst exponent. Some of them have been related to the phenomena of turbulence [31], while others have attracted interest because of their relationship with random wavefunctions [32]. In both cases, one would have to adjust the model to accomodate different kernels and then examine the scaling at the precise value of H. This would further serve as evidence of the specific universality class and additionally of conformal invariance.

The observable proposed here —the two-point connectivity function— is both quite natural to the statistics of clusters and has also been studied by Conformal Field Theory methods. Other observables like the three-point function can also be explored and an description of the mechanism by which this function may factorize into two-point functions is at reach.

From the numerical perspective, our algorithms generate most of the relevant behavior reported in this thesis even for modest sizes and runtimes. Considering that it was written on Python, one could study more intensively the scaling behavior of plateaus and coefficients of the finite-size corrections after translating to a language like C. One could further modify it by devising a method to include correlations in a Monte Carlo approach (which would open the way for fast algorithms [21]). We note however that the Hoshen-Kopelman scheme allows already the introduction of more statistical quantities for the clusters. In fact, we only included cluster detection in the Appendix, but both cluster masses and different boundary conditions can be easily implemented. This is because the principle behind the algorithm is to manage equivalence classes within the clusters rather than exploiting memory resources. Thus, even the connectivity observable is in principle adaptable to this scheme. In addition, different lattice configurations (e.g. triangular) are a simple yet interesting modification, which can provide alternatives to the convergence of other correction terms of p_{12}. This would not increase the complexity of the code Other types of percolation networks can be studied based on the work presented here, as well as other statistical lattice systems. It is our hope that the work presented in this thesis serves to aid and inspire future results into this line of research.

Chapter 5

Appendix

5.1 Generating correlated surfaces

```python
import numpy as np

def kernel(L,H):
    '''Computes the spectral density in momentum space'''
    ker = np.zeros((L,L))
    for k1 in range(-L//2, L//2):
        for k2 in range(-L//2, L//2):
            ker[k1,k2] = np.abs(2*np.cos(2*np.pi*k1/L)+2*np.cos(2*np.pi*k2/L)-4))
    ker[0,0]=1
    return 1/ker**(H+1)


def gaussian_field(L,H,cov_kernel = kernel(L,H)):
    '''Builds a correlated gaussian field on a surface LxL'''

    # FFT of gaussian noise:
    noise_real = np.random.normal(0, 1, size = (L, L))
    noise_fourier = np.fft.fft2(noise_real)

    # Add correlations by Fourier Filtering Method:
    convolution = noise_fourier*np.sqrt(cov_kernel)

    # Take IFFT and exclude residual complex part
    correlated_noise = np.fft.ifft2(convolution).real

    # Return normalized field
    return correlated_noise * (L/np.sqrt(np.sum(cov_kernel)) )
```

Code 5.1 – Generating a Correlated Gaussian Field.

5.2 Detecting clusters with the Hoshen-Kopelman algorithm.

```python
import numpy as np

```

```
# Define UNION and FIND functions:
################################## UNION-FIND ########################################
def find(x, labels):
    '''
    Finds the equivalence class of an element x in an array
    '''
    y = x
    # first follow the tree assigned to y to see its equivalence class (seed)
    while labels[y] != y:
        y = labels[y]
    # assign the label of y to all the tree (improves speed).
    while labels[x] != x:
        z = labels[x] # store original pointer
        labels[x] = y # relabel pointer
        x = z # continue relabelling with original pointer
    return y

def union(x, y, labels):
    '''
    Make the seed of x equal to that of y and returns
    said class
    '''
    target = find(y, labels)
    labels[find(x, labels)] = target
    return target

def new_seed(labels):
    '''
    Creates a new equivalence class
    '''
    labels[0] += 1 # add to slot that counts No. of classes
    labels[labels[0]] = labels[0] # condition that defines seed
    return labels[0] # returns updated equivalence class label

#Get clusters
################ Hoshen-Kopelman Algorithm ####################
def get_clusters(surface, open=False):
    '''
    Calculate clusters of the excursion set (Using the Hoshen-Kopelman Algorithm)
    '''
    M = surface.shape[0]
    N = surface.shape[1]
    labels = np.zeros(M*N, dtype=np.int32) # Assuming M*N equivalence classes

    for i in range(M):
        for j in range(N):
            if surface[i][j]:  #if active site
                up = (i>0)*surface[i-1][j] # upper boundary
                left = (j>0)*surface[i][j-1] # left boundary
                #
                if up and left: surface[i][j] = union(up, left, labels)  #add to an equivalence
     class
                if (up and not left) or (not up and left): surface[i][j] = max(up, left)  #put the
      nonzero label
                if not up and not left: surface[i][j] = new_seed(labels)      #new cluster

    # Periodic Boundary Conditions:
    if not open:
        for k in range(N):
```

```
            if surface[0][k] and surface[M-1][k]:
                union(surface[0][k], surface[M-1][k], labels)
        for k in range(M):
            if surface[k][0] and surface[k][N-1]:
                union(surface[k][0], surface[k][N-1], labels)

    # Relabel matrix so that only seeds are shown:
    for i in range(M):
        for j in range(N):
            if surface[i][j]:
                surface[i][j] = find(surface[i][j],labels)

    return surface
```

Code 5.2 – Hoshen Kopelman algorithm for labelling clusters in a 2D lattice.

II Open XXZ Spin Chain and Boundary Modes at Zero Temperature

Chapter 6

Introduction

In this second part, we will study a different model: the open Heisenberg quantum spin chain with longitudinal boundary fields. The Hamiltonian of this model for a chain of length L is given by

$$\mathbf{H}_{\mathrm{XXZ}}^{(\mathrm{open})} = \sum_{j=1}^{L-1} \left\{ \sigma_j^x \sigma_{j+1}^x + \sigma_j^y \sigma_{j+1}^y + \Delta \left(\sigma_j^z \sigma_{j+1}^z - 1 \right) \right\} + h_- \sigma_1^z + h_+ \sigma_L^z, \tag{6.1}$$

in which σ_n^α, $\alpha \in \{x, y, z\}$, are quantum spin operators (represented as Pauli matrices) acting on a local site n of the chain, Δ represents an anisotropy of the coupling constant along the z-direction, and h_-, h_+ are boundary magnetic fields, i.e., fields localized respectively on the first and last sites on the chain. This model is often called the *XXZ model*, to distinguish it from its isotropic ($\Delta = 1$) version which is called *XXX model*, or its completely anisotropic version (i.e., with different coupling constants along x, y and z) which is called *XYZ model*.

The origin of this model goes back to Heisenberg who proposed it as a model of magnetism [33]. Historically, the Heisenberg spin chain is, in its periodic and isotropic version, the first model to have been solved by a method which is nowadays known as *Bethe Ansatz*: in its pioneering paper [34], H. Bethe managed to exactly characterize the Hamiltonian eigenvalues and eigenfunctions by postulating that the latter could be represented as a simple superposition of plane waves. His *Ansatz* (see [35] for a review) was then successively applied to a variety of other one-dimensional quantum models, which include the anisotropic XXZ version of the spin chain [36], with periodic boundary conditions. Since then, this model has been widely studied. Let us in particular mention the works of Hulthen [37], Walker [38], and Yang and Yang [39–41] who performed a precise study of the ground state of the periodic model for $\Delta > -1$, as well as the works of Takahashi [42] and Gaudin [43] who studied the thermodynamics of the model following the approach developed

in [44].

It has also been realized that Bethe's method was not limited to the study of one-dimensional quantum models, but could also be used to compute to the partition function of some two-dimensional models of statistical physics [45–47], and that in fact there exists a deep connexion between these solvable classical two-dimensional models and one-dimensional quantum models such as the Heisenberg spin chain [48, 49]: in particular, the Hamiltonian of the XXZ spin chain can be obtained as the logarithmic derivative of the transfer matrix of the corresponding two-dimensional model of statistical physics, the so-called *six-vertex model*. This connexion, together with the impressive series of works of Baxter (see [50] for a review), helped to understand Bethe's solution in a more algebraic framework with the development, in the late seventies, of the *Quantum Inverse Scattering Method* (QISM) [51–54]. QISM appears as a quantum version of the *Classical Inverse Scattering Method* [55] and its developments in classical integrability [56, 57]. Models that can be formulated within the QISM framework are then naturally called *quantum integrable model*. The Heisenberg spin chain is nowadays considered as an archetype of such quantum integrable models. The explicit construction of the eigenstates of the periodic model can be done within QISM by the *Algebraic Bethe Ansatz* (ABA) [58], which can be seen as the algebraic version of Bethe's method. In the next chapter, we briefly recall for completeness the ABA solution of the periodic XXZ spin chain.

This algebraic framework, which can also be understood in terms of representation theory of *Quantum Groups* [59–61], appeared to be a very convenient framework for the computation of more complicated physical quantities, such as *correlation functions*. The first explicit results concerning correlation functions of the Heisenberg spin chain were obtained directly in the infinite volume limit, by considering the full (non-abelian) algebra of symmetry of the model in this limit [62, 63]: the correlation functions at zero temperature, or more precisely their elementary building blocks, were represented in the form of multiple integrals. These results were recovered later on by the consideration of the finite size (periodic) model in the ABA framework [64]. The advantage of the ABA approach is that it also provides very convenient determinant representations for more elementary quantities, the finite volume *form factors* (i.e., the matrix elements of local operators in the basis given by the transfer matrix eigenstates) [65]. Since each correlation function can be expressed as a sum over the corresponding form factors, these determinant representations for the form factors proved to be very useful for the derivation of the long-distance asymptotic behaviour for the correlation functions, either numerically [66, 67], or analytically [68–74]. Temperature correlation functions can also be computed [75–79], in particular by means of the *Quantum Transfer Matrix* (QTM) approach [80–83].

All these results concern essentially the Heisenberg spin chain with periodic boundary conditions, which appears to be the simplest one for the point of view of its exact resolution by Bethe Ansatz. In this thesis, we are however interested in the open version (6.1) of this model. The latter is still integrable [84], and the Hamiltonian (6.1) can be diagonalized in the framework of the representation theory of the reflection algebra [85], by means of the boundary version of the algebraic Bethe ansatz introduced by Sklyanin in [86].

There are important aspects that differentiate the open-boundary case to its periodic counterpart. The parameters acting at the first and last site (representing a magnetic field at the boundaries of the spin chain) generate a more elaborate phase diagram and, as we will see, allow the existence of *boundary modes*. These have been actively studied in the context of the *Kitaev chain* (related to the transverse-field XY chain via a Jordan-Wigner transformation), which presents localized *Majorana Fermions* [87] at the edges of the system, thus forming degenerate states that combine both boundary modes. More recently, in [88], it was shown that the gapped XYZ chain contains so-called *Strong Zero Modes*, which are operators defined at the edges of the chain and which commute with the Hamiltonian up to finite-size correction operators whose expectation values vanish exponentially with the system size. These strong zero modes act on a state in one sector of the discrete symmetry and give a different-sector eigenstate of the Hamiltonian with the same energy, up to $\mathrm{O}(L^{-\infty})$ corrections. These quasi-degeneracies are remarkably a feature not limited to the ground state but to a family of states in the entire spectrum.

In this thesis, we will be interested in studying some of the signatures of such boundary modes. In particular, an interesting quantity to calculate is the spin autocorrelation at the edge of the open-boundary XXZ chain. The presence of boundary modes and of a strong zero mode should have consequences in the evolution of the σ_1^z spin operator at any temperature T:

$$\lim_{t\to\infty}\lim_{L\to\infty}\langle\sigma_1^z(t)\sigma_1^z\rangle_T^c \neq 0 \tag{6.2}$$

with $\langle\mathcal{O}_1\mathcal{O}_2\rangle_T^c = \langle\mathcal{O}_1\mathcal{O}_2\rangle_T - \langle\mathcal{O}_1\rangle\langle\mathcal{O}_2\rangle_T$ the connected two-point correlation function and $\langle\mathcal{O}\rangle_T = \frac{\mathsf{Tr}[e^{-\beta H}\mathcal{O}]}{\mathsf{Tr}[e^{-\beta H}]}$ the thermal expectation value. Even if we perturb the model away from the integrable point, the coherence time should remain long –as was shown in [89–91] –, so this quantity is of physical interest because of its long-living plateau at intermediate times.

As a first step to investigate this question, we will take advantage of the framework of the QISM to obtain an exact and explicit expression of the autocorrelation function at zero temperature, at the thermodynamic and large-time limit. Indeed,

the integrable structure of the model allows us to explain the emergence of the quasi-degeneracy of the ground state and the range of values in the system's parameters for which this phenomenon is possible.

The scheme is the following: in Chapter 7, we review the Algebraic Bethe Ansatz solution of the Heisenberg Spin Chain, first in the periodic case and then with the corresponding modifications in the open-boundary case. In Chapter 8 we describe in detail the structure of the ground state of the open-boundary XXZ model, and we schematise the different regions that emerge according to the values of the boundary fields. We characterize in particular the role played by some isolated complex roots (the *boundary roots*) among the solutions of the corresponding Bethe equations. Finally, in Chapter 9, we perform the analytic calculation of two edge quantities: the boundary magnetization —and we show that, interestingly, this quantity depends on *both* boundary fields, even in the thermodynamic (semi-infinite chain) limit— and the zero-temperature autocorrelation function itself. We conclude with a discussion of the results and of the open questions which arise.

Chapter 7

The Heisenberg Spin Chain in the Quantum Inverse Scattering Method framework

In the framework of the QISM, we first briefly review the solution periodic chain by algebraic Bethe ansatz, and give a few indications about the computation its correlation functions. Then, we review the solution of the open-boundary chain, which requires a modification of the Bethe Ansatz —the *boundary Bethe ansatz*.

7.1 A brief review of the periodic case

Let us first consider the periodic XXZ spin-1/2. Heisenberg chain of L sites. Its Hamiltonian is given by:

$$\mathbf{H}_{\mathrm{XXZ}}^{(\mathrm{periodic})} = \sum_{j=1}^{L} \left\{ \sigma_j^x \sigma_{j+1}^x + \sigma_j^y \sigma_{j+1}^y + \Delta \sigma_j^z \sigma_{j+1}^z \right\}, \tag{7.1}$$

where $\sigma_j^{x,y,z}$ denote the local spin-1/2 operators (Pauli matrices) at site j. We impose here the following periodic boundary conditions: $\sigma_{L+1}^{\alpha} = \sigma_1^{\alpha}$. The total quantum space of the chain is then $\mathcal{H} = \bigotimes_{j=1}^{L} \mathcal{H}_j$, each local quantum space $\mathcal{H}_j$ being isomorphic to $\mathbb{C}^2$. Also $\Delta \in \mathbb{R}$ determines the anisotropy of the coupling constant along the z-direction.

7.1.1 Diagonalization by ABA

In the framework of the Quantum Inverse Scattering Method, each quantum integrable model defined on a one-dimensional lattice is characterized by a *quantum Lax operator* (or quantum L-operator) $L_n(\lambda)$ associated to a given site n of the model and which is a matrix of local operators at this site. Hence, it can be considered as

an operator acting on the tensor product $V_a \otimes \mathcal{H}_n$ of an auxiliary space V_a (the matrix space) and the local quantum space $\mathcal{H}_n$ of the model at site n. This L-operator depends in addition on a complex parameter λ which is called *spectral parameter*. The commutation relations between the local operators at a given site n of the model can then be rewritten as the following quadratic relation on the L-operators:

$$R(\lambda-\mu)\,(L_n(\lambda)\otimes \mathrm{Id})\,(\mathrm{Id}\otimes L_n(\mu)) = (\mathrm{Id}\otimes L_n(\mu))\,(L_n(\lambda)\otimes \mathrm{Id})\,R(\lambda-\mu), \quad (7.2)$$

which can be conveniently rewritten as

$$R_{ab}(\lambda-\mu)\,L_{an}(\lambda)\,L_{bn}(\mu) = L_{bn}(\mu)\,L_{an}(\lambda)\,R_{ab}(\lambda-\mu), \quad (7.3)$$

Equation (7.3) should be understood as a relation on $V_a \otimes V_b \otimes \mathcal{H}_n$, where V_a and V_b are two copies of the auxiliary space, and the indices label on which space of the tensor product the corresponding operators act. The operator $R(\lambda) \equiv R_{ab}(\lambda) \in \mathrm{End}(V_a \otimes V_b)$ is the so-called *R-matrix* of the model, which satisfies the *Yang-Baxter equation*:

$$\mathrm{R}_{ab}(\lambda-\mu)\,\mathrm{R}_{ac}(\lambda)\,\mathrm{R}_{bc}(\mu) = \mathrm{R}_{bc}(\mu)\,\mathrm{R}_{ac}(\lambda)\,\mathrm{R}_{ab}(\lambda-\mu) \quad (7.4)$$

on three copies on the auxiliary space $V_a \otimes V_b \otimes V_c$. The advantage of writing commutation of local operators in the form (7.3) is that they can be easily transposed at the global level, by defining the *monodromy matrix* as the following product of local operators along the chain:

$$\mathrm{T}(\lambda) \equiv \mathrm{T}_a(\lambda) \equiv \mathrm{T}_{a,1\ldots L}(\lambda) = L_{aL}(\lambda)\,L_{aL-1}(\lambda)\ldots L_{a1}(\lambda). \quad (7.5)$$

which satisfies the analog of (7.3):

$$\mathrm{R}_{ab}(\lambda-\mu)\,\mathrm{T}_a(\lambda)\,\mathrm{T}_b(\mu) = \mathrm{T}_b(\mu)\,\mathrm{T}_a(\lambda)\,\mathrm{R}_{ab}(\lambda-\mu). \quad (7.6)$$

The monodromy matrix is an operator on $V_a \otimes \mathcal{H}$, where $\mathcal{H} = \bigotimes_{j=1}^{L} \mathcal{H}_j$, i.e., it is a matrix whose entries are quantum global operators of the model. The relation (7.6) hence provides commutation relations for these operator entries of the mododromy matrix. The algebra defined by these commutation relations is often called the *Yang-Baxter algebra*. The idea of QISM is then to use the operators entries of the monodromy matrix, satisfying the Yang-Baxter commutation relations, so as to

1. Define a family of operators commuting between themselves and with the Hamiltonian;
2. Construct their common eigenstates.

In the case of the XXZ model (7.1), the R-matrix is a numerical 4×4 matrix

acting on $\mathbb{C}^2 \otimes \mathbb{C}^2$ (the auxiliary space is of dimension 2) which is the *trigonometric* solution of (7.4):

$$\mathrm{R}(\lambda) = \begin{pmatrix} \sin(\lambda - i\zeta) & 0 & 0 & 0 \\ 0 & \sin(\lambda) & \sin(-i\zeta) & 0 \\ 0 & \sin(-i\zeta) & \sin(\lambda) & 0 \\ 0 & 0 & 0 & \sin(\lambda - i\zeta) \end{pmatrix}. \tag{7.7}$$

The parameter $\zeta \in \mathbb{C}$ is here related to the anisotropy parameter Δ of the Hamiltonian by $\Delta = \cosh \zeta$. The Heisenberg chain of spin $1/2$ is a fundamental model, in the sense that the dimension of the auxiliary space coincides with the dimension of the local quantum space at a given site of the lattice, and that the L-operator $L_{an}(\lambda)$ coincides with the R-matrix $\mathrm{R}_{an}(\lambda - w_n)$ in which the second space is identified with the local quantum space at site n, and where w_n is an arbitrary complex parameter (called *inhomogeneity parameter* at site n): (7.3) is then automatically satisfied from (7.4). The *monodromy matrix* is then defined as

$$\mathrm{T}_a(\lambda) = \mathrm{R}_{aL}(\lambda - \omega_L)\, \mathrm{R}_{aL-1}(\lambda - \omega_{L-1}) \cdots \mathrm{R}_{a1}(\lambda - \omega_1) = \begin{pmatrix} \mathrm{A}(\lambda) & \mathrm{B}(\lambda) \\ \mathrm{C}(\lambda) & \mathrm{D}(\lambda) \end{pmatrix}_a. \tag{7.8}$$

With respect to the auxiliary space, the monodromy matrix is a 2×2 matrix with entries $\mathrm{A}(\lambda), \mathrm{B}(\lambda), \mathrm{C}(\lambda), \mathrm{D}(\lambda)$ which are operators acting on the full quantum space $\mathcal{H}$ of the chain. These operators obey the commutation relations derived from (7.6).

Let us define the *transfer matrix* as the trace on the auxiliary space of the monodromy matrix:

$$\mathbf{t}(\lambda) = \mathsf{Tr}_a\Big(\mathrm{T}_a(\lambda)\Big). \tag{7.9}$$

It is easy to see from (7.6) that these transfer matrices commute between themselves for different values of the spectral parameter:

$$\Big[\mathbf{t}(\mu), \mathbf{t}(\lambda)\Big] = 0.$$

Moreover, one can show that, in the limit where all inhomogeneity parameters tend to the same value $-i\zeta/2$, the transfer matrix is closely related to the Hamiltonian of the XXZ chain by:

$$\mathbf{H}_{\mathrm{XXZ}}^{(\mathrm{periodic})} = -2i \sin\zeta \frac{\partial}{\partial\lambda} \log \mathbf{t}(\lambda)\Big|_{\lambda=-i\zeta/2}, \tag{7.10}$$

and in particular it verifies the following commutation relation:

$$\left[\mathbf{H}_{\mathrm{XXZ}}^{(\mathrm{periodic})}, \mathbf{t}(\lambda)\right] = 0,$$

thus defining a set of commuting operators that are conserved. The eigenstates of $\mathbf{t}(\lambda)$ then correspond, in the homogeneous limit, to the eigenstates of $\mathbf{H}_{\mathrm{XXZ}}{}^{(\mathrm{periodic})}$.

The eigenstates of the transfer matrix can be constructed in the framework of the *Algebraic Bethe Ansatz* (ABA). The idea of this ansatz is to find a *reference state* $|\mathbf{0}\rangle$ such that

$$\begin{aligned} \mathrm{A}(\lambda)|\mathbf{0}\rangle &= \mathrm{a}(\lambda)|\mathbf{0}\rangle, \\ \mathrm{D}(\lambda)|\mathbf{0}\rangle &= \mathrm{d}(\lambda)|\mathbf{0}\rangle, \\ \mathrm{C}(\lambda)|\mathbf{0}\rangle &= 0, \end{aligned} \tag{7.11}$$

so that $B(\lambda)$ can be used as a creation operator on this state to generate the space of state ($C(\lambda)$ then acts as an annihilation operator). In particular, the eigenstates of the transfer matrix are looked for in the form of *Bethe states*, i.e., of states of the form:

$$|\boldsymbol{\lambda}\rangle = \prod_{j=1}^{N} \mathrm{B}(\lambda_j)|\mathbf{0}\rangle, \tag{7.12}$$

for a set $\boldsymbol{\lambda} = \{\lambda_1 \cdots, \lambda_N\}$ of spectral parameters. In the case of the XXZ chain, it is easy to see that such a state $|\mathbf{0}\rangle$ (7.11) exists and is given by the fully ferromagnetic state will all spins pointing up. The eigenvalues $\mathrm{a}(\lambda), \mathrm{d}(\lambda)$ will then be:

$$\mathrm{a}(\lambda) = \prod_{j=1}^{N} \sin(\lambda - \omega_j - i\zeta), \quad \mathrm{d}(\lambda) = \prod_{j=1}^{N} \sin(\lambda - \omega_j). \tag{7.13}$$

By using the commutation relations issued from (7.6), one can act with the transfer matrix on the Bethe state $|\boldsymbol{\lambda}\rangle$ and obtain the conditions that ensure it is an eigenstate: $\mathbf{t}(\mu)|\boldsymbol{\lambda}\rangle = \widehat{t}(\mu|\boldsymbol{\lambda})|\boldsymbol{\lambda}\rangle$ for any value of μ. These conditions take the form of a set of equations known as *Bethe Equations*:

$$\mathrm{a}(\lambda_j) \prod_{i=1}^{N} \sin(\lambda_k - \lambda_j - i\zeta) + \mathrm{d}(\lambda_j) \prod_{i=1}^{N} \sin(\lambda_k - \lambda_j + i\zeta) = 0, \quad j = 1, \ldots, N. \tag{7.14}$$

The corresponding eigenvalue of $\mathbf{t}(\mu)$ is then

$$\widehat{t}(\mu|\boldsymbol{\lambda}) = \mathrm{a}(\mu) \prod_{k=1}^{N} \frac{\sin(\lambda_k - \mu - i\zeta)}{\sin(\lambda_k - \mu)} + \mathrm{d}(\mu) \prod_{k=1}^{N} \frac{\sin(\mu - \lambda_k - i\zeta)}{\sin(\mu - \lambda_k)}. \tag{7.15}$$

The dual Bethe states can be constructed in a similar way, by multiple action on the dual reference state $\langle \mathbf{0}|$ of the operator $\mathrm{C}(\lambda)$:

$$\langle \boldsymbol{\lambda}| = \langle \mathbf{0}| \prod_{j=1}^{N} \mathrm{C}(\lambda_j), \tag{7.16}$$

and one obtains similarly that a state of the form (7.16) is an eigenstateof the transfer matrix if the Bethe equations (7.14), and that the corresponding eigenvalue is (7.15). In the homogeneous limit, the eigenvalue (7.15) can be plugged into (7.10) giving the energy of a Bethe state:

$$E^{(\mathrm{periodic})}(\boldsymbol{\lambda}) = \sum_{j=1}^{N} \varepsilon_0^{(\mathrm{periodic})}(\lambda_j), \tag{7.17}$$

where $\epsilon_0^{(\mathrm{periodic})}(\lambda)$ is the *bare energy* given by $\varepsilon_0^{(\mathrm{periodic})}(\lambda) = -\frac{2\sinh^2\zeta}{\sin(\lambda+i\zeta/2)\sin(\lambda-i\zeta/2)}$.

7.1.2 Description of the spectrum

Ground State

In the ferromagnetic region, $\Delta < -1$, the ground state is particularly simple: it is doubly degenerated and given by the two states where all spins are aligned, i.e., by $|\mathbf{0}\rangle$ with all spins pointing up, or by $|\bar{\mathbf{0}}\rangle$ with all spins pointing down.

The ground state for $\Delta > -1$ has been characterized in [39, 40], by studying the minimal-energy solution of the Bethe equations written in logarithmic form:

$$Lp_0(\lambda_j) + \sum_{j=1}^{N} \theta(\lambda_j - \lambda_k) = 2\pi n_j \tag{7.18}$$

for $p_0(\lambda) = i\log\frac{\sinh(\lambda+i\zeta/2)}{\sinh(\lambda-i\zeta/2)}$ and $\theta(\lambda) = i\log\frac{\sin(i\zeta-\lambda)}{\sin(i\zeta+\lambda)}$. In (7.18), n_j are integers if N is odd and half-integers if N is even. To characterize the ground state in terms of Bethe roots, it is convenient to distinguish the notations between the domains $|\Delta| < 1$ and $\Delta > 1$, and to perform the change of variables:

$$\alpha_j = -i\lambda_j \qquad \text{for} \quad -1 < \Delta < 1, \tag{7.19}$$

$$\alpha_j = \lambda_j \qquad \text{for} \quad \Delta > 1. \tag{7.20}$$

We remark that our notation is in fact adapted to the study of the regime $\Delta > 1$, which is the regime we will consider more particularly in the next chapters. Then, in terms of these new notations, the ground state corresponds to a state, in the sector

$N = L/2$ of zero magnetization, where all Bethe roots α_j are real and are solutions to the logarithmic Bethe equations (7.18) with consecutive (half-)integers n_j:

$$n_j = -\frac{N+1}{2} + j, \qquad j = 1, 2, \ldots, N. \tag{7.21}$$

In the thermodynamic limit, the solutions are condensed in a symmetric interval $[-\Lambda, \Lambda]$, with $\Lambda = \pi/2$ for $\Delta > 1$ and $\Lambda = \infty$ for $|\Delta| < 1$ (see [92] for a rigorous proof of this condensation of Bethe roots for the ground state). This allows us to define the local density of (real) solutions:

$$\rho(\alpha_j) = \lim_{L\to\infty} \frac{1}{L(\alpha_{j+1} - \alpha_j)}, \tag{7.22}$$

Equation (7.18) then becomes a linear integral equation for the density ρ:

$$\rho(\alpha) + \int_{-\Lambda}^{\Lambda} K(\alpha - \beta)\rho(\beta)\beta = \frac{p_0'(\alpha)}{2\pi}, \tag{7.23}$$

with $K = -\theta'/2\pi$. This equation can be solved explicitly by using the Fourier transform. we obtain:

$$\begin{aligned} \rho(\alpha) &= \frac{1}{2\tilde{\zeta}\cosh(\pi\alpha/\tilde{\zeta})} \quad , \quad \text{for } |\Delta| < 1, \text{ with } \tilde{\zeta} = i\zeta, \\ \rho(\alpha) &= \frac{1}{2\pi}\sum_{k\in\mathbb{Z}} \frac{e^{2ik\alpha}}{\cosh(k\zeta)} \quad , \quad \text{for } \Delta > 1. \end{aligned} \tag{7.24}$$

It can be shown that the spectrum is gapless when $-1 < \Delta < 1$ and is gapped when $\Delta > 1$. In the gapped regime $\Delta > 1$, there is another real set of solutions giving a state which becomes quasi-degenerate with the ground state in the thermodynamic limit $L \to \infty$, having the same energy up to exponentially small corrections in L. It is given by a shift $n_j \to n_j - 1$ in the quantum numbers $\{n_j\}$ that describe the set of roots (7.18).

Excited states and String Hypothesis

As mentioned above, each eigenstate can be represented in terms of a set of Bethe roots. When L becomes large, while the ground state is described by a continuous real distribution of roots, the excited states can contain complex roots. These complex roots appear in pairs of conjugated roots $z, \bar{z}$ [93, 94]. Moreover, it is common to assume [34, 42, 43] that these complex roots always appear in so-called *strings*, which are ordered complexes of roots with common real part and whose complex parts are arranged in an equidistant fashion. This assumption comes from the fol-

lowing argument: when considering a complex root λ_j of the Bethe equations (7.14), for which one can rewrite the equation in the homogeneous limit as

$$\left(\frac{\sinh(\lambda_j + i\zeta/2)}{\sinh(\lambda_j - i\zeta/2)}\right)^L = \prod_{\substack{n=1 \\ n\neq j}}^{N} \frac{\sinh(\lambda_j - \lambda_n + i\zeta)}{\sinh(\lambda_j - \lambda_n - i\zeta)}, \tag{7.25}$$

one sees that the first member of the equation tends exponentially fast with L to zero or ∞; for $N \ll L$, this imposes that λ_j coincide with a zero or a pole of the second member up to exponentially small corrections in L, i.e., that there exists another root λ_k such that $\lambda_j = \lambda_k \pm i\zeta$. Of course, this argument is not valid when N is of order L, and it has been shown that the string hypothesis does *not* give a complete description of the excited spectrum [95–97]. Assuming the string hypothesis allows nevertheless the description of many aspects of spin chains at finite-temperature [42, 43, 98], being the basis of what is known as the *Thermodynamic Bethe Ansatz*.

The analysis of the Bethe equations without assuming the string hypothesis has been performed in [93]. The authors of [93] study separately the Bethe equations for real and complex solutions. Since the real solutions are described in terms of an integral equation, one can solve it for *arbitrary complex* roots and then use this solution in the remaining equations for the complex roots. This produces a closed system, using in particular the conservation of spin number. The result is a set of equations (different according to the regime of Δ) similar in structure to the Bethe equations but this time describing excited states. There also emerges a picture of "close" and "wide" complex roots, as well as the strings mentioned above.

Finally, more recently, there have been many developments using the *Quantum Transfer Matrix* approach (see e.g. [99] for an introduction to the method) where finite-temperature expressions can be obtained by using a Trotter formula for the thermal part of expectation values, $e^{\mathbf{H}\beta}$, and then expressing it in terms of a (quantum) transfer matrix (QTM) of the integrable model, which assumes an extra auxiliary space for the thermal evolution. The eigenvalues of the QTM are then found using the ABA in terms of a set of parameters that are solutions of the Bethe equations.

7.1.3 Form Factors and Correlation Functions

The calculation of correlation functions is essential for the study of time-asymptotic and large scale behavior of quantum lattice models. Although the characterization of the spectrum of the Heisenberg chain goes back to the work of Bethe in 1931, and the description of the ground state was achieved in the 1960's, the first explicit results concerning correlation functions were obtained only in the 1990's. We briefly

recall here the strategy to compute such correlation functions using the ABA solution presented above.

Let us for instance consider a two-point correlation functions at zero temperature. It is given as the ground-state expectation value of the product of two local operators $\mathcal{O}$ and $\widetilde{\mathcal{O}}$ in two sites of the lattice:

$$\langle \mathrm{GS}|\mathcal{O}_p\widetilde{\mathcal{O}}_q|\mathrm{GS}\rangle \tag{7.26}$$

for $p, q \in \{1, \dots, L\}$. For the periodic XXZ chain, where there is translation invariance, one can restrict to the case $p = 1$, $q = m$. A computation of such quantities within ABA was made possible thanks to the solution of the quantum inverse problem [65, 100, 101], which consists in expressing local operators as a simple elements of the monodromy matrix dressed by a product of transfer matrices, and also by use of the *Slavnov formula* [102], which expresses the scalar product of two Bethe states, one on-shell $|\boldsymbol{\lambda}\rangle$ (i.e., for $\boldsymbol{\lambda}$ solution of the Bethe equations) and one off-shell $|\boldsymbol{\mu}\rangle$ (i.e., for arbitrary $\boldsymbol{\mu}$) in terms of a simple determinant.

In the case of the spin chain, local operators $\mathcal{O}_j$ and $\widetilde{\mathcal{O}}_j$ at some site j are local spin operators $\sigma_j^{+,-,z}$, or equivalently elementary matrices $E_j^{\epsilon_j,\epsilon'_j}$ at the position $j \in \{1, \dots, L\}$, with $\epsilon_j \in \{1, 2\}$ and $(E_j^{\epsilon_j,\epsilon'_j})_{\ell m} = \delta_{\ell,\epsilon_j}\delta_{m,\epsilon'_j}$. The solution of the quantum inverse problem for such elementary matrices is [65]:

$$E_j^{\epsilon_j,\epsilon'_j} = \left[\prod_{k=1}^{j-1} \mathbf{t}(\omega_k)\right] \mathrm{T}_{\epsilon'_j,\epsilon_j}(\omega_j) \left[\prod_{k=1}^{j} \mathbf{t}^{-1}(\omega_k)\right]. \tag{7.27}$$

This allows one to compute the action of one (or several) local operators on a Bethe state by using the commutation relations of the monodromy matrix elements given by (7.6). The result is in general express as a sum over off-shell Bethe states. One can then use Slavnov's formula [102] to compute the resulting scalar products:

$$\langle \mathbf{0}| \prod_{k=1} \mathrm{C}(\lambda_k) \prod_{j=1} \mathrm{B}(\mu_j)|\mathbf{0}\rangle = \frac{\mathsf{Det}\, \mathrm{H}(\boldsymbol{\mu}, \boldsymbol{\lambda})}{\prod_{\ell<n} \sin(\mu_n - \mu_\ell) \prod_{j<k} \sin(\lambda_k - \lambda_j)}, \tag{7.28}$$

where

$$\big[\mathrm{H}(\boldsymbol{\mu}, \boldsymbol{\lambda})\big]_{ab} = \frac{\sin\zeta}{\sin(\lambda_a - \mu_b)} \left\{ \mathrm{a}(\mu_b) \prod_{m\neq a} \sin(\lambda_m - \mu_b - i\zeta) - \mathrm{d}(\mu_b) \prod_{m\neq a} \sin(\lambda_m - \mu_b + i\zeta) \right\}, \tag{7.29}$$

for $\boldsymbol{\lambda}$ a solution of the Bethe equations and $\boldsymbol{\mu}$ an arbitrary set of parameters.

At this point, two strategies are possible:

(a) One computes the action of both operators on the ground state on the right

and then calculate the scalar product $\big(\langle \mathrm{GS}|\big) \cdot \big(\mathcal{O}_1 \widetilde{\mathcal{O}}_m |\mathrm{GS}\rangle\big)$. This strategy was first used in [64, 103], leading to multiple integral representations for the correlation functions in the thermodynamic limit.

(b) One can expand the correlation function in terms of a complete set of eigenstates of the Hamiltonian:

$$\langle \mathrm{GS}|\mathcal{O}_1 \widetilde{\mathcal{O}}_m|\mathrm{GS}\rangle = \sum_{\{|n\rangle\} \text{ eigenstates of } \mathbf{H}} \frac{\langle \mathrm{GS}|\mathcal{O}_1|n\rangle\langle n|\widetilde{\mathcal{O}}_m|\mathrm{GS}\rangle}{\langle n|n\rangle}. \tag{7.30}$$

This reduces the computation of the correlation functions to the calculation of much simpler quantities, the *form factors* $\langle \boldsymbol{\lambda}|\mathcal{O}|\boldsymbol{\mu}\rangle$. Compact and simple determinant representations for the finite size spin chain form factors were obtained in [65].

These two approaches were shown to be explicitly equivalent in [104] (see [105] in the dynamical case), in which a *master representation* for the two-point function was obtained, leading both to the expansions *(a)* and *(b)*.

It is possible to analytically derive the large distance asymptotic behavior ($m \to \infty$) of the two-point functions in the thermodynamic limit from their exact representations on the lattice. This was first done in [68] directly from the master representation. However, it was shown later (see [69–74, 106, 107]) that is was easier to start directly from the expansion (7.30), so that it is also possible to consider more general multiple-point correlation functions [73], or time-dependent correlation functions [74, 106]. Such results could also be extended to the study of the large-distance asymptotic behavior of correlation functions at non-zero temperature, in particular by means of the quantum transfer matrix approach [77, 79, 108]. Note that the expansion (7.30), together with the determinant representations for the form factors [65], were also used for the numerical study of the correlation functions [66, 67, 109, 110].

To conclude this section, let us also mention that there exist other approaches to the exact computation of the correlation functions of the XXZ chain, not based on the Bethe Ansatz. In particular, the pioneering approach of [62, 63, 111] was based on the identification of the non-abelian symmetries of the quantum spin chain in infinite volume, and on the use of some q-deformed versions of the *vertex operators* and *Knizhnik-Zamolodchikov equations*, two notions at the heart of the study of conformal field theories. This approach led to the first explicit representations, in the form of multiple integrals, for the correlations functions of the XXZ chain (or more precisely for their elementary building blocks), representations that were recovered later in [64] by means of ABA. One should also mention the more recent

approach developed in the series of papers [112–120], based on the identification of a hidden Grassmann structure in the XXZ model.

7.2 The Open Case

In this part of the thesis, as mentioned in the introduction, we are more particularly interested in the open spin chain with boundary longitudinal magnetic fields, with Hamiltonian (6.1). Our aim is to study some of the boundary effects due to the presence of the boundary magnetic fields.

7.2.1 Boundary Bethe Ansatz

The Hamiltonian (6.1) can still be diagonalized in the QISM framework, by means of a modified version of the ABA, originally proposed by Sklyanin in [86]. The strategy consists once again in building a monodromy matrix, leading on the one hand to a one-parameter family of commuting transfer matrices which also commute with the Hamiltonian, and used on the other hand to construct the space of states in the form of Bethe states, i.e., by multiple action of one of its entries on a well chosen reference state. This boundary monodromy matrix will be given in terms of the standard (bulk) monodromy matrix we introduced in the previous section, and of some numerical matrices which encode the boundary conditions, the so-called boundary K-matrices.

In the case of longitudinal boundary fields such as in (6.1), the two boundary K-matrices $K_-(\lambda)$ and $K_+(\lambda)$, which encode the boundary conditions of the model, are diagonal and take the following form:

$$K_-(\lambda) = K(\lambda;\xi_-), \qquad K_+(\lambda) = K(\lambda - i\zeta;\xi_+), \tag{7.31}$$

where the parameters $\xi_\pm$ are related to the boundary fields $h_\pm$ as

$$h_\pm = -\sinh\zeta\,\coth\xi_\pm, \tag{7.32}$$

and

$$K(u;\xi) = \begin{pmatrix} \sin(u + i\zeta/2 + i\xi) & 0 \\ 0 & \sin(i\xi - u - i\zeta/2) \end{pmatrix}. \tag{7.33}$$

The matrix (7.33) is a solution of the *reflection equation* [85], also called *Boundary*

Yang-Baxter Equation:

$$R_{12}(u-v)K_1(u)R_{12}(u+v)K_2(v) = K_2(v)R_{12}(u+v)K_1(u)R_{12}(u-v), \tag{7.34}$$

where R is the trigonometric R-matrix (7.7).

The *boundary monodromy matrix* $\mathcal{U}(\lambda)$ can then be constructed from the bulk monodromy matrix $T(\lambda)$ (7.8) and the boundary matrix $K_+(\lambda)$ as the following "double-row" monodromy matrix:

$$\mathcal{U}^t(\lambda) = T^t(\lambda)K_+^t(\lambda)\widehat{T}^t(\lambda) = \begin{pmatrix} \mathcal{A}(\lambda) & \mathcal{C}(\lambda) \\ \mathcal{B}(\lambda) & \mathcal{D}(\lambda) \end{pmatrix}, \tag{7.35}$$

where $T(\lambda)$ is given by (7.8) and $\widehat{T}(\lambda)$ is the following backwards propagating product of R-matrices:

$$\widehat{T}(\lambda) = R_{1a}(\lambda+\omega_1+i\zeta)R_{2a}(\lambda+\omega_2+i\zeta)\cdots R_{La}(\lambda+\omega_L+i\zeta) = (-1)^L\sigma_a^y T^t(-\lambda)\sigma_a^y. \tag{7.36}$$

The boundary monodromy matrix is also a 2×2 matrix with operator entries $\mathcal{A},\mathcal{B},\mathcal{C},\mathcal{D}$, that we denote by calligraphic letters so as to distinguish them from the entries of the *bulk* monodromy matrix (7.8). One can show that $\mathcal{U}^t(-\lambda)$ is also a solution of the boundary Yang-Baxter equation (7.34), which provides the commutation relations of the operators $\mathcal{A},\mathcal{B},\mathcal{C},\mathcal{D}$. One can then construct the boundary transfer matrix as

$$\mathcal{T}(\lambda) = \mathsf{Tr}_a\left\{K_+(\lambda)T(\lambda)K_-(\lambda)\widehat{T}(\lambda)\right\} = \mathsf{Tr}_a\left\{K_-(\lambda)\mathcal{U}(\lambda)\right\}, \tag{7.37}$$

which forms a one-parameter family of commuting operators.

With diagonal boundary K-matrices as in (7.31)–(7.33), the Algebraic Bethe Ansatz can still be applied to construct the space of states, in the sense that $|\mathbf{0}\rangle$ is still a reference state for the boundary monodromy matrix (7.35). The *boundary Bethe states* are then constructed similarly as in the bulk case, by multiple action of the operator entries $\mathcal{B},\mathcal{C}$ of the "double-row" monodromy matrix on the reference state $|\mathbf{0}\rangle$ or on the dual reference state $\langle\mathbf{0}|$:

$$\begin{aligned} |\boldsymbol{\lambda}\rangle &= \prod_{j=1}^{N}\mathcal{B}(\lambda_j)|\mathbf{0}\rangle, \\ \langle\boldsymbol{\lambda}| &= \langle\mathbf{0}|\prod_{j=1}^{N}\mathcal{C}(\lambda_j). \end{aligned} \tag{7.38}$$

Acting with the transfer matrix (7.37) on (7.38) by means of the commutation relations given by the boundary Yang-Baxter equation, one obtains that the states (7.38) are common eigenstates to the boundary transfer matrix (7.37) provided the set of parameters $\boldsymbol{\lambda} = \{\lambda_1, \dots, \lambda_N\}$ obey the following system of Bethe equations:

$$\mathtt{A}(\lambda_j) \prod_{k=1}^{N} \mathfrak{s}(\lambda_j + i\zeta) + \mathtt{A}(-\lambda_j) \prod_{k=1}^{N} \mathfrak{s}(\lambda_j - i\zeta) = 0, \quad j = 1, \dots, N, \tag{7.39}$$

where we have defined for compactness:

$$\begin{aligned} \mathfrak{s}(\lambda, \mu) &= \sin(\lambda + \mu) \sin(\lambda - \mu) = \sin^2 \lambda - \sin^2 \mu, \\ \mathtt{A}(\mu) &= \frac{\sin(2\mu - i\zeta)}{\sin 2\mu} a(\mu) d(-\mu) \sin(\mu + i\xi_+ + i\zeta/2) \sin(\mu + i\xi_- + i\zeta/2), \end{aligned} \tag{7.40}$$

in terms of (7.13). In that case the Bethe states (7.38) are called *on-shell*, and the corresponding transfer matrix eigenvalue is:

$$\tau(\mu|\boldsymbol{\lambda}) = (-1)^L \left[\mathtt{A}(\mu) \prod_{k=1}^{N} \frac{\mathfrak{s}(\mu + i\zeta, \lambda_k)}{\mathfrak{s}(\mu, \lambda_k)} + \mathtt{A}(-\mu) \prod_{k=1}^{N} \frac{\mathfrak{s}(\mu - i\zeta, \lambda_k)}{\mathfrak{s}(\mu, \lambda_k)} \right], \tag{7.41}$$

If instead the set of parameters $\boldsymbol{\lambda} = \{\lambda_1, \dots, \lambda_N\}$ is arbitrary, i.e., does not satisfies the Bethe equations (7.39), the corresponding Bethe states (7.38) are called *off-shell*.

When we take the homogeneous limit $\omega_j \to -i\zeta/2$, $j \in \{1 \dots, L\}$, the transfer matrix can be used to obtain the open-boundary XXZ Hamiltonian (6.1):

$$\mathbf{H}_{\mathrm{XXZ}}^{(\mathrm{open})} = \frac{-i \sinh \zeta}{\mathcal{T}(\lambda)} \frac{\mathrm{d}}{\mathrm{d}\lambda} \mathcal{T}(\lambda) \Big|_{\lambda = -i\zeta/2} + \frac{1}{\cosh \zeta} - 2L \cosh \zeta, \tag{7.42}$$

and the eigenstates of the transfer matrix become also eigenstates of the Hamiltonian with energy:

$$E(\boldsymbol{\lambda}) = h_+ + h_- + \sum_{j=1}^{N} \varepsilon_0(\lambda_j), \tag{7.43}$$

where the *bare energy* $\varepsilon_0(\lambda)$ is defined as:

$$\varepsilon_0(\lambda) = -\frac{2 \sinh^2 \zeta}{\mathfrak{s}(\lambda, i\zeta/2)}. \tag{7.44}$$

This energy spectrum has been studied in [121, 122] based on the solutions of the Bethe equations (7.39). As in the periodic case, the real roots describing the ground state are described, in the thermodynamic limit, by a density function $\rho(\lambda)$ which

happens to be the same, up to a factor 2, as in the periodic case. An important difference with respect to the periodic case is that the set of Bethe roots for the ground state may also contain some isolated complex root (i.e., with no conjugated partner). The domain of existence and contribution to the ground state of this isolated complex root according to the values of h_+ and h_- is however not so clear from [121, 122]. We will discuss this point in details in the next chapter for the regime $\Delta > 1$.

To conclude this section, let us mention that it is possible to consider spin chains with more general boundary fields, i.e., not only along the z-direction as in (6.1), but with components along all three directions x, y, z. An XXZ chain with such boundary fields is still integrable in the QISM framework, but the corresponding boundary K-matrices solution of the boundary Yang-Baxter equation (7.34) are in that case no longer diagonal, and the state $|\mathbf{0}\rangle$ can no longer be used as a reference state. ABA can therefore not be used directly to construct the common eigenstates of the transfer matrices. In that case, the model can be solved by means of the quantum version of the *Separation of Variables* (see [123, 124] for an explanation of the method in the case of the quasi-periodic Heisenberg spin chain, and [125–128] for more recent results about the solution of the open spin chain by this method). Some attempts have also been made by modifying the Bethe Ansatz approach [129–133]. We will not discuss these more general —and complicated— cases which were not considered during this thesis.

7.2.2 Computation of correlation Functions: State of the Art and Problems

The problem of computing correlation functions is much more complicated in the open case than in the periodic case. In particular, determinant representations as those of the periodic case for the form factors do not exist in general. It is still possible to express the scalar product of an off-shell and an on-shell Bethe states of the form (7.38) as a generalized version of the Slavnov determinant (7.28) [134, 135] (see (9.11)), but a convenient expression of the local spin operators in terms of the boundary monodromy matrix elements dressed by a product of *boundary* transfer matrices is presently not known, except at the first (or last) site of the chain [136].

It was nevertheless possible, in [135, 137], to obtain multiple integral representations for the zero-temperature correlation functions in the thermodynamic limit (half-infinite chain), similar to those obtained in the bulk case in [64]. In fact, the formulas obtained in [135, 137] relied on a cumbersome use of the *bulk* inverse problem (7.27), and on the explicit connexion between boundary Bethe states (7.38) and bulk Bethe states (7.12). Note that such multiple integral representations where pre-

viously directly obtained by the q-vertex operator approach in the half-infinite chain in [138]. A convenient representation enabling ones to extract the explicit dependance on the distance from the boundary of these correlation functions is however still missing, even in the simplest case of a one-point function of a local operator at distance m from the boundary.

At the first (or last) site of the chain, however, the situation is different. Indeed, the solution of the quantum inverse problem proposed in [136] is in that case sufficient, together with the determinant representation for the scalar products, to obtain determinant representations for the form factors of local operators at site 1 which are very similar to the bulk ones. Hence, we are able to study their thermodynamic limit similarly as what has been done in [69, 70, 107, 139]. In particular, we are in position to compute and study the thermodynamic limit of the form factors which are relevant for the long-time limit of the boundary autocorrelation (6.2). This is the purpose of the next sections.

Chapter 8

The Ground State of the XXZ Chain with open boundaries

In this chapter, we study the ground state of the open XXZ chain for large L. We concentrate on the regime when $\Delta > 1$, in which we expect to find a configuration of boundary fields for which the spectrum is gapped and the ground state double degenerate in the thermodynamic limit. We will more generally discuss here the set of Bethe roots for the ground state, and the presence of a peculiar isolated complex root in this set — the so-called *boundary root* — according to the value of the two boundary fields h_+ and h_- and to the parity of the number of sites L of the chain. We also discuss the presence of an energy gap in the spectrum, and the possible degeneracy of the ground state.

From now on, we use the following parametrization:

$$\Delta = \cosh\zeta, \quad \zeta > 0, \tag{8.1}$$

$$h_\sigma = -\sinh\zeta\coth\xi_\sigma, \quad \xi_\sigma = -\tilde{\xi}_\sigma + i\delta_\sigma\frac{\pi}{2}, \tag{8.2}$$

where $\tilde{\xi}_\sigma \in \mathbb{R}$, and $\delta_\sigma = 1$ if $|h_\sigma| < \sinh\zeta$ and zero otherwise.

From the form of the Bethe equations for the open-boundary chain, eq. (7.39), which can be rewritten in the homogeneous limit as

$$\left(\frac{\sin(\lambda_j + i\zeta/2)}{\sin(\lambda_j - i\zeta/2)}\right)^{2L} = \left(\frac{\sin(\lambda_j + i[\zeta/2 + \xi_-])\sin(\lambda_j + i|\zeta/2 + \xi_+])}{\sin(\lambda_j - i[\zeta/2 + \xi_-])\sin(\lambda_j - i[\zeta/2 + \xi_+])}\right) \times \prod_{k\neq j}\frac{\sin(\lambda_j + \lambda_k + i\zeta)\sin(\lambda_j - \lambda_k + i\zeta)}{\sin(\lambda_j + \lambda_k - i\zeta)\sin(\lambda_j - \lambda_k - i\zeta)}, \tag{8.3}$$

one can see that there is π-periodicity and sign parity in the set $\boldsymbol{\lambda}$. Therefore, we

can, without loss of generality, restrict our analysis to roots in the following domain in the complex plane:

$$D_{\text{solutions}} = \left\{ \lambda \in \mathbb{C} \;\middle|\; 0 < \mathfrak{Re}(\lambda) < \pi/2 \quad \text{or} \quad \big(\mathfrak{Re}(\lambda) \in \{0, \pi/2\} \text{ and } \mathfrak{Im}(\lambda) < 0\big) \right\}. \tag{8.4}$$

The ground state of the open boundary XXZ chain in the regime $\Delta > 1$ was studied previously by [122]. It was argued in that paper that all the Bethe roots for the ground state (which we will label with $\boldsymbol{\alpha}$ as opposed to a general Bethe state $\boldsymbol{\lambda}$) are real, except for a possible isolated complex root that could arise due to the presence of the boundary factor in the Bethe equations. In the $L \to \infty$ limit, the real roots of the set $\boldsymbol{\alpha}$ form a dense distribution $\rho(\alpha)$ on the interval $(0, \pi/2)$, which can be extended by parity to $(-\pi/2, \pi/2)$. The distribution $\rho(\alpha)$ can be written as the solution to the following integral equation:

$$\rho(\alpha) + \int_{-\pi/2}^{\pi/2} K(\alpha - y)\rho(y)dy = \frac{p'(\alpha)}{\pi}, \tag{8.5}$$

where K and p' are given by $K(\lambda) = \frac{\sinh(2\zeta)}{2\pi \mathfrak{s}(\lambda, i\zeta)}$ and $p'(\lambda) = \frac{\sinh\zeta}{\mathfrak{s}(\lambda, i\zeta/2)}$. This integral equation can be solved in terms of a Fourier series, so that the density of real roots in the ground state reads:

$$\rho(\alpha) = \frac{1}{\pi} \sum_{k \in \mathbb{Z}} \frac{e^{2ik\alpha}}{\cosh(k\zeta)} = \frac{1}{\pi} \frac{\vartheta_1'(0,q)}{\vartheta_1'(0,q)} \frac{\vartheta_3(\alpha, q)}{\vartheta_4(\alpha, q)}, \tag{8.6}$$

with the last equality being a representation in terms of the elliptic Theta functions[1] of nome $q = e^{-\zeta}$, which display more clearly the double periodicity of the function $\rho(\alpha)$.

It was also argued in [122] that the additional boundary factors of the Bethe equations, depending on $\xi_\pm$, would lead to isolated complex roots in the large L limit and placed around one of the two zeroes of the boundary factors. Such kind of roots would emerge similarly to the "string solutions" in the bulk of the chain: as L becomes large, the left hand side of (8.3) diverges or vanishes for a complex root, but this may be compensated in the right hand side by the fact that the complex root tends to a pole or a zero (in the large-L limit) of the boundary factors. With our choice (8.4) of the domain of solution of the Bethe equation, this argument would

[1] We have adopted the conventions of [140].

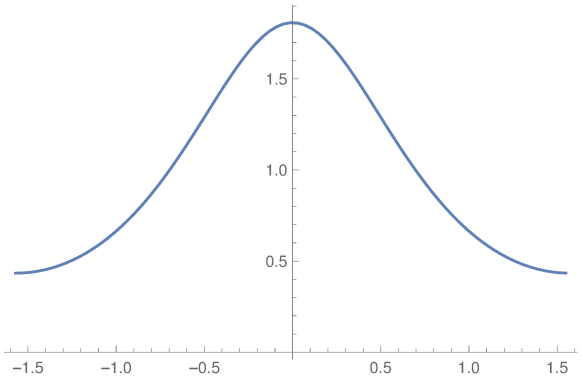

Figure 8.1 – Distribution of real roots $\rho(\alpha)$ for $\Delta = 3$. As defined in (8.6), the density function has period π and is even.

mean that the boundary root would take the value:

$$\alpha_{\mathrm{BR}}^{\sigma} = -i[\zeta/2 - \tilde{\xi}_{\sigma} + \epsilon_{\sigma}] + \delta_{\sigma}\frac{\pi}{2}, \quad \sigma \in \{+,-\}, \tag{8.7}$$

with exponentially small corrections $\epsilon_\sigma = \mathrm{O}(L^{-\infty})$. In [122], this boundary root is predicted to exist for $\tilde{\xi}_\sigma < \zeta/2$, which corresponds to a boundary field h_σ *outside* of an interval delimited by two critical fields $h_{\mathrm{cr}}^{(1)}$ and $h_{\mathrm{cr}}^{(2)}$ defined as [122, 138]

$$h_{\mathrm{cr}}^{(1)} = \Delta - 1, \qquad h_{\mathrm{cr}}^{(2)} = \Delta + 1. \tag{8.8}$$

In this chapter, we clarify (and correct) this assertion, and we study more precisely, in the large L limit, the structure of Bethe roots for the ground state, and more generally for the low energy states, in terms of the values of the boundary fields and of the parity of the chain. We will notably show how to control the finite-size corrections up to exponentially small order in L.

8.1 Properties of the states of low energy for large L

In the following, we restrict our study to states of low energy in the spectrum, which are expected to be described, in the large L limit, by a set $\boldsymbol{\lambda}$ of Bethe roots consisting in an extensive, $\mathrm{O}(L/2)$ set of real roots, and a finite number of complex roots. Following the same argument as in [93], it is possible to show that, for L large enough, complex roots appear only in conjugated pairs, except if their real part is 0 or $\pi/2$ (in our chosen domain of solutions (8.4)). We will be particularly interested here in the role of these isolated complex roots, which are peculiar to the open chain and will play the role of "boundary modes" when localizing at one of the two zeroes of the boundary factor. To elucidate their role in the description of the ground state and low-energy states, we have to perform a careful study of the solutions of the

Bethe equations. As in [93], we study separately the Bethe equations for the real roots and for the complex roots.

8.1.1 Bethe equations for real roots and Counting Function

As usual, it is convenient to rewrite the Bethe equations for the real roots in the logarithmic form. This allows us to characterize the real Bethe roots by mapping them into a set of integer quantum numbers. This mapping is given by the so-called *counting function*.

Let $\lambda_j \in \mathbb{R}$. We rewrite the Bethe equation for λ_j in logarithmic form, which defines a map $\lambda_j \mapsto n_j \in \mathbb{N}$:

$$\mathfrak{Z}(\lambda_j|\boldsymbol{\lambda}) = \frac{\pi n_j}{L}, \tag{8.9}$$

where the *counting function* $\mathfrak{Z}$ is defined —for a given set of N Bethe roots $\boldsymbol{\lambda}$— as the following function on $\mathbb{R}$:

$$\mathfrak{Z}(x|\boldsymbol{\lambda}) = p(x) + \frac{1}{2L}\Big(g(x) - \theta(2x) + \sum_{j=1}^{N} \Theta(x,\lambda_j)\Big), \tag{8.10}$$

with:

$$p(x) = \int_0^x \varphi'(\mu,\zeta/2)\,\mathrm{d}\mu \tag{8.11}$$

$$\theta(x) = -\int_0^x \varphi'(\mu,\zeta)\,\mathrm{d}\mu \tag{8.12}$$

$$\Theta(x,\lambda_j) = -\frac{1}{2}\int_0^x \Big[\varphi'(\mu-\lambda_j,\zeta) + \varphi'(\mu-\bar{\lambda}_j,\zeta) + \varphi'(\mu+\lambda_j,\zeta) + \varphi'(\mu+\bar{\lambda}_j,\zeta)\Big]\mathrm{d}\mu \tag{8.13}$$

$$g(x) = -\int_0^x \Big[\varphi'(\mu,\zeta/2+\xi_+) + \varphi'(\mu,\zeta/2+\xi_-)\Big]\mathrm{d}\mu, \tag{8.14}$$

and where we use the following function:

$$\varphi'(\mu,\gamma) = \frac{\sinh(2\gamma)}{\mathfrak{s}(\mu,i\gamma)}, \quad \gamma > 0, \tag{8.15}$$

and the fact that complex Bethe roots appear in conjugate pairs $\lambda_j, \bar{\lambda}_j$, except if $\mathfrak{Re}(\lambda_j) \in \{0, \pi/2\}$.

Allowed set of quantum numbers

The allowed range of quantum numbers n_j can easily be determined by continuity from the Ising limit $\Delta \to +\infty$ (i.e., $\zeta \to +\infty$). In this limit, we see from the above expressions that:

$$\begin{aligned} p(x) &\to 2x \\ \theta(x) &\to -2x \\ \Theta(x,\lambda_k) &\to \begin{cases} -4x & \text{if } |\mathrm{Im}(\lambda_j)| = \mathrm{o}(\zeta) \\ 0 & \text{if } \zeta = \mathrm{o}(|\mathrm{Im}(\lambda_j)|) \end{cases} \\ g(x) &\to -2(\tilde{\delta}_+ + \tilde{\delta}_-)x \end{aligned} \tag{8.16}$$

where $\tilde{\delta}_\sigma = -1$ if $h_{\mathrm{cr}}^{(1)} < h_\sigma < h_{\mathrm{cr}}^{(2)}$ (i.e., if. $\tilde{\xi}_\sigma > \zeta/2$) and 1 otherwise ($\sigma = \pm$).

Then, for large Δ, the counting function for $x \in \mathbb{R}$ takes the simple form

$$\mathfrak{Z}(x|\boldsymbol{\lambda}) \sim_{\zeta\to+\infty} \frac{2M}{L}x, \tag{8.17}$$

where $M = L - N + n_w + 1 - \frac{1}{2}(\tilde{\delta}_+ + \tilde{\delta}_-)$. Notice that this means that a real root λ_j behaves as

$$\lambda_j \sim_{\zeta\to+\infty} \frac{\pi n_j}{2M}, \tag{8.18}$$

and since the real solutions are in the interval $(0, \pi/2)$, we conclude that the integers n_j can take only the values $n_j \in \{1, 2, \ldots, M-1\}$.

We can therefore rewrite the Bethe equations for the real roots λ_j as

$$\mathfrak{Z}(\lambda_j|\boldsymbol{\lambda}) = \frac{\pi j}{L}, \quad j \in \{1,\ldots,M-1\} \setminus \{h_1,\ldots,h_n\} \tag{8.19}$$

where $h_1, \ldots, h_n$ label the positions of the *holes*, i.e., of the unoccupied quantum numbers in the range of all allowed quantum numbers.

Thermodynamic form of the Bethe equations

In the thermodynamic limit $L \to \infty$, if we make the usual assumption that the real roots λ_j for the low energy states form a dense distribution on the interval $(0, \pi/2)$ (that can be extended by parity to $(-\pi/2, \pi/2)$) and that sums over such real roots transform to integrals on the interval $(0, \pi/2)$ (see [92] for a rigorous proof of this in the periodic case), we obtain that the limit $\frac{\mathfrak{Z}(\lambda_{j+1})-\mathfrak{Z}(\lambda_j)}{\lambda_{j+1}-\lambda_j}$ in (8.10) gives:

$$\mathfrak{Z}'(x|\boldsymbol{\lambda}) \to \pi\rho(x) \tag{8.20}$$

where ρ is the solution of the integral equation (8.5) and where $K = \frac{1}{2\pi}\Theta'$. The Bethe equations for the real roots then turn, in the leading order order in L, into the integral equation (8.5) for the density ρ of real roots.

In the following, we study the corrections to this integral equations, and in particular the corrections due to the presence of holes and/or complex roots in a given state of low energy. We also show that we can control these corrections up to exponentially small order in L.

Controlling the sum-to-integral transformation

It follows from (8.20) that, for L large enough, $\mathfrak{Z}$ is a monotonous increasing function. Thus, in the interval $(0, \pi/2)$, for any $j \in \{1, \dots, M-1\}$, there exists a single $\check{\lambda}_j$ such that

$$\mathfrak{Z}(\check{\lambda}_j|\boldsymbol{\lambda}) = \frac{\pi j}{L}, \quad j \in \{1, \dots, M-1\} \setminus \{h_1, \dots, h_{n_{\text{holes}}}\}. \tag{8.21}$$

Thus:

- When j corresponds to an "occupied" quantum number, then $\check{\lambda}_j$ coincides with the Bethe root λ_j.
- If on the contrary $j = h_k \in \{1, \dots, N\}$, $k \in \{1, \dots, n_{\text{holes}}\}$ is the index that corresponds to the quantum number of a hole, Eq. (8.21) gives then a definition for the hole rapidity $\check{\lambda}_{h_k}$.

In addition to equation (8.20), $\mathfrak{Z}$ verifies the following properties:

(i) $\mathfrak{Z}(-x|\boldsymbol{\lambda}) = -\mathfrak{Z}(x|\boldsymbol{\lambda})$

(ii) $\mathfrak{Z}(x+\pi|\boldsymbol{\lambda}) = \mathfrak{Z}(x|\boldsymbol{\lambda}) + \frac{2M}{L}\pi$

(iii) $\mathfrak{Z}(0|\boldsymbol{\lambda}) = 0, \quad$ and $\quad \mathfrak{Z}(\pi/2|\boldsymbol{\lambda}) = -\mathfrak{Z}(-\pi/2|\boldsymbol{\lambda}) = \frac{M\pi}{L}$.

This enables us to precisely control the sum-to-integral transformation for real roots of a low energy state. In fact, we have shown in [141] the following proposition and corollary. We refer to our paper [141] for the proofs.

Proposition 1. *Let f be a $\mathcal{C}^\infty$, π-periodic and even function on $\mathbb{R}$. Let $\boldsymbol{\lambda}$ be a solution of the Bethe equations (8.3). Let $\mathfrak{Z}(x|\boldsymbol{\lambda})$ be the corresponding counting function. Then, the sum of all the values $f(\lambda_j)$ corresponding to the real roots λ_j,*

with $j \in \{1,\dots,M-1\} \setminus \{h_1,\dots,h_{n_{holes}}\}$ can be replaced by an integral in the large L limit according to the following rule:

$$\frac{1}{L}\sum_{\substack{j=1\\ j\neq h_1,\dots,h_n}}^{M-1} f(\lambda_j) = \frac{1}{2\pi}\int_{-\pi/2}^{\pi/2} f(y)\mathfrak{Z}'(y|\boldsymbol{\lambda})\mathrm{d}y - \frac{1}{L}\left(\frac{f(0)+f(\pi/2)}{2} + \sum_{j=1}^{n_{holes}} f(\check{\lambda}_{h_j})\right) + \mathrm{O}(L^{-\infty}). \tag{8.22}$$

Corollary 1. (I) *Let f be a $\mathcal{C}^\infty$ and π-periodic function on $\mathbb{R}$. Then, with the same notations as the previous proposition:*

$$\frac{1}{L}\sum_{\substack{j=1\\ j\neq h_1,\dots,h_n}}^{M-1} \Big[f(\lambda_j)+f(-\lambda_j)\Big] = \frac{1}{\pi}\int_{-\pi/2}^{\pi/2} f(y)\mathfrak{Z}'(y|\boldsymbol{\lambda})\mathrm{d}y \tag{8.23}$$

$$- \frac{1}{L}\left(f(0)+f(\pi/2)+\sum_{j=1}^{n_{holes}}\Big[f(\check{\lambda}_{h_j})+f(-\check{\lambda}_{h_j})\Big]\right) + \mathrm{O}(L^{-\infty}) \tag{8.24}$$

(II) *Let g be a $\mathcal{C}^\infty$ function such that its derivative g' is π-periodic:*

$$\frac{1}{L}\sum_{\substack{j=1\\ j\neq h_1,\dots,h_n}}^{M-1} \Big[g(\lambda_j)+g(-\lambda_j)\Big] = \frac{1}{\pi}\int_{-\pi/2}^{\pi/2} g(y)\mathfrak{Z}'(y|\boldsymbol{\lambda})\mathrm{d}y$$

$$- \frac{1}{L}\left(\frac{g(\pi/2)+2g(0)+g(-\pi/2)}{2} + \sum_{j=1}^{n_{holes}}\Big[g(\check{\lambda}_{h_j})+g(-\check{\lambda}_{h_j})\Big]\right) + \mathrm{O}(L^{-\infty} \tag{8.25}$$

Finite-size correction to the counting function: contributions of the complex roots and holes

We can in particular apply the second corollary to transform the sum over real roots in the definition of the counting function:

$$\mathfrak{Z}(x|\boldsymbol{\lambda}) = p(x) + \frac{g(x)}{2L} - \frac{\theta(2x)}{2L} + \frac{1}{2\pi}\int_{-\frac{\pi}{2}}^{\frac{\pi}{2}} \theta(x-y)\,\mathfrak{Z}'(y|\boldsymbol{\lambda})\,\mathrm{d}y + \frac{1}{2L}\sum_{k\in\mathfrak{C}}\Theta(x,\lambda_k)$$
$$- \frac{\theta(x-\frac{\pi}{2})+\theta(x+\frac{\pi}{2})+2\theta(x)}{4L} - \frac{1}{2L}\sum_{j=1}^{n}\big[\theta(x-\check{\lambda}_{h_j})+\theta(x+\check{\lambda}_{h_j})\big] + O(L^{-\infty}), \tag{8.26}$$

Taking the derivative with respect to x, we obtain the following integral equation for $\mathfrak{Z}'$:

$$\mathfrak{Z}'(x|\boldsymbol{\lambda})+\int_{-\frac{\pi}{2}}^{\frac{\pi}{2}} K(x-y)\,\mathfrak{Z}'(y|\boldsymbol{\lambda})\,\mathrm{d}y = p'(x) + \frac{1}{2L}\Bigg(g'(x) - 2\theta'(2x) - \theta'(x) - \theta'(x+\pi/2) + \sum_{k\in\mathfrak{C}} \Theta'(x,\lambda_k) - \sum_{j=1}^{n}\Big[\theta'(x-\check{\lambda}_{h_j}) + \theta'(x+\check{\lambda}_{h_j})\Big]\Bigg) + \mathrm{O}(L^{-\infty}), \tag{8.27}$$

where $\mathfrak{C}$ is the set of indices corresponding to complex roots ($k \in \mathfrak{C} \Rightarrow \mathrm{Im}(\lambda_k) \neq 0$). Hence, by linearity, the solution of the integral equation can be decomposed into a sum of term corresponding to real roots, complex roots and holes:

$$\mathfrak{Z}(x|\boldsymbol{\lambda}) = \mathfrak{Z}_0(x|\boldsymbol{\lambda}) + \frac{1}{L}\Bigg(\sum_{k\in\mathfrak{C}} \mathfrak{Z}_{\lambda_k}(x|\boldsymbol{\lambda}) - \sum_{j=1}^{n} \mathfrak{Z}_{\check{\lambda}_{h_j}}(x|\boldsymbol{\lambda})\Bigg) + \mathrm{O}(L^{-\infty}), \tag{8.28}$$

In this expression, we have used the following definitions:

(i) $\mathfrak{Z}_0(x|\boldsymbol{\lambda})$ is the common contribution of the "Fermi sea" of real roots. It is an odd function, and its derivative is defined as the solution of the integral equation

$$\mathfrak{Z}_0'(x|\boldsymbol{\lambda}) + \int_{-\frac{\pi}{2}}^{\frac{\pi}{2}} K(x-y)\,\mathfrak{Z}_0'(y|\boldsymbol{\lambda})\,\mathrm{d}y = p'(x) + \frac{1}{2L}\Big(g'(x) - 2\theta'(2x) - \theta'(x) - \theta'(x+\pi/2)\Big). \tag{8.29}$$

Note that $\mathfrak{Z}_0'(x|\boldsymbol{\lambda})$ can itself be decomposed as

$$\mathfrak{Z}_0'(x|\boldsymbol{\lambda}) = \pi\rho(x) + \frac{1}{L}\,\mathfrak{Z}_{\mathrm{open}}'(x|\boldsymbol{\lambda}), \tag{8.30}$$

where ρ is the density of Bethe roots, and where $\mathfrak{Z}_{\mathrm{open}}'$ is the correction due to the $1/L$ terms in (8.29), which is defined as the solution to the integral equation

$$\mathfrak{Z}_{\mathrm{open}}'(x|\boldsymbol{\lambda}) + \int_{-\frac{\pi}{2}}^{\frac{\pi}{2}} K(x-y)\,\mathfrak{Z}_{\mathrm{open}}'(y|\boldsymbol{\lambda})\,\mathrm{d}y = \frac{1}{2}\Big(g'(x) - 2\theta'(2x) - \theta'(x) - \theta'(x+\pi/2)\Big). \tag{8.31}$$

(ii) The function $\mathfrak{Z}_\mu$, which corresponds to the contribution to the counting function of an excitation (an additional complex root or a hole at position μ) with

respect to the above Fermi sea of real roots, is also an odd function with derivative being the solution of the integral equation:

$$\mathfrak{Z}'_\mu(x|\boldsymbol{\lambda}) + \int_{-\frac{\pi}{2}}^{\frac{\pi}{2}} K(x-y)\,\mathfrak{Z}'_\mu(y|\boldsymbol{\lambda})\,\mathrm{d}y = \frac{\Theta'(x,\mu)}{2}. \tag{8.32}$$

This latter can be computed in Fourier modes. We obtain that $\mathfrak{Z}'_\mu(x|\boldsymbol{\lambda}) = \frac{1}{2}\big[\mathfrak{f}'_\mu(x) + \mathfrak{f}'_{\bar{\mu}}(x)\big]$, with

$$\mathfrak{f}'_\mu(x) = \begin{cases} -\displaystyle\sum_{k=-\infty}^{+\infty} \frac{e^{-|k|\zeta}}{\cosh(k\zeta)}\,\cos(2k\mu)\,e^{2ikx} & \text{if } |\mathfrak{Im}(\mu)| < \zeta, \\ 2\displaystyle\sum_{k=-\infty}^{\infty} e^{|k|\zeta}\,\sinh(|k|\zeta)\,e^{2i|k|\,\mathsf{sign}[\mathfrak{Im}(\mu)]\mu}\,e^{2ikx} & \text{if } |\mathfrak{Im}(\mu)| > \zeta. \end{cases} \tag{8.33}$$

8.1.2 Bethe equations for complex roots: is an isolated complex root a boundary root ?

Let us now consider the Bethe equations for the complex roots. We are more particularly interested in the isolated complex roots which are specific to the open chain. We want to determine notably the domain of existence of the boundary roots, thus being more precise than the predictions of [122].

To this aim, let us separate the factors in the Bethe equations that can lead to divergences depending on L. Let the function F be defined by:

$$F(z) = ip(z) + \frac{i}{2}\int_{-\pi/2}^{\pi/2} \theta(z-y)\rho(y)\mathrm{d}y, \tag{8.34}$$

where p, θ are defined by: $\exp(ip(z)) = \frac{\sin(i\zeta/2-z)}{\sin(i\zeta/2+z)}$ and $\exp(i\theta(z)) = \frac{\sin(i\zeta+z)}{\sin(i\zeta-z)}$.

Then, for a complex root $\lambda_j \in \boldsymbol{\lambda}$, $\lambda_j \in \mathbb{C}$, we rewrite the Bethe equations as:

$$\begin{aligned} \exp\Bigg(& 2LF(\lambda_j) + \frac{i}{\pi}\int_{-\pi/2}^{\pi/2} \theta(\lambda_j - y)\Big[\mathfrak{Z}'_{\mathrm{open}}(y) + \sum_{\ell\in\mathfrak{C}} \mathfrak{Z}'_{\lambda_\ell}(y) - \sum_{\ell=1}^{n_{\mathrm{holes}}} \mathfrak{Z}'_{\check{\lambda}_{h_\ell}}(y)\Big]\mathrm{d}y \\ & - \frac{i}{2}\Big(\theta(\lambda_j - \pi/2) + \theta(\lambda_j + \pi/2) + 2\theta(\lambda_j)\Big) - i\sum_{\ell=1}^{n}\Big(\theta(\lambda_j - \check{\lambda}_{h_\ell}) + \theta(\lambda_j - \check{\lambda}_{h_\ell})\Big) + \mathrm{O}(L^{-\infty})\Bigg) \\ & \times \frac{\sin(\lambda_j + i\xi_- + i\zeta/2)\sin(\lambda_j + i\xi_+ + i\zeta/2)}{\sin(\lambda_j - i\xi_- - i\zeta/2)\sin(\lambda_j - i\xi_+ - i\zeta/2)} \times \prod_{k\neq j, k\in\mathfrak{C}} \frac{\mathfrak{s}(\lambda_j + i\zeta, \lambda_k)}{\mathfrak{s}(\lambda_j - i\zeta, \lambda_k)} = 1, \end{aligned} \tag{8.35}$$

where we have substituted in the first line the decomposition of contributions to the counting function. Hence, we see that the real part of $F(\lambda_j)$ may lead to an exponential growth or an exponential vanishing with L of the first line of Eq. (8.35), which should be compensated by the fact that λ_j becomes exponentially close to a zero or a pole of the remaining factors —and especially of the boundary factors if λ_j is an isolated complex root. We need therefore to investigate the behavior of the real part of F to determine whether an isolated complex root is, or not, a boundary root.

We can integrate directly (8.5) only when $|\mathfrak{Im}(\lambda_j)| < \zeta$ since then we can assure that the meromorphic function $\theta'(z)$ will have no poles. This is the condition that defines a *close root*. Roots such that $\mathfrak{Im}(\lambda_j) > \zeta$ are called *wide roots*. The function F then gives:

$$F(\lambda_j) = i\pi \int_0^{\lambda_j} \rho(w)dw = i \int_0^{\lambda_j} \sum_{k\in\mathbb{Z}} \frac{e^{2ik\mu}}{\cosh(k\zeta)} \mathrm{d}\mu \tag{8.36}$$

When we evaluate it on $z = \beta + i\alpha$, and $\beta \in \{0, \pi/2\}$, $\alpha < 0$ (recall that this is within the range of allowed values we assumed for the isolated Bethe roots), F has the following form :

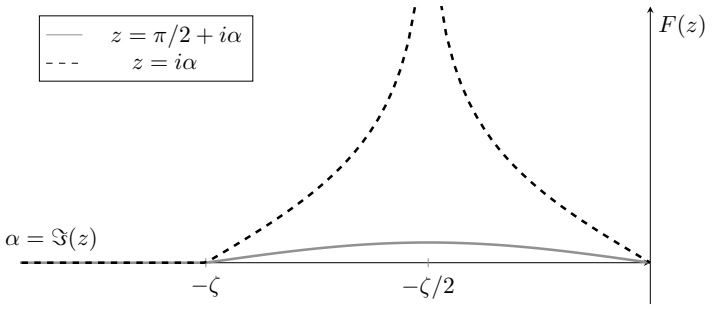

Figure 8.2 – The function (8.34) evaluated at $z = \beta + i\alpha$ and $\beta \in \{0, \pi/2\}$. Notice that $F(z)$ takes positive values only when $|\mathfrak{Im}(z)| < \zeta$. This causes a diverging term in the Bethe equations.

We are interested in the sign of the real part of F, since it will determine whether the first line of (8.35) vanishes or diverges for large L. We find that $\Re(F(\lambda_j)) > 0$ for $-\zeta < \mathfrak{Im}(\lambda_j) < 0$ (i.e., if λ_j is a close root), which gives a diverging factor in the first line of (8.35), whereas $\Re(F(\lambda_j)) = 0$ for $\mathfrak{Im}(\lambda_j) < -\zeta$ (i.e., if λ_j is a wide root), and the corresponding factor in the first line of (8.35) remains finite.

If we expect the Bethe equations to be satisfied and if the first line of (8.35) diverges, the corresponding complex root needs to approach simultaneously a zero in some other term. If it is the case that there is only one complex root (which, from the previous study, should be a close root), then the boundary factors are the

only ones who can provide this compensation. A zero of a boundary factor is of the form $-i\zeta/2 - i\xi_\sigma$, for some $\sigma \in \{+,-\}$. So we arrive at the existence domain of the boundary root in terms of the boundary fields (recall the parametrization of (8.1)):

$$-\zeta < \mathfrak{Im}\left(-i\zeta/2 - i\left[-\widetilde{\xi}_\sigma + i\delta_\sigma \frac{\pi}{2}\right]\right) < 0 \quad \Rightarrow \quad \left|\widetilde{\xi}_\sigma\right| < \zeta/2, \tag{8.37}$$

or, in terms of the corresponding boundary field h_σ:

$$h_\sigma \notin [-h_{\rm cr}^{(2)}, -h_{\rm cr}^{(1)}] \cup [h_{\rm cr}^{(1)}, h_{\rm cr}^{(2)}]. \tag{8.38}$$

Note that this domain of existence is more restrictive that the one found in [122].

8.1.3 Expression of the energy

We now apply the results of the previous subsections so as to compute, up to exponentially small corrections in L, the energy (7.43) associated with a given solution $\boldsymbol{\lambda}$ describing a state of low energy for large L. Using the sum-to-integral transformation result (8.22) on the bare energy and the decomposition of the counting function (8.28), we obtain that

$$E(\boldsymbol{\lambda}) = E_0 + \sum_{k\in\mathfrak{C}} \varepsilon(\lambda_k) + \sum_{j=1}^{n} \varepsilon(\check{\lambda}_{h_j}) + \mathrm{O}(L^{-\infty}). \tag{8.39}$$

Here, the common contribution E_0 of the real roots is

$$E_0 = h_+ + h_- + \frac{L}{2\pi}\int_{-\frac{\pi}{2}}^{\frac{\pi}{2}} \varepsilon_0(\mu)\, \mathfrak{Z}_0'(\mu|\boldsymbol{\lambda})\, \mathrm{d}\mu - \frac{\varepsilon_0(0)+\varepsilon_0(\frac{\pi}{2})}{2}, \tag{8.40}$$

and $\varepsilon(\mu)$ is the dressed energy of an excitation with rapidity μ, defined as

$$\varepsilon(\mu) = \varepsilon_0(\mu) + \frac{1}{2\pi}\int_{-\frac{\pi}{2}}^{\frac{\pi}{2}} \varepsilon_0(\beta)\, \mathfrak{Z}_\mu'(\beta)\, d\beta. \tag{8.41}$$

in terms of the bare energy (7.44) and of the correction to the counting function due to the root μ, see (8.32)–(8.33). We can compute the expression of (8.41) in Fourier modes, by using (8.32) and the expression (8.33) of $\mathfrak{Z}_\mu(\alpha)$:

$$\varepsilon(\mu) = \frac{\varepsilon_\mu + \varepsilon_{\bar{\mu}}}{2}, \tag{8.42}$$

where

$$\varepsilon_\mu = -2\sinh\zeta\left[\varphi'(\mu,\zeta/2) + \frac{1}{2\pi}\int_{-\frac{\pi}{2}}^{\frac{\pi}{2}} \varphi'(\beta,\zeta/2)\,\mathfrak{Z}'_\mu(\beta)\,\mathrm{d}\beta\right], \tag{8.43}$$

$$= \begin{cases} -2\sinh\zeta \sum_{k\in\mathbb{Z}} \dfrac{e^{2ik\mu}}{\cosh(k\zeta)} = -2\pi\sinh\zeta\,\rho(\mu) & \text{if } |\mathfrak{Im}(\mu)| < \zeta/2, \\ 2\sinh\zeta \sum_{k\in\mathbb{Z}} \dfrac{e^{2ik\left(\mu - i\,\mathsf{sign}[\mathfrak{Im}(\mu)]\zeta\right)}}{\cosh(k\zeta)} = -2\pi\sinh\zeta\,\rho(\mu) & \text{if } \zeta/2 < |\mathfrak{Im}(\mu)| < \zeta, \\ 4\,\mathsf{sign}[\mathfrak{Im}(\mu)]\sinh\zeta \sum_{k\in\mathbb{Z}} \sinh(k\zeta)\,e^{2i|k|\,\mathsf{sign}[\mathfrak{Im}(\mu)]\mu} = 0 & \text{if } |\mathfrak{Im}(\mu)| > \zeta, \end{cases}$$

in which ρ is the distribution of Bethe roots. Here we have notably used the quasi-periodicity property $\rho(\mu \pm i\zeta) = -\rho(\mu)$.

In particular, the dressed energy of a wide root vanishes, the dressed energy of a hole with rapidity $\check{\lambda}_h \in (0, \frac{\pi}{2})$ is given by

$$\varepsilon_h(\check{\lambda}_h) = -\varepsilon(\check{\lambda}_h) = 2\sinh\zeta \sum_{k\in\mathbb{Z}} \frac{e^{2ik\check{\lambda}_h}}{\cosh(k\zeta)} = 2\pi\sinh\zeta\,\rho(\check{\lambda}_h), \tag{8.44}$$

whereas the dressed energy of the boundary root (8.7) is given by

$$\varepsilon(\alpha^\sigma_{\mathrm{BR}}) = -2\pi\sinh\zeta\,\rho(\alpha^\sigma_{\mathrm{BR}}) = -2\pi\sinh\zeta\,\rho\Big(i\tilde{\xi}_\sigma - i\frac{\zeta}{2} + \delta_\sigma\frac{\pi}{2}\Big) + O(L^{-\infty}), \tag{8.45}$$

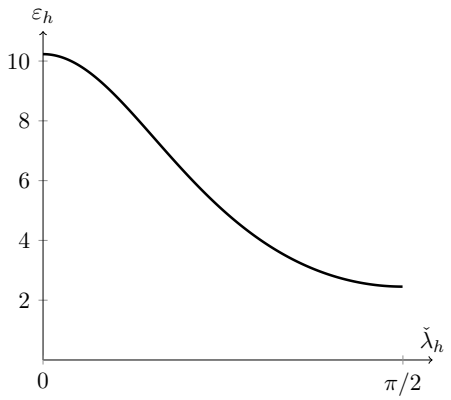

Figure 8.3 – Dressed energy (8.44) of a hole as a function of its rapidity $\check{\lambda}_h \in (0, \pi/2)$ for a chain at $\Delta = 3$.

Note that the expression (8.44) for the dressed energy of a hole is a positive and decreasing function of $\check{\lambda}_h$ on the interval $[0, \frac{\pi}{2}]$, see Fig. 8.3. The expression (8.45) for the dressed energy of the boundary root is an odd function of $\tilde{\xi}_\sigma$ (and therefore

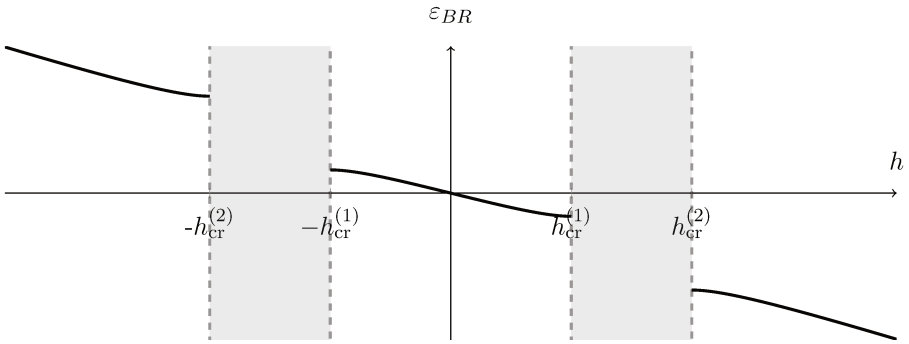

Figure 8.4 – Dressed energy $\varepsilon_{\mathbf{BR}} = \varepsilon(\alpha^{\sigma}_{\mathbf{BR}})$ of the boundary root as a function of the boundary field $h = h_\sigma$ at $\Delta = 3$, as given by (8.45), in its domain of existence (8.38). The two critical fields are here $h_{\rm cr}^{(1)} = 2$ and $h_{\rm cr}^{(2)} = 4$. The dressed energy $\varepsilon_{\rm BR}$ is an odd and decreasing function of h. Moreover, the dressed energy of the boundary root tends to the one of a hole with rapidity $\check{\lambda}_h = \frac{\pi}{2}$ when $h \to -h_{\rm cr}^{(1)}$, $h > -h_{\rm cr}^{(1)}$, and it tends to the one of a hole with rapidity $\check{\lambda}_h = 0$ when $h \to -h_{\rm cr}^{(2)}$, $h < -h_{\rm cr}^{(2)}$.

of h_σ). It is moreover a decreasing function of h_σ if $|h_\sigma| \notin [h_{\rm cr}^{(1)}, h_{\rm cr}^{(2)}]$, and we have

$$\varepsilon(\alpha^{\sigma}_{\rm BR}) \underset{\substack{h_\sigma \to -h_{\rm cr}^{(2)} \\ h_\sigma < -h_{\rm cr}^{(2)}}}{\longrightarrow} \varepsilon_h(0), \qquad \varepsilon(\alpha^{\sigma}_{\rm BR}) \underset{\substack{h_\sigma \to -h_{\rm cr}^{(1)} \\ h_\sigma > -h_{\rm cr}^{(1)}}}{\longrightarrow} \varepsilon_h(\pi/2), \tag{8.46}$$

so that the dressed energy (8.45) of the boundary root can be compared to the dressed energy (8.44) of a hole with rapidity $\check{\lambda}_h$ as

$$\varepsilon(\alpha^{\sigma}_{\rm BR}) > \varepsilon_h(\check{\lambda}_h), \qquad \forall \check{\lambda}_h \in \big(0, \frac{\pi}{2}\big) \qquad \text{if} \quad h_\sigma < -h_{\rm cr}^{(2)}, \tag{8.47}$$

$$|\varepsilon(\alpha^{\sigma}_{\rm BR})| < \varepsilon_h(\check{\lambda}_h), \qquad \forall \check{\lambda}_h \in \big(0, \frac{\pi}{2}\big) \qquad \text{if} \quad |h_\sigma| < h_{\rm cr}^{(1)}. \tag{8.48}$$

The dressed energy of the boundary root $\alpha^{\sigma}_{\rm BR}$ is plotted as a function of the field h_σ for a specific value of Δ in Fig. 8.4.

We finally recall that, according to [93], the bulk close complex roots are arranged either in 2-strings or in quartets whose dressed energy vanishes.

8.2 Root configurations in the ground state

8.2.1 Allowed configurations of Bethe roots

We have seen that the number of allowed quantum numbers for real roots is:

$$\text{Allowed} = L - N + n_w - \frac{1}{2}(\tilde{\delta}_+ + \tilde{\delta}_-). \tag{8.49}$$

One begins by determining $\tilde{\delta}_+ + \tilde{\delta}_-$ according to the boundary field values, and from there, the number of allowed quantum numbers for real roots from eq. (8.49). We now analyze succesively the magnetization sectors with $N \leq L/2$ and determine the composition of $\boldsymbol{\lambda}$ for cases with and without wide roots:

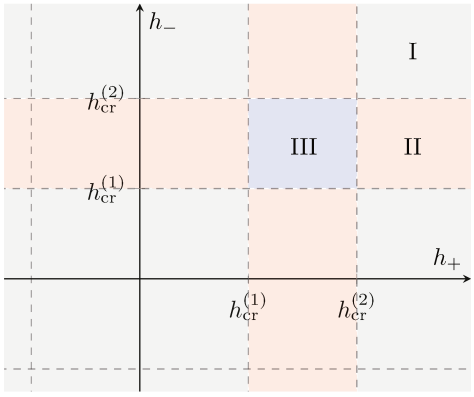

Figure 8.5 – Different cases for the values $\tilde{\delta}_\pm$ according to the field strengths. This determine the maximum number of real Bethe roots.

Case I: Both fields are *not* in the interval $[h_{\rm cr}^{(1)}, h_{\rm cr}^{(2)}]$ (so $\tilde{\delta}_+ + \tilde{\delta}_- = 2$).

L Even: When $N = L/2$, there are $N + n_w - 1$ possible quantum numbers for the real roots.

- If there is no wide root, there can be a state with $N - 1$ real roots (no hole) and a boundary root *only if the corresponding field* $h_\sigma \notin [-h_{cr}^{(2)}, -h_{cr}^{(1)}]$. If the boundary field is in that region, we have at least one hole, corresponding to a state with $N - 2$ real roots and a 2-string.
- If there is a wide root ($\zeta = \mathrm{o}(|\mathrm{Im}(\lambda_k)|)$), since now there is a maximum of $N - 1$ remaining real roots mapping to N available quantum numbers, there has to be at least one hole.

When $N = L/2 - 1$ there are $N + n_w + 1$ possible quantum numbers for the real roots.

- If there's a wide root, one has at least $N - 1$ real roots and three holes, which is energetically costly.
- If there is no wide root, then one gets N real roots and a hole. Other solutions have more complex solutions and holes.

For $N < L/2 - 1$ one has higher energy configurations which will not describe the ground state.

L Odd: When $N = (L-1)/2$, we now have $N + n_w$ allowed quantum numbers. The state of lowest energy in that sector can be either the state with N real roots (no hole) or a state with $N-1$ real roots, one hole and one Boundary Root (we have to compare the energy of the hole and the energy of the boundary root). The states in sectors $N < (L-1)/2$ have more holes and cannot describe the ground state.

Case II: Only one of the fields is in the interval $[h_{\rm cr}^{(1)}, h_{\rm cr}^{(2)}]$ (so $\tilde{\delta}_+ + \tilde{\delta}_- = 0$).

L Even: When $N = L/2$, there are $N + n_w$ possible quantum numbers for the real roots and a maximum of N real and adjacent roots (no hole and no complex root). The possibilities $N < L/2$ bring extra holes and complex roots which will not describe the ground state.

L Odd: For $N = (L-1)/2$, we have $N + n_w + 1$ allowed quantum numbers for the real roots. So the state with the minimum numbers of holes is a state with 1 hole and N real roots.

Case III: Both fields are in the interval $[h_{\rm cr}^{(1)}, h_{\rm cr}^{(2)}]$ (so $\tilde{\delta}_+ + \tilde{\delta}_- = -2$).

L Even: If $N = L/2$, there are $N + n_w + 1$ possible quantum numbers for the real roots and a maximum of N real roots. This means that there is at least one hole in the solution. The possibilities $N < L/2$ bring extra holes and complex roots which will not describe the ground state.

L Odd: If $N = (L-1)/2$, the allowed quantum numbers for the real roots is $N + n_w + 2$, so there's at least N real roots and two holes. States in sectors $N < (L-1)/2$ contain more holes.

We see that Case I includes the largest variety of configurations of real roots accompanied by a complex root. As we will see this case will indeed contain a ground state with boundary roots. To verify this we need to be able to compare the energy of each candidate configuration:

8.2.2 Configuration of Bethe roots for the ground state

The number of Bethe roots of a given Bethe state $\prod_{j=1}^{N} \mathcal{B}(\lambda_j)|\mathbf{0}\rangle$ is related to its total *magnetization*, defined as

$$m = \left\langle \sum_{n=1}^{L} S_n^z \right\rangle = \frac{L}{2} - N. \tag{8.50}$$

States with negative magnetization would correspond to more than $L/2$ roots. To avoid going "beyond the equator", one can describe these states by reproducing the Algebraic Bethe Ansatz solution starting from the reference state $|\bar{\mathbf{0}}\rangle$ with all spins down and then act with $\mathcal{C}(\lambda)$ as a creation operator. Otherwise, one can simply describe the sectors with negative magnetization by using the invariance of the model with respect to reversal of all spins and change of sign of the boundary fields.

The ground state is given by a configuration of Bethe roots that minimizes the number of holes, unless there is a boundary root that compensates. Here we concentrate on values of the boundary fields such that $h_+ + h_- \leq 0$ so as to make sure that the magnetization of the ground state is $m \geq 0$ and that we don't exceed $L/2$ Bethe roots.

We review the results obtained by analyzing the energy contributions of each candidate configuration (obtained from the previous section). A more thorough analysis can be found in chapter 4 of [141].

Even Chain

Case A: Both fields are below $-h_{\rm cr}^{(2)}$
In this case the dressed energies are $\varepsilon_{\rm hole} < \varepsilon_{\rm BR}$. So the state with $L/2-1$ roots (so that $m=1$) which are all real and a hole is preferred.

Case B: The boundary field of maximal value is the region $(-h_{\rm cr}^{(2)}, -h_{\rm cr}^{(1)})$
Here we will have a transition from a $m=1$ state (sector $N = L/2-1$) to a $m=0$ state (sector $N=L/2$). This means that a new root comes into play, and from the study of the Ising limit, we see that we are passing to a state where a wide root (whose dressed energy vanishes) is added to the set.

Case C: The boundary field of maximal value is above $-h_{\rm cr}^{(1)}$
There are three possibilities:

- $C1$: The boundary field of maximal value is in the region $(-h_{\rm cr}^{(1)}, h_{\rm cr}^{(1)})$, in which case we have a ground state with magnetization $m=0$, $\frac{L}{2}-1$ real roots and a boundary root corresponding to the boundary field with the higher value.
- $C2$: The boundary field of maximal value is in the region $(h_{\rm cr}^{(1)}, h_{\rm cr}^{(2)})$ and the other field is below $h_{\rm cr}^{(1)}$, we have a ground state with $m=0$, $L/2$ real roots and no hole.
- $C3$: The boundary field of maximal value is above $h_{\rm cr}^{(2)}$ and the other field is below $h_{\rm cr}^{(1)}$. Here, the ground state has magnetization $m=0$, it corresponds to $L/2-1$ real Bethe roots (it fills all available quantum number

spots for real roots) and a boundary root corresponding to the field of maximal value.

The other cases, for which $h_- + h_+ > 0$, can be obtained by symmetry. We summarize these results in the following table:

	m	Real roots	Holes	Complex Roots
A	1	$L/2-1$	1	None
B	$1 \leftrightarrow 0$	$L/2-1$	1	None $\leftrightarrow$ Wide
$C1$	0	$L/2-1$	0	Boundary
$C2$	0	$L/2$	0	None
$C3$	0	$L/2-1$	0	Boundary

Table 8.1 – Root Configurations for the ground state of the even length chain for different values of boundary fields (with $h_+ + h_- \leq 0$). In the B region, there is a transition from a $m = 0$ to a $m = +1$ state. The boundary root, when it is present, corresponds always to the boundary field of maximal value.

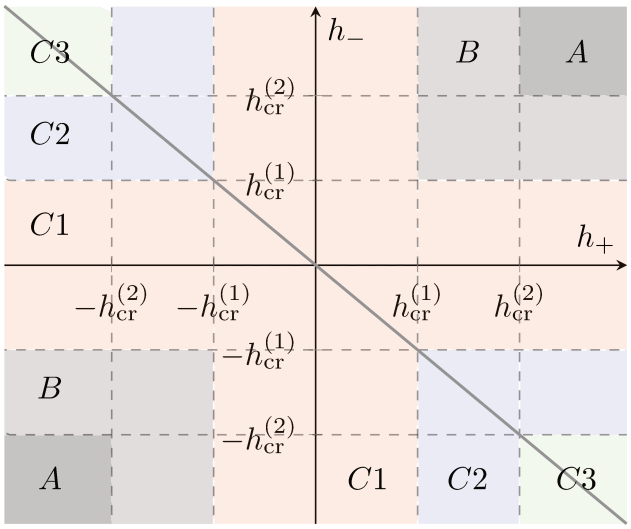

Figure 8.6 – Ground State composition according to the values of the boundary fields. Even length chain. Only in cases C1, C2, C3 there is a gap between the ground state and the rest of the spectrum at the thermodynamic limit.

Odd Chain

In the odd-length case, all Bethe eigenstates (and therefore the ground state) have non-zero magnetization. For $h_+ + h_- < 0$, the ground state is in a sector of magnetization $1/2$ with $N = (L-1)/2$. The corresponding configuration of Bethe roots

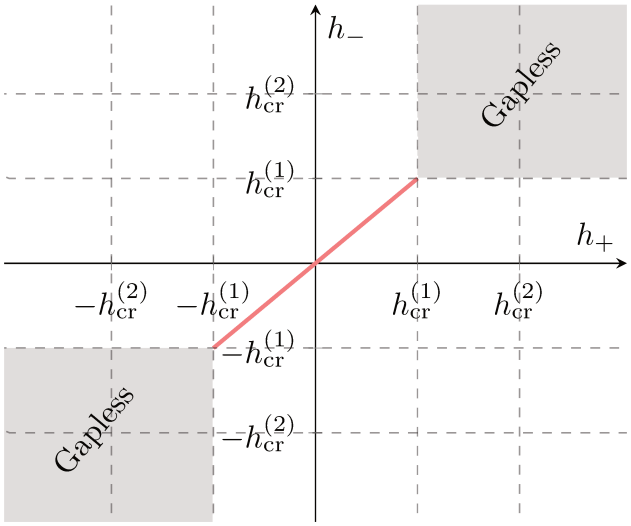

Figure 8.7 – Phase diagram of the Open XXZ chain for $\Delta > 1$ and L even according to the values of the boundary fields. For the shaded regions there is a gapless phase, while the rest of the values present a gap in the low-energy spectrum. The red line indicates the values of $h_\pm$ for which there is a doubly quasi-degenerate ground state.

can be summarized (see Table 8.2) according to the regions schematized as in Figure 8.8. The ground states in the regions where $h_- + h_+ > 0$ are in sectors of negative magnetization $-1/2$ and can be obtained from the previously studied cases by symmetry.

	m	Real roots	Holes	Complex Roots
A	$1/2$	$(L-1)/2$	0	None
B	$1/2$	$(L-1)/2$	1	None
C	$1/2$	$(L-3)/2$	1	Boundary

Table 8.2 – Root Configurations for the ground state of the odd length chain for different values of boundary fields ($h_+ + h_- < 0$). The boundary root, when it is present, corresponds always to the boundary field of maximal value.

Moreover, at $h_+ + h_- = 0$, the magnetization symmetry produces a doubly degenerate spectrum, which is entirely related to the parity of the chain. The two degenerate ground states are in that case in two different magnetization sectors ($m = +1/2$ and $m = -1/2$).

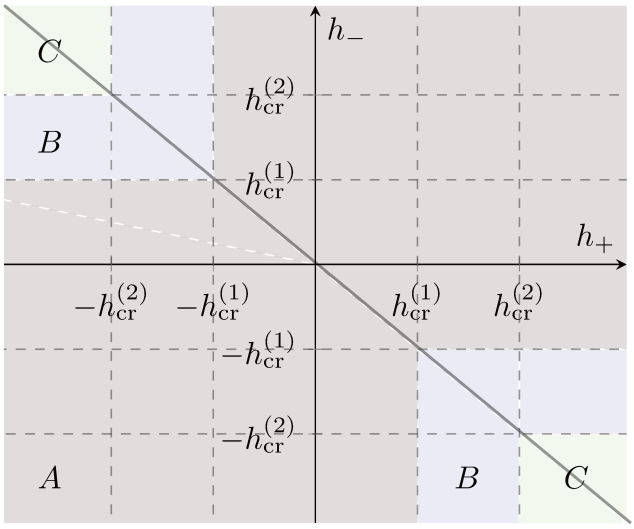

Figure 8.8 – Ground State composition according to the values of the boundary fields. Odd length chain. The gapless region is now switched to a region of opposing boundary fields, while the gapped region (A) is described without boundary roots.

8.3 The two lowest-energy states when $|h_\pm| < \Delta - 1$ in the even chain

In the remaining part of this thesis, we will concentrate more particularly on the regime of the even length chain for which both boundary fields $h_\pm$ are such that $|h_\pm| < h_{\rm cr}^{(1)}$. In this regime, the spectrum is gapped in the thermodynamic limit, and we expect a double quasi-degeneracy of the ground state when $h_+ = h_-$. This regime will be of particular interest for the consideration of the zero-temperature boundary correlation functions at the vicinity of $h_+ = h_-$. Therefore we now investigate more thoroughly the ground state and the first excited state in this regime.

The case $h_+ \neq h_-$

If $h_{\sigma_1} > h_{\sigma_2}$ (with $\{\sigma_1, \sigma_2\} = \{+, -\}$), we have seen that the ground state is the state in the sector $N = \frac{L}{2}$ with $\frac{L}{2} - 1$ real roots with adjacent quantum numbers $n_j = 1, \ldots, \frac{L}{2} - 1$ (no hole) and the boundary root $\alpha_{\rm BR}^{\sigma_1}$. Moreover, it is easy to see from similar arguments that the excited state with lowest energy is the state in the sector $N = \frac{L}{2}$ with $\frac{L}{2} - 1$ real roots with adjacent quantum numbers $n_j = 1, \ldots, \frac{L}{2} - 1$ (no hole) and the boundary root $\alpha_{\rm BR}^{\sigma_2}$.

Let us denote by $\{\alpha^+\}$ and $\{\alpha^-\}$ the two sets of $N = \frac{L}{2}$ Bethe roots corresponding to each of these two states, with $\alpha_1^\pm, \ldots, \alpha_{N-1}^\pm$ being real roots, and

$$\alpha_N^\pm = \alpha_{\rm BR}^\pm = -i(\zeta/2 + \xi_\pm + \epsilon_\pm), \tag{8.51}$$

being the corresponding boundary root. It follows from the study of section 8.1.2 that the deviation $\epsilon_\pm$ is exponentially small in L:

$$\epsilon_\pm = e^{-2L\,F(-i\zeta/2-i\xi_\pm)+O(1)} = O(L^{-\infty}). \tag{8.52}$$

Hence, since $\xi_+ \neq \xi_-$, these two boundary roots remain at finite distance from each other:

$$\alpha_N^+ - \alpha_N^- = \alpha_{\rm BR}^+ - \alpha_{\rm BR}^- = -i(\xi_+ - \xi_- + O(L^{-\infty})), \tag{8.53}$$

so that the difference of energy between these two states remains finite in the thermodynamic limit:

$$E_+ - E_- = \varepsilon(-i\zeta/2 - i\xi_+) - \varepsilon(-i\zeta/2 - i\xi_-) + O(L^{-\infty}). \tag{8.54}$$

Note that there also exists a finite gap of energy between these two states and the remaining part of the spectrum, the latter corresponding to Bethe states with one or more hole(s) and therefore leading to continuous distributions of energy in the thermodynamic limit.

If we denote by $\mathfrak{Z}_\pm$ the counting functions corresponding to these two states, we obtain from (8.28) that

$$\mathfrak{Z}_+(\alpha) - \mathfrak{Z}_-(\alpha) = \frac{1}{L}\left(\mathfrak{Z}_{\alpha_{\rm BR}^+}(\alpha) - \mathfrak{Z}_{\alpha_{\rm BR}^-}(\alpha)\right) + O(L^{-\infty}). \tag{8.55}$$

Hence, using the fact that $\mathfrak{Z}_+(\alpha_j^+) = \mathfrak{Z}_-(\alpha_j^-)$ for $j = 1, \ldots, N-1$,

$$\begin{aligned}\mathfrak{Z}_+(\alpha_j^-) - \mathfrak{Z}_-(\alpha_j^-) &= (\alpha_j^- - \alpha_j^+)\,\mathfrak{Z}_+'(\alpha_j^+) + O\left((\alpha_j^- - \alpha_j^+)^2\right) \\ &= \frac{1}{L}\left(\mathfrak{Z}_{\alpha_{\rm BR}^+}(\alpha_j^-) - \mathfrak{Z}_{\alpha_{\rm BR}^-}(\alpha_j^-)\right) + O(L^{-\infty}),\end{aligned} \tag{8.56}$$

so that the deviation δ_j between the real Bethe roots of the two states is of order $1/L$:

$$\delta_j = \alpha_j^- - \alpha_j^+ = \frac{1}{L}\frac{\mathfrak{Z}_{\alpha_{\rm BR}^+}(\alpha_j^-) - \mathfrak{Z}_{\alpha_{\rm BR}^-}(\alpha_j^-)}{\mathfrak{Z}_+'(\alpha_j^+)} + O(L^{-2}) = O(L^{-1}). \tag{8.57}$$

The ground state degeneracy at $h_+ = h_-$

Let us now consider the particular case $h_- = h_+ = h$, at which the ground state becomes degenerate in the thermodynamic limit. When $h_+ = h_- = h$, namely $\xi_- = \xi_+ = \xi$, the Bethe equations (9.30) contain a zero of second order which is

given by the product of the two field-dependent factors:

$$\left(\frac{\sin(\alpha+i\xi_-+i\zeta/2)}{\sin(\alpha-i\xi_--i\zeta/2)}\right)\left(\frac{\sin(\alpha+i\xi_++i\zeta/2)}{\sin(\alpha-i\xi_+-i\zeta/2)}\right)=\left(\frac{\sin(\alpha+i\xi+i\zeta/2)}{\sin(\alpha-i\xi-i\zeta/2)}\right)^2. \quad (8.58)$$

Let us consider a state, in the sector $N=\frac{L}{2}$, with $N-1$ real roots $\alpha_1,\dots,\alpha_{N-1}$ with adjacent quantum numbers $n_j=1,\dots,N-1$ and a complex root $\alpha_{\rm BR}$ at

$$\alpha_{\rm BR}=-i(\zeta/2+\xi+\epsilon)=-i(\zeta/2-\tilde{\xi}+\epsilon)+\frac{\pi}{2}, \quad (8.59)$$

and let us evaluate more precisely the deviation ϵ of this complex root with respect to the position of the double zero in the large L limit. The Bethe equation (9.30) for the complex root is

$$\left(\frac{\sin(\alpha_{\rm BR}-i\zeta/2)}{\sin(\alpha_{\rm BR}+i\zeta/2)}\right)^{2L}\left(\frac{\sin(\alpha_{\rm BR}+i\xi+i\zeta/2)}{\sin(\alpha_{\rm BR}-i\xi-i\zeta/2)}\right)^2 \times\prod_{k=1}^{N-1}\frac{\sin(\alpha_{\rm BR}-\alpha_k+i\zeta)\,\sin(\alpha_{\rm BR}+\alpha_k+i\zeta)}{\sin(\alpha_{\rm BR}-\alpha_k-i\zeta)\,\sin(\alpha_{\rm BR}+\alpha_k-i\zeta)}=1. \quad (8.60)$$

Hence, using (8.59) and keeping the leading order terms in ϵ, we obtain

$$\left(\frac{\sinh(\zeta+\xi)}{\sinh\xi}\right)^{2L}\left(\frac{\sinh\epsilon}{\sinh(2\xi+\zeta)}\right)^2\exp\big[L\,O(\epsilon)\big] \times\exp\left\{-i\sum_{k=1}^{N-1}\Big[\theta\big(i(\zeta/2+\xi)+\alpha_k\big)+\theta\big(i(\zeta/2+\xi)-\alpha_k\big)\Big]\right\}=1. \quad (8.61)$$

We can now use Corollary 8.23 so as to replace the sum over the real roots in (8.60) by an integral in the large L limit by means of (8.25). It leads to

$$\begin{aligned}\epsilon\,\exp\big[L\,O(\epsilon)\big]&=\pm\Bigg\{\sinh^2(\zeta+2\xi)\left(\frac{\sinh\xi}{\sinh(\zeta+\xi)}\right)^{2L}\\&\quad\times\exp\left[\frac{\theta\big(i(\zeta/2+\xi)+\frac{\pi}{2}\big)+\theta\big(i(\zeta/2+\xi)-\frac{\pi}{2}\big)+2\theta\big(i(\zeta/2+\xi)\big)}{2i}\right]\\&\quad\times\exp\left[\frac{iL}{\pi}\int_{-\frac{\pi}{2}}^{\frac{\pi}{2}}\theta\big(i(\zeta/2+\xi)-x\big)\,\mathfrak{Z}'(x)\,dx\right]\Bigg\}^{1/2}\Big(1+O(L^{-\infty})\Big),\\&=\pm\exp\Big[-L\,F(-i\zeta/2-i\xi)+G(\xi)\Big]\Big(1+O(L^{-\infty})\Big),\end{aligned} \quad (8.62)$$

where $F(-i\zeta/2-i\xi)$ is given by (8.34) and $G(\xi)$ is a term of order 1 when $L\to+\infty$. We recall that $F(-i\zeta/2-i\xi)$ is positive for $|h|<h_{\rm cr}^{(1)}$ (see Fig. 8.9 in which this term

is plotted as a function of the boundary magnetic field h), so that the deviation ϵ is exponentially decreasing in L in this regime, as expected[2]. Moreover, we see from

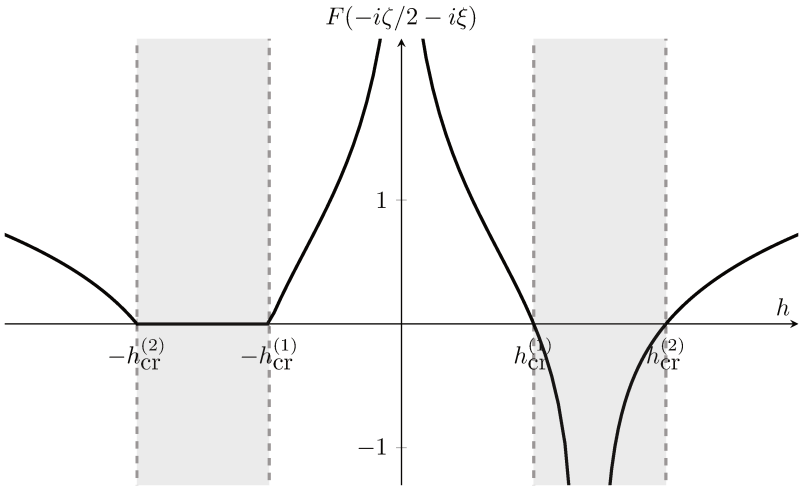

Figure 8.9 – Values of the coefficient $F(-i\zeta/2 - i\xi)$ as a function of the magnetic field h and for $\Delta = 3$ (therefore $h_{\rm cr}^{(1)} = 2$ and $h_{\rm cr}^{(2)} = 4$).

(8.62) that there are two possible choices $\epsilon_\pm$ for the deviation ϵ, corresponding to the two possible choices of the sign in (8.62). Hence there are two different states with $N-1$ real roots $\alpha_1^\pm \dots, \alpha_{N-1}^\pm$ and one boundary complex root $\alpha_{\rm BR}^\pm$, that we shall denote by superscripts: $\boldsymbol{\alpha}^+$ or $\boldsymbol{\alpha}^-$, according to the sign of the leading correction of the complex root in (8.62) (note that the $+$ or $-$ denomination is here not related to the left or right boundary, but only to the fact that there are two different solutions for the complex root position corresponding to the two different signs in (8.62)).

From (8.62), the boundary roots for these two states are exponentially close in L. If we denote by $\mathfrak{Z}_\pm(\cdot)$ the corresponding counting function $\mathfrak{Z}(\,\cdot\,|\boldsymbol{\alpha}^\pm)$, it follows from their decomposition property (8.28) that

$$\mathfrak{Z}_+(\alpha) - \mathfrak{Z}_-(\alpha) = \frac{1}{L}\Big(\mathfrak{Z}_{\alpha_{\rm BR}^+}(\alpha) - \mathfrak{Z}_{\alpha_{\rm BR}^-}(\alpha)\Big) + O(L^{-\infty}) = O(L^{-\infty}). \tag{8.63}$$

Hence, using the fact that $\mathfrak{Z}_+(\alpha_j^+) = \mathfrak{Z}_-(\alpha_j^-)$ for $j = 1, \dots, N-1$, we can deduce from (8.63) that

$$\mathfrak{Z}_+(\alpha_j^-) - \mathfrak{Z}_-(\alpha_j^-) = (\alpha_j^- - \alpha_j^+)\,\mathfrak{Z}'_+(\alpha_j^+) + o(\alpha_j^- - \alpha_j^+) = O(L^{-\infty}), \tag{8.64}$$

so that the real roots of these two states are also exponentially close in L. It moreover follows that the difference of energy between these two states is also exponentially

[2]Note that we more generally recover from Fig. 8.9 the regimes (8.37) of existence of the boundary root ($h \notin [-h_{\rm cr}^{(2)}, -h_{\rm cr}^{(1)}] \cup [h_{\rm cr}^{(1)}, h_{\rm cr}^{(2)}]$) for which $F(-i\zeta/2 - i\xi) < 0$.

small in L:

$$E_+ - E_- = O(L^{-\infty}). \tag{8.65}$$

Furthermore, since other types of states are given by solutions of the Bethe equations with at least one hole, there is a gap of energy between these two quasi-degenerate ground states and the other excited states.

Let us finally remark that the exponential degeneracy at $h_+ = h_-$ and the gap in the spectrum are no longer present in the other regimes. Indeed, in the regimes $h \in (-h_{\rm cr}^{(2)}, -h_{\rm cr}^{(1)})$ and $h < -h_{\rm cr}^{(2)}$, it follows from our previous study that the lowest energy states contain one hole, and that their difference of energy is a direct consequence of the difference of rapidities of the hole.

Chapter 9

Boundary Correlation Functions

In the previous chapter, we have characterized, in terms of Bethe roots, the ground state of the open spin chain (6.1) according to the values of the boundary fields $h_\pm$ and to the parity of the length L. We have seen in particular that the ground state and the first excited state are quasi-degenerate at $h_+ = h_- = h$ within the region $|h_\pm| < \Delta - 1$ for L even. We now use this information to calculate two zero-temperature boundary correlation functions and to evaluate their behavior in the thermodynamic (half-infinite chain) limit: the boundary magnetization and the autocorrelation function of the σ_1^z operator at zero temperature.

The zero-temperature boundary magnetization, i.e., the mean value, in the ground state, of the σ_1^z operator at the first site of the chain,

$$\langle \sigma_1^z \rangle = \langle \mathrm{GS} | \sigma_1^z | \mathrm{GS} \rangle, \tag{9.1}$$

has already been computed as the simplest example of correlation function in [138] (directly in the half-infinite chain limit by the q-vertex operator approach), and in [135] (from the study of the finite chain by Bethe Ansatz). However, the results of [135, 138] for $L \to \infty$ were limited to the case of a null boundary field h_+ at infinity. Here we show that, even in the thermodynamic $L \to \infty$ limit, the boundary magnetization still depends on the boundary field at infinity. This is due to the fact that the characterization of the ground state depends in fact from *both* boundary fields. In particular, for L even, the presence —or not— of a boundary root at the left edge of the chain, which directly affects the value of the boundary magnetization at this edge, depends also from the value of the boundary field at the right edge of the chain. Hence, if h_+ is inside the interval $(-h_{\mathrm{cr}}^{(1)}, h_{\mathrm{cr}}^{(1)})$, the thermodynamic limit of the boundary magnetization, as a function of h_-, is discontinuous at $h_- = h_+$: this is due to the fact that, in the description of the ground state, one changes from a boundary root associated with one edge to a boundary root associated with the

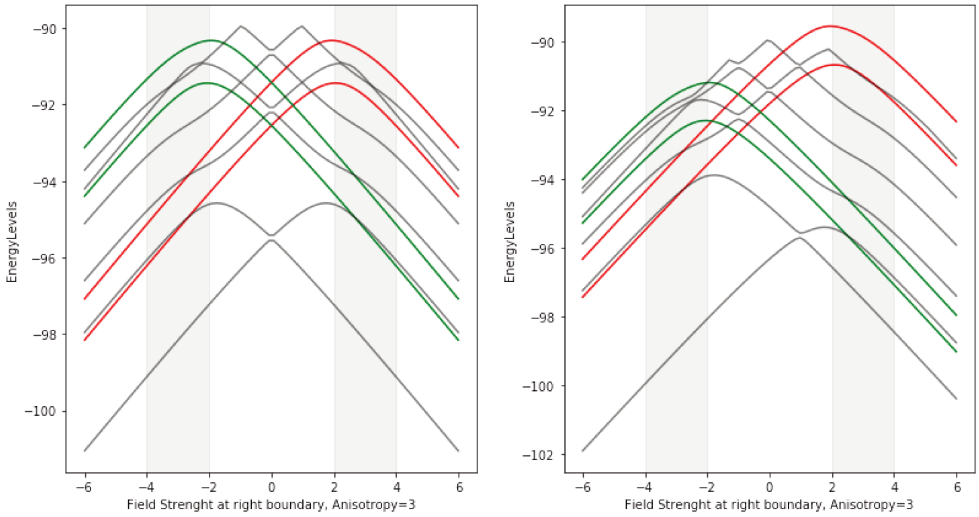

Figure 9.1 – Spectrum of the XXZ chain with open-boundary conditions for a chain of even length and anisotropy $\Delta = 3$. The left-edge field has been fixed to 0 (left) and to 1 (right). We then vary the field at the opposite edge. The lowest states with magnetization ± 1 are colored in red and green while the other states (in gray) have zero magnetization. Notice that when the fields are equal there is a closing in the distance between the two lowest energy states. This distance is exponentially vanishing with system size.

other edge of the chain. The discontinuity is therefore given by the contribution $\langle \sigma_1^z \rangle_{\mathrm{BR}}$ of the left boundary root to the boundary magnetization:

$$\lim_{\substack{h_- \to h_+ \\ h_- < h_+}} \lim_{L\to\infty} \langle \sigma_1^z \rangle - \lim_{\substack{h_- \to h_+ \\ h_- > h_+}} \lim_{L\to\infty} \langle \sigma_1^z \rangle = - \lim_{\substack{h_- \to h_+ \\ h_- > h_+}} \langle \sigma_1^z \rangle_{\mathrm{BR}}.$$
$$= -2 \langle \sigma_1^z \rangle_{\mathrm{BR}} \Big|_{h_- = h_+}. \tag{9.2}$$

At exactly $h_- = h_+$, the boundary root becomes delocalized between the two edges of the chain and contributes equally to the left or the right boundary magnetization, hence the factor 2 in (9.2). For L odd, we also recover a discontinuity at $h_- = -h_+$, but the microscopic mechanism is different: it is due to the change of magnetization sector of the ground state.

We also present in this chapter a computation of the boundary autocorrelation function of σ_1^z. We show in particular that it does not decay to zero in the thermodynamic limit when $h_- = h_+$ and $|h_\pm| < \Delta - 1$ for L even, due to the presence of the two quasi-degenerate ground states at this point. We moreover compute its limiting value and show that it is directly related to the discontinuity of the boundary magnetization.

Since this is a quite technical calculation, let us briefly review the main steps that

will follow. At $T = 0$, the expectation values are calculated uniquely with respect to the ground state, which we write $|\mathrm{GS}\rangle$. Thus, the autocorrelation function can be expanded in the energy eigenbasis as:

$$\begin{aligned}\langle\sigma_1^z(t)\sigma_1^z\rangle\big|_{T=0} &= \langle\mathrm{GS}|\sigma_1^z(t)\sigma_1^z|\mathrm{GS}\rangle \\ &= \sum_{\substack{|n\rangle \\ \text{eigenstates} \\ \text{of } \mathbf{H}}} \langle\mathrm{GS}|e^{iHt}\sigma_1^z e^{-iHt}|n\rangle\langle n|\sigma_1^z|\mathrm{GS}\rangle \\ &= \sum_{|n\rangle} e^{i(E_{\mathrm{GS}}-E_n)t}\langle\mathrm{GS}|\sigma_1^z|n\rangle\langle n|\sigma_1^z|\mathrm{GS}\rangle \\ &= \sum_{[n\rangle} e^{i(E_{\mathrm{GS}}-E_n)t}|\langle n|\sigma_1^z|\mathrm{GS}\rangle|^2\end{aligned} \tag{9.3}$$

where we are expressing the time evolution in the Heisenberg picture: $\sigma_1^z(t) = e^{iHt}\sigma_1^z e^{-iHt}$. As the system size grows, the number of contributing frequencies ($E_{\mathrm{GS}} - E_n$) increases and add up incoherently among them, except for those states which are degenerate with the ground state. If there is a degenerate state $|\widetilde{\mathrm{GS}}\rangle$ *at the thermodynamic limit*, then:

$$\lim_{L\to\infty}\langle\sigma_1^z(t)\sigma_1^z\rangle^c\big|_{T=0} = \lim_{L\to\infty}|\langle\widetilde{\mathrm{GS}}|\sigma_1^z|\mathrm{GS}\rangle|^2 \tag{9.4}$$

where we consider the connected correlation function. Note that this is a time independent function so that it is constant at the long time limit. Since we have found that the lowest states can be expressed with sets of Bethe roots in the ABA framework, we can express the autocorrelation function by using form factors. Let us denote by $|\mathrm{GS}_\sigma, h_\sigma\rangle$, $\sigma \in \{+,-\}$, the two (normalized) quasi-degenerate ground states that we found on the previous section. Then:

$$\lim_{t\to\infty}\lim_{L\to\infty}\lim_{h_-\to h_+}\langle\sigma_1^z(t)\sigma_1^z\rangle^c\big|_{T=0} = \lim_{L\to\infty}\left|\langle\mathrm{GS}_\sigma, h|\sigma_1^z|\mathrm{GS}_{-\sigma}, h\rangle\right|^2 \neq 0. \tag{9.5}$$

Indeed, to see how this non zero result emerges, we place ourselves in the interval of boundary fields where there is quasi-degeneracy, and write the ground states in the representation of the sets of ground-state Bethe roots $\boldsymbol{\alpha}^\pm$:

$$\lim_{t\to\infty}\lim_{L\to\infty}\lim_{h_-\to h_+}\langle\sigma_1^z(t)\sigma_1^z\rangle^c\big|_{T=0} = \left|\frac{\langle\boldsymbol{\alpha}^+|\sigma_1^z|\boldsymbol{\alpha}^-\rangle}{\langle\boldsymbol{\alpha}^+|\boldsymbol{\alpha}^+\rangle^{1/2}\langle\boldsymbol{\alpha}^-|\boldsymbol{\alpha}^-\rangle^{1/2}}\right|^2. \tag{9.6}$$

We rewrite the last expression in terms of two ratios:

$$\lim_{t\to\infty}\lim_{L\to\infty}\lim_{h_-\to h_+}\langle\sigma_1^z(t)\sigma_1^z\rangle^c\big|_{T=0}=\left|\frac{\langle\boldsymbol{\alpha}^+|\boldsymbol{\alpha}^+\rangle}{\langle\boldsymbol{\alpha}^-|\boldsymbol{\alpha}^-\rangle}\right|\left|\frac{\langle\boldsymbol{\alpha}^+|\sigma_1^z|\boldsymbol{\alpha}^-\rangle}{\langle\boldsymbol{\alpha}^+|\boldsymbol{\alpha}^+\rangle}\right|^2. \tag{9.7}$$

We will prove, in (9.66), that the first ratio has an exponentially subleading term:

$$\frac{\langle\boldsymbol{\alpha}^+|\boldsymbol{\alpha}^+\rangle}{\langle\boldsymbol{\alpha}^-|\boldsymbol{\alpha}^-\rangle}=1+\mathrm{O}(L^{-\infty}), \tag{9.8}$$

whereas the second ratio will be shown, in (9.78), to have a finite value in the thermodynamic limit, which is remarkably equal to the boundary root contribution to the boundary magnetization when $\xi_+=\xi_-=\xi$:

$$\frac{\langle\boldsymbol{\alpha}^+|\sigma_1^z|\boldsymbol{\alpha}^-\rangle}{\langle\boldsymbol{\alpha}^+|\boldsymbol{\alpha}^+\rangle}\sim(-\pi i\sinh^2\xi)\,\rho'(-i\zeta/2-i\xi)=-\langle\sigma_1^z\rangle_{\mathrm{BR}}\big|_{\xi_+=\xi_-=\xi} \tag{9.9}$$

The result for the autocorrelation function is then:

$$\lim_{t\to\infty}\lim_{L\to\infty}\lim_{h_-\to h_+}\langle\sigma_1^z(t)\sigma_1^z\rangle^c\big|_{T=0}\sim\left|\langle\sigma_1^z\rangle_{\mathrm{BR}}\big|_{\xi_+=\xi_-=\xi}\right|^2, \tag{9.10}$$

thus relating the entire calculation to that of the boundary magnetization in the semi-infinite chain limit, which we do explicitly in (9.49).

9.1 Computation of the Boundary Form Factors in Finite Volume

The finite-size form factors of local spin operators on the first site of the chain can be computed similarly as in the periodic case [65], by using the solution of the quantum inverse problem on the first site of the chain [136] together with the generalization of Slavnov's determinant representation for the scalar product of boundary Bethe states [134, 135].

The determinant representation for the scalar product of an on-shell $\langle\,\boldsymbol{\lambda}\,|$ with an off-shell $|\,\boldsymbol{\mu}\,\rangle$ Bethe states (7.38) is given by [134, 135]:

$$\begin{aligned}\langle\,\boldsymbol{\lambda}|\boldsymbol{\mu}\,\rangle=&\prod_{j=1}^{N}\left[a(\lambda_j)\,d(-\lambda_j)\,\frac{\sin(2\lambda_j-i\zeta)\sin(2\mu_j-i\zeta)}{\sin(2\mu_j)}\,\frac{\sin(\lambda_j+i\xi_+ +i\frac{\zeta}{2})}{\sin(\lambda_j-i\xi_- -i\frac{\zeta}{2})}\right]\\&\times(-1)^{NL}\prod_{j<k}\left[\frac{\sin(\lambda_j+\lambda_k-i\zeta)}{\sin(\lambda_j+\lambda_k+i\zeta)}\,\frac{1}{\mathfrak{s}(\lambda_j,\lambda_k)\mathfrak{s}(\mu_k,\mu_j)}\right]\mathsf{Det}_N\big[H(\boldsymbol{\lambda},\boldsymbol{\mu})\big],\end{aligned} \tag{9.11}$$

where the elements of the $N \times N$ matrix $H(\boldsymbol{\lambda}, \boldsymbol{\mu})$ are

$$\big[H(\boldsymbol{\lambda}, \boldsymbol{\mu})\big]_{jk} = \frac{\sin(-i\zeta)}{\mathfrak{s}(\mu_k, \lambda_j)} \Bigg[\mathsf{a}(\mu_k) \prod_{\ell \neq j} \mathfrak{s}(\mu_k + i\zeta, \lambda_\ell) - \mathsf{a}(-\mu_k) \prod_{\ell \neq j} \mathfrak{s}(\mu_k - i\zeta, \lambda_\ell) \Bigg], \quad (9.12)$$

and where we have written for brevity

$$\mathsf{a}(\mu) = (\sin(\mu - i\zeta/2))^{2L} \sin(\mu + i[\zeta/2 + \xi_+]) \sin(\mu + i[\zeta/2 + \xi_-]). \quad (9.13)$$

The normalization of a Bethe state is then given by taking the on-shell limit $\mu \to \lambda$:

$$\begin{aligned} \langle \boldsymbol{\lambda} | \boldsymbol{\lambda} \rangle = \prod_{j=1}^{N} \Bigg[\big(\sin(\lambda_j - i\zeta/2) \big)^{2L} \sin(2\lambda_j - i\zeta) \, \frac{\sin(\lambda_j + i[\xi_+ + \frac{\zeta}{2}])}{\sin(\lambda_j - i[\xi_- + \frac{\zeta}{2}])} \Bigg] \\ \times \prod_{j<k} \frac{\sin(\lambda_j + \lambda_k - i\zeta)}{\sin(\lambda_j + \lambda_k + i\zeta)} \prod_{k=1}^{N} \frac{\mathsf{a}(-\lambda_k) \prod_{\ell=1}^{N} \mathfrak{s}(\lambda_k - i\zeta, \lambda_\ell)}{i \sin^2(2\lambda_k) \prod_{\ell \neq k} \mathfrak{s}(\lambda_k, \lambda_\ell)} \, \mathsf{Det}_N \big[\mathcal{M}(\boldsymbol{\lambda}, \boldsymbol{\lambda}) \big]. \quad (9.14) \end{aligned}$$

On the other hand the operator at the edge of the chain can be expressed in terms of the operator entries of the boundary transfer matrix as:

$$\begin{aligned} \sigma_1^z &= \Big[\sin(i\xi_- + \omega + i\zeta/2) \, \mathcal{A}(\omega) - \sin(i\xi_- - \omega - i\zeta/2) \, \mathcal{D}(\omega) \Big] \mathcal{T}(\omega)^{-1} & (9.15) \\ &= 2 \sin(i\xi_- + \omega + i\zeta/2) \, \mathcal{A}(\omega) \, \mathcal{T}(\omega)^{-1} - \mathbb{I}, & (9.16) \end{aligned}$$

where ω is a generic inhomogeneity parameter that should be sent to $-i\zeta/2$ at the end of the computation. We also recall the action of the boundary monodromy matrix element $\mathcal{A}(\omega)$ on an off-shell Bethe state, which follows from the commutation relations that are created by the boundary Yang Baxter equation, (7.34):

$$\mathcal{A}(\omega) \prod_{j=1}^{N} \mathcal{B}(\mu_j) | \, \mathbf{0} \, \rangle = \Omega(\omega | \boldsymbol{\mu}) \prod_{j=1}^{N} \mathcal{B}(\mu_j) | \, \mathbf{0} \, \rangle + \sum_{j=1}^{N} \Omega_j(\omega | \boldsymbol{\mu}) \, \mathcal{B}(\omega) \prod_{\substack{k=1 \\ k \neq j}}^{N} \mathcal{B}(\mu_j) | \, \mathbf{0} \, \rangle. \quad (9.17)$$

with

$$\Omega(\omega|\boldsymbol{\mu}) = \frac{2\,\tau(\omega|\boldsymbol{\mu})}{\sin(i\xi_- + \omega + i\zeta/2)}, \tag{9.18}$$

$$\Omega_j(\omega|\boldsymbol{\mu}) = \frac{\sin(-i\zeta)\sin(2\mu_j - i\zeta)}{\mathfrak{s}(\omega,\mu_j)\sin(2\mu_j)}\left[\frac{\mathsf{a}(\mu_j)\,\sin(\omega+\mu_j+i\zeta)}{\sin(\mu_j+i\xi_-+i\zeta/2)}\prod_{\substack{k=1\\k\neq j}}^{N}\frac{\mathfrak{s}(\mu_j+i\zeta,\mu_k)}{\mathfrak{s}(\mu_j,\mu_k)}\right.$$
$$\left. + \frac{\mathsf{a}(-\mu_j)\,\sin(\omega-\mu_j+i\zeta)}{\sin(\mu_j-i\xi_--i\zeta/2)}\prod_{\substack{k=1\\k\neq j}}^{N}\frac{\mathfrak{s}(\mu_j-i\zeta,\mu_k)}{\mathfrak{s}(\mu_j,\mu_k)}\right], \tag{9.19}$$

The matrix element of the σ_1^z operator between two eigenstates $\langle\,\boldsymbol{\lambda}\,|$ and $|\,\boldsymbol{\mu}\,\rangle$ is therefore

$$\begin{aligned}\langle\,\boldsymbol{\lambda}\,|\,\sigma_1^z\,|\,\boldsymbol{\mu}\,\rangle &= \frac{2\sin(i\xi_- + \omega + i\zeta/2)}{\tau(\xi_1|\boldsymbol{\mu})}\,\langle\,\boldsymbol{\lambda}\,|\,\mathcal{A}(\omega)\,|\,\boldsymbol{\mu}\,\rangle - \langle\,\boldsymbol{\lambda}\,|\,\boldsymbol{\mu}\,\rangle \\ &= 2\sum_{j=1}^{N}\frac{\Omega_j(\omega|\boldsymbol{\mu})}{\Omega(\omega|\boldsymbol{\mu})}\,\langle\,\boldsymbol{\lambda}\,|\,(\boldsymbol{\mu}\setminus\{\mu_j\})\cup\{\omega\}\,\rangle + \langle\,\boldsymbol{\lambda}|\,\boldsymbol{\mu}\,\rangle.\end{aligned} \tag{9.20}$$

The summands are scalar products $\frac{\Omega_j(\omega|\boldsymbol{\mu})}{\Omega(\omega|\boldsymbol{\mu})}\langle\,\boldsymbol{\lambda}\,|\,(\boldsymbol{\mu}\setminus\{\mu_j\})\cup\{\omega\}\,\rangle$ which differ from $\langle\,\boldsymbol{\lambda}\,|\,\boldsymbol{\mu}\,\rangle$ by the prefactors and a change of variable in the j-th column. We can regroup these factors and include them into the j-th column of the corresponding scalar product determinant. We now use the identity

$$\sum_j \mathsf{Det}[H^{(j)}] + \mathsf{Det}[H] = \mathsf{Det}[H + wv^T] \tag{9.21}$$

where $[H^{(j)}]_{\ell m}$ has its j-th column equal to $[H^{(j)}]_{\ell j} = w_\ell v_j$, while the other columns are those of H, $[H^{(j)}]_{\ell,m\neq j} = H_{\ell m}$, for vectors w and v. This results in the following closed expresion for the form factor:

$$\begin{aligned}\langle\,\boldsymbol{\lambda}\,|\,\sigma_1^z\,|\,\boldsymbol{\mu}\,\rangle = \prod_{j=1}^{N}&\left[(\sin(\lambda_j - i\zeta/2))^{2L}\,\frac{\sin(2\lambda_j - i\zeta)\sin(2\mu_j - i\zeta)}{\sin(2\mu_j)}\,\frac{\sin(\lambda_j + i\xi_+ + i\frac{\zeta}{2})}{\sin(\lambda_j - i\xi_- - i\frac{\zeta}{2})}\right] \\ &\times\prod_{j=1}^{N}\frac{\mathfrak{s}(\lambda_j,\xi_1+i\zeta)}{\mathfrak{s}(\mu_j,\xi_1+i\zeta)}\prod_{j<k}\left[\frac{\sin(\lambda_j+\lambda_k-i\zeta)}{\sin(\lambda_j+\lambda_k+i\zeta)}\,\frac{1}{\mathfrak{s}(\lambda_j,\lambda_k)\mathfrak{s}(\mu_k,\mu_j)}\right] \\ &\times\mathsf{Det}_N\big[H(\boldsymbol{\lambda},\boldsymbol{\mu}) - 2P(\boldsymbol{\lambda},\boldsymbol{\mu})\big],\end{aligned} \tag{9.22}$$

where $H(\boldsymbol{\lambda},\boldsymbol{\mu})$ is the matrix (9.12) and $P(\boldsymbol{\lambda},\boldsymbol{\mu})$ is a rank one matrix[1] with elements

$$\big[P(\boldsymbol{\lambda},\boldsymbol{\mu})\big]_{jk} = \mathsf{a}(-\mu_k)\prod_{\ell\neq k}\mathfrak{s}(\mu_k-i\zeta,\mu_\ell)\left[\frac{\sin(\mu_k-\omega-i\zeta)}{\sin(\mu_k-i\xi_--i\frac{\zeta}{2})}-\frac{\sin(\mu_k+\omega+i\zeta)}{\sin(\mu_k+i\xi_-+i\frac{\zeta}{2})}\right] \\ \times\sin(\omega+i\xi_-+i\zeta/2)\,\frac{\sin^2(-i\zeta)}{\mathfrak{s}(\omega+i\zeta,\lambda_j)\,\mathfrak{s}(\omega,\lambda_j)}. \quad (9.23)$$

So as to express the determinant in a more convenient form before taking the thermodynamic limit, let us introduce, as in [139], an $N\times N$ matrix $\mathcal{X}(\boldsymbol{\lambda},\boldsymbol{\mu})$ with elements

$$\big[\mathcal{X}(\boldsymbol{\lambda},\boldsymbol{\mu})\big]_{ij} = \frac{1}{\mathfrak{s}(\mu_i,\lambda_j)}\frac{\prod_{\ell=1}^N\mathfrak{s}(\lambda_j,\mu_\ell)}{\prod_{\ell\neq j}\mathfrak{s}(\lambda_j,\lambda_\ell)}. \quad (9.24)$$

Its determinant is

$$\mathsf{Det}\big[\mathcal{X}(\boldsymbol{\lambda},\boldsymbol{\mu})\big] = (-1)^N\prod_{j>k}\frac{\mathfrak{s}(\mu_k,\mu_j)}{\mathfrak{s}(\lambda_k,\lambda_j)}. \quad (9.25)$$

Multiplying and dividing (9.22) by $\mathsf{Det}[\mathcal{X}(\boldsymbol{\lambda},\boldsymbol{\mu})]$, computing the matrices $\mathcal{X}H$ and $\mathcal{X}P$, and factorizing the quantity

$$i^N\prod_{k=1}^N\frac{\mathsf{a}(-\mu_k)\prod_{\ell=1}^N\mathfrak{s}(\mu_k-i\zeta,\mu_\ell)}{\sin(2\mu_k)\,\sin(2\mu_k-i\zeta)} \quad (9.26)$$

outside of the determinant, we obtain:

$$\langle\,\boldsymbol{\lambda}\,|\,\sigma_1^z\,|\,\boldsymbol{\mu}\,\rangle = \prod_{j=1}^N\left[(\sin(\lambda_j-i\zeta/2))^{2L}\,\sin(2\lambda_j-i\zeta)\,\frac{\sin(\lambda_j+i\xi_++i\frac{\zeta}{2})}{\sin(\lambda_j-i\xi_--i\frac{\zeta}{2})}\right] \\ \times\prod_{j<k}\frac{\sin(\lambda_j+\lambda_k-i\zeta)}{\sin(\lambda_j+\lambda_k+i\zeta)}\prod_{k=1}^N\frac{\mathsf{a}(-\mu_k)\,\prod_{\ell=1}^N\mathfrak{s}(\mu_k-i\zeta,\mu_\ell)}{i\sin^2(2\mu_k)\,\prod_{\ell\neq k}\mathfrak{s}(\mu_k,\mu_\ell)} \\ \times\,\mathsf{Det}_N\big[\mathcal{M}(\boldsymbol{\lambda},\boldsymbol{\mu})-2\mathcal{P}(\boldsymbol{\lambda},\boldsymbol{\mu})\big], \quad (9.27)$$

[1] which implies it can be written as $P=wv^T$, for vectors w,v

with

$$\big[\mathcal{M}(\boldsymbol{\lambda},\boldsymbol{\mu})\big]_{jk} = i\delta_{jk}\,\sin(2\mu_j)\,\frac{\prod_{\ell\neq j}\mathfrak{s}(\mu_j,\mu_\ell)}{\prod_{\ell=1}^{N}\mathfrak{s}(\mu_j,\lambda_\ell)}\prod_{\ell=1}^{N}\frac{\mathfrak{s}(\mu_j-i\zeta,\lambda_\ell)}{\mathfrak{s}(\mu_j-i\zeta,\mu_\ell)}\,\big[\mathfrak{a}(\mu_j|\boldsymbol{\lambda})-1\big]$$
$$-\,i\sin(2\mu_j)\left[\frac{\mathfrak{a}(\mu_k|\boldsymbol{\mu})}{\mathfrak{s}(\mu_k-i\zeta,\mu_j)}-\frac{1}{\mathfrak{s}(\mu_k+i\zeta,\mu_j)}\right], \tag{9.28}$$

$$\big[\mathcal{P}(\boldsymbol{\lambda},\boldsymbol{\mu})\big]_{jk} = -i\sin(\omega+i\xi_-+i\zeta/2)\left[\frac{\sin(\mu_k-\omega-i\zeta)}{\sin(\mu_k-i\xi_--i\frac{\zeta}{2})}-\frac{\sin(\mu_k+\omega+i\zeta)}{\sin(\mu_k+i\xi_-+i\frac{\zeta}{2})}\right]$$
$$\times\,\frac{\sin(2\mu_j)}{\sin(2\omega+i\zeta)}\left[\frac{\prod_{\ell\neq j}\mathfrak{s}(\omega,\mu_\ell)}{\prod_{\ell=1}^{N}\mathfrak{s}(\omega,\lambda_\ell)}-\frac{\prod_{\ell\neq j}\mathfrak{s}(\omega+i\zeta,\mu_\ell)}{\prod_{\ell=1}^{N}\mathfrak{s}(\omega+i\zeta,\lambda_\ell)}\right], \tag{9.29}$$

(notice the difference between (9.23) and (9.29)) in which we have defined

$$\mathfrak{a}(\mu|\boldsymbol{\nu}) = \frac{\mathsf{a}(\mu)}{\mathsf{a}(-\mu)}\frac{\sin(i\zeta-2\mu)}{\sin(i\zeta+2\mu)}\prod_{\ell=1}^{N}\frac{\mathfrak{s}(\mu+i\zeta,\nu_\ell)}{\mathfrak{s}(\mu-i\zeta,\nu_\ell)}. \tag{9.30}$$

Using the Bethe equations for $\boldsymbol{\mu}$ and taking the homogeneous limit $\omega\to -i\zeta/2$, we can rewrite (9.28) and (9.29) using the functions that compose the logarithmic Bethe equations:

$$\big[\mathcal{M}(\boldsymbol{\lambda},\boldsymbol{\mu})\big]_{jk} = i\,\delta_{jk}\,\sin(2\mu_j)\,\frac{\prod_{\ell\neq j}\mathfrak{s}(\mu_j,\mu_\ell)}{\prod_{\ell=1}^{N}\mathfrak{s}(\mu_j,\lambda_\ell)}\prod_{\ell=1}^{N}\frac{\mathfrak{s}(\mu_j-i\zeta,\lambda_\ell)}{\mathfrak{s}(\mu_j-i\zeta,\mu_\ell)}\,\big[\mathfrak{a}(\mu_j|\boldsymbol{\lambda})-1\big]$$
$$-\,2\pi\big[K(\mu_j-\mu_k)-K(\mu_j+\mu_k)\big], \tag{9.31}$$

$$\big[\mathcal{P}(\boldsymbol{\lambda},\boldsymbol{\mu})\big]_{jk} = -i\sinh\xi_-\left[\frac{\sin(\mu_k-i\frac{\zeta}{2})}{\sin(\mu_k-i[\xi_-+\frac{\zeta}{2}])}-\frac{\sin(\mu_k+i\frac{\zeta}{2})}{\sin(\mu_k+i[\xi_-+\frac{\zeta}{2}])}\right]$$
$$\times\,\frac{\sin(2\mu_j)}{\mathfrak{s}(\mu_j,i\frac{\zeta}{2})}\prod_{\ell=1}^{N}\frac{\mathfrak{s}(\mu_\ell,i\frac{\zeta}{2})}{\mathfrak{s}(\lambda_\ell,i\frac{\zeta}{2})}\left[\sum_{\ell=1}^{N}[p'(\mu_\ell)-p'(\lambda_\ell)]-p'(\mu_j)\right]. \tag{9.32}$$

The matrix $\mathcal{M}(\boldsymbol{\lambda},\boldsymbol{\lambda})$ can be written as:

$$\big[\mathcal{M}(\boldsymbol{\lambda},\boldsymbol{\lambda})\big]_{jk} = -2L\,\delta_{jk}\,\mathfrak{Z}'(\lambda_j|\boldsymbol{\lambda})-2\pi\big[K(\lambda_j-\lambda_k)-K(\lambda_j+\lambda_k)\big], \tag{9.33}$$

in which we have used the definition of the counting function $\mathfrak{Z}$ defined in (8.21). Equations (9.33),(9.32) thus express the form factor (9.27) in a manageable form before taking the thermodynamic limit.

9.2 Form Factors in the thermodynamic limit: the even-length open chain

We now compute the thermodynamic limit $L \to \infty$ (L even) of the expression for the boundary form factor of σ_1^z obtained in the previous section in two particular cases. We first consider the case of the boundary magnetization (i.e., both Bethe states coincide with each other and with the ground state) for generic values of the boundary magnetic fields. We then consider the form factor between the two states of lowest energy in the regime $|h_\pm| < h_{\rm cr}^{(1)}$: when $h_+ \neq h_-$, we show that this form factor vanishes exponentially fast with L whereas, for $h_+ = h_- = h$, it tends to a finite value which gives the large time limit of the boundary spin-spin autocorrelation function (9.5).

9.2.1 Boundary magnetization in the ground state

Let us first explain how to obtain from (9.27) the value of the boundary magnetization in the thermodynamic limit, namely the mean value $\langle\, \sigma_1^z \,\rangle$ in the ground state. This quantity has already been computed by different methods for $T = 0$ and $h_+ = 0$ in [135, 137, 138], and for finite T in [142], together with [143] where the boundary free energy was obtained for generic boundary conditions at one edge of the chain. It is relevant to see how one can derive it directly from the finite-size form factor by taking into account the precise large-L structure of the Bethe roots for the ground state that we have obtained in the previous section. We shall see in particular that, since this structure depends on *both* boundary fields (and therefore also on the right boundary field h_+ at infinity), so does the large-L limit of the boundary magnetization.

From the expressions (9.27) and (9.14), the mean value of the operator σ_1^z in an eigenstate $|\, \boldsymbol{\lambda} \,\rangle$ is

$$\begin{aligned} \frac{\langle\, \boldsymbol{\lambda} \,|\, \sigma_1^z \,|\, \boldsymbol{\lambda} \,\rangle}{\langle\, \boldsymbol{\lambda} | \boldsymbol{\lambda} \,\rangle} &= \frac{\mathsf{Det}_N[\mathcal{M}(\boldsymbol{\lambda},\boldsymbol{\lambda}) - 2\mathcal{P}(\boldsymbol{\lambda},\boldsymbol{\lambda})]}{\mathsf{Det}_N \mathcal{M}(\boldsymbol{\lambda},\boldsymbol{\lambda})} \\ &= 1 - 2\,\mathsf{Tr}\left[\mathcal{M}(\boldsymbol{\lambda},\boldsymbol{\lambda})^{-1} \cdot \mathcal{P}(\boldsymbol{\lambda},\boldsymbol{\lambda})\right], \end{aligned} \tag{9.34}$$

in which $\mathcal{M}(\boldsymbol{\lambda},\boldsymbol{\lambda})$ is given by (9.33), and $\mathcal{P}(\boldsymbol{\lambda},\boldsymbol{\lambda})$ by (see (9.32))

$$\left[\mathcal{P}(\boldsymbol{\lambda},\boldsymbol{\lambda})\right]_{jk} = p''(\lambda_j)\, \mathsf{v}(\lambda_k) \tag{9.35}$$

where p'' is the derivative of the function defined in (8.11) and

$$\begin{aligned}\mathsf{v}(\lambda) &= i\sinh\xi_-\left[\frac{\sin(\lambda+i\frac{\zeta}{2})}{\sin(\lambda+i\xi_-+i\frac{\zeta}{2})}-\frac{\sin(\lambda-i\frac{\zeta}{2})}{\sin(\lambda-i\xi_--i\frac{\zeta}{2})}\right]\\ &= \frac{\sinh^2\xi_-\,\sin(2\lambda)}{\sin(\lambda-i\xi_--i\frac{\zeta}{2})\,\sin(\lambda+i\xi_-+i\frac{\zeta}{2})}.\end{aligned} \tag{9.36}$$

Let us now particularise the state $|\,\boldsymbol{\lambda}\,\rangle$ in (9.34) to be the ground state of the open XXZ spin chain. We denote by $\boldsymbol{\alpha}=\{\alpha_1,\dots,\alpha_N\}$ the corresponding Bethe roots of the ground state. From the results of the previous chapter, either all N Bethe roots are real, or $N-1$ of them are real whereas one of them, say α_N, is an isolated complex root. We need then to compute the following trace in the thermodynamic limit:

$$\begin{aligned}\mathsf{Tr}\left[\mathcal{M}(\boldsymbol{\alpha},\boldsymbol{\alpha})^{-1}\cdot\mathcal{P}(\boldsymbol{\alpha},\boldsymbol{\alpha})\right] &= \sum_{j,k=1}^{N}\left[\mathcal{M}(\boldsymbol{\alpha},\boldsymbol{\alpha})^{-1}\right]_{kj}\left[\mathcal{P}(\boldsymbol{\alpha},\boldsymbol{\alpha})\right]_{jk}\\ &= \sum_{j,k=1}^{N}\left[\mathcal{M}(\boldsymbol{\alpha},\boldsymbol{\alpha})^{-1}\right]_{kj}p''(\alpha_j)\,\mathsf{v}(\alpha_k)\\ &= \sum_{k=1}^{N}\mathsf{u}(\alpha_k)\,\mathsf{v}(\alpha_k),\end{aligned} \tag{9.37}$$

in which the vector $(\mathsf{u}(\alpha_1),\dots,\mathsf{u}(\alpha_N))$ is obtained as the result of the action of the matrix $\mathcal{M}(\boldsymbol{\alpha},\boldsymbol{\alpha})^{-1}$ on the vector $(p''(\alpha_1),\dots,p''(\alpha_N))$, i.e., is such that

$$\sum_{\ell=1}^{N}[\mathcal{M}(\boldsymbol{\alpha},\boldsymbol{\alpha})]_{j\ell}\,\mathsf{u}(\alpha_\ell)=p''(\alpha_j),\qquad 1\le j\le N. \tag{9.38}$$

Let us suppose that this vector can be obtained from an odd π-periodic function u (so that in particular $\mathsf{u}(0)=\mathsf{u}(\frac{\pi}{2})=0$) which is moreover $\mathcal{C}^\infty$ on the real axis. Then we can use our Corollary, Eq. (8.23), to change the sum over real roots into

an integral in the left hand side of (9.38). It gives

$$\begin{aligned}
&\sum_{\ell=1}^{N}[\mathcal{M}(\boldsymbol{\alpha},\boldsymbol{\alpha})]_{j\ell}\,\mathsf{u}(\alpha_\ell)\\
&\quad= -2L\,\mathfrak{Z}'(\alpha_j|\boldsymbol{\alpha})\,\mathsf{u}(\alpha_j) - 2\pi\sum_{\ell=1}^{N}\big[K(\alpha_j-\alpha_\ell)-K(\alpha_j+\alpha_\ell)\big]\,\mathsf{u}(\alpha_\ell)\\
&\quad= -2L\Bigg\{\mathfrak{Z}'(\alpha_j|\boldsymbol{\alpha})\,\mathsf{u}(\alpha_j) + \int_{-\frac{\pi}{2}}^{\frac{\pi}{2}} K(\alpha_j-\nu)\,\mathfrak{Z}'(\nu|\boldsymbol{\alpha})\,\mathsf{u}(\nu)\,d\nu\\
&\qquad + \frac{\pi}{L}\sum_{\ell\in\mathfrak{C}}\big[K(\alpha_j-\alpha_\ell)-K(\alpha_j+\alpha_\ell)\big]\,\mathsf{u}(\alpha_\ell)\\
&\qquad - \frac{\pi}{L}\sum_{\ell=1}^{n_{\rm holes}}\big[K(\alpha_j-\check\alpha_{h_\ell})-K(\alpha_j+\check\alpha_{h_\ell})\big]\,\mathsf{u}(\check\alpha_{h_\ell}) + O(L^{-\infty})\Bigg\}.
\end{aligned}\tag{9.39}$$

Note that, in the case of the ground state that we consider here, the set of complex roots is either empty or equal to α_N, and the number of holes $n_{\rm holes}$ is either 0 or 1. It is easy to solve (9.38) at leading order in L, by noticing that the function p'' can be obtained as

$$p''(\alpha) = \pi\rho'(\alpha) + \pi\int_{-\frac{\pi}{2}}^{\frac{\pi}{2}} K(\alpha-\nu)\,\rho'(\nu)\,d\nu,\tag{9.40}$$

in terms of the derivative ρ' of the function (8.6), see (8.5). Therefore, the u solving (9.38) is of the form

$$\mathsf{u}(\alpha) = -\frac{\pi}{2L\,\mathfrak{Z}'(\alpha|\boldsymbol{\alpha})}\left[\rho'(\alpha)+\mathsf{u}_1(\alpha)\right],\tag{9.41}$$

where $\mathsf{u}_1(\alpha)$ is a correction of order $O(\frac{1}{L})$ (or even of order $O(L^{-\infty})$ if the ground state does neither contain a complex root nor a hole). Note that the leading term in (9.41) is indeed an odd π-periodic meromorphic function with no pole on the real axis. Hence, combining this result with (9.37), we obtain that

$$\begin{aligned}
\mathsf{Tr}\left[\mathcal{M}(\boldsymbol{\alpha},\boldsymbol{\alpha})^{-1}\cdot\mathcal{P}(\boldsymbol{\alpha},\boldsymbol{\alpha})\right] &= -\frac{\pi}{2L}\sum_{k=1}^{N}\frac{\rho'(\alpha_k)+\mathsf{u}_1(\alpha_k)}{\mathfrak{Z}'(\alpha_k|\boldsymbol{\alpha})}\,\mathsf{v}(\alpha_k)\\
&= -\frac{1}{4}\int_{-\frac{\pi}{2}}^{\frac{\pi}{2}}\left[\rho'(\alpha)+\mathsf{u}_1(\alpha)\right]\mathsf{v}(\alpha)\,d\alpha + \frac{\pi}{2L}\sum_{j=1}^{n_{\rm holes}}\frac{\rho'(\check\alpha_{h_j})+\mathsf{u}_1(\check\alpha_{h_j})}{\mathfrak{Z}'(\check\alpha_{h_j}|\boldsymbol{\alpha})}\,\mathsf{v}(\check\alpha_{h_j})\\
&\quad - \frac{\pi}{2L}\sum_{k\in\mathfrak{C}}\frac{\rho'(\alpha_k)+\mathsf{u}_1(\alpha_k)}{\mathfrak{Z}'(\alpha_k|\boldsymbol{\alpha})}\,\mathsf{v}(\alpha_k) + O(L^{-\infty}),
\end{aligned}\tag{9.42}$$

in which we have again replaced the sum over real roots by integrals. Note that the

contributions of the complex root and/or hole vanish in the thermodynamic limit $L \to \infty$, except for the case of the boundary root $\alpha^-_{\rm BR} = -i(\zeta/2+\xi_-+\epsilon_-)$ for which the coefficient $\mathsf{v}(\alpha^-_{\rm BR})$ (defined in (9.36)) diverges as the inverse of the boundary root deviation ϵ_-:

$$\mathsf{v}(\alpha^-_{\rm BR}) = i\,\frac{\sinh^2\xi_-}{\epsilon_-}\,\big(1+O(\epsilon_-)\big). \tag{9.43}$$

This divergence is compensated in (9.42) by the fact that the function $2L\,\mathfrak{Z}'$ itself diverges at $\alpha^-_{\rm BR}$, via the contribution $g'(\alpha^-_{\rm BR})$, as the inverse of the boundary root deviation ϵ_-:

$$2L\,\mathfrak{Z}'(\alpha^-_{\rm BR}) = \frac{1+\delta_{\xi_+,\xi_-}}{\epsilon_-}\,\big(1+O(\epsilon_-)\big). \tag{9.44}$$

In other words, the divergence in (9.43) is compensated by a divergence of the same order in the last row of the matrix $\mathcal{M}(\boldsymbol{\alpha},\boldsymbol{\alpha})$ (9.33) if $\alpha_N = \alpha^-_{\rm BR}$:

$$[\mathcal{M}(\boldsymbol{\alpha},\boldsymbol{\alpha})]_{Nk} = -\frac{1}{\epsilon_-}\,\big[(1+\delta_{\xi_-,\xi_+})\,\delta_{Nk} + O(\epsilon_-)\big]. \tag{9.45}$$

The presence of the factor $(1+\delta_{\xi_-,\xi_+})$ in (9.44) or in (9.45), which is equal to 1 when the two boundary fields are different and to 2 when they are equal, is due to the fact that the term g', see eq. (8.11), is summed over the two boundary fields: hence, when the latter are equal, the boundary root approaches a pole for both factors. Finally,

$$\lim_{L\to\infty} \mathsf{Tr}\,\big[\mathcal{M}(\boldsymbol{\alpha},\boldsymbol{\alpha})^{-1}\cdot\mathcal{P}(\boldsymbol{\alpha},\boldsymbol{\alpha})\big] = -\frac{1}{4}\int_{-\frac{\pi}{2}}^{\frac{\pi}{2}} \rho'(\alpha)\,\mathsf{v}(\alpha)\,d\alpha \\ - \delta_{\alpha_N,\alpha^-_{\rm BR}}\,\frac{i\pi\,\sinh^2\xi_-}{1+\delta_{\xi_-,\xi_+}}\,\rho'(\alpha^-_{\rm BR}), \tag{9.46}$$

in which the symbol $\delta_{\alpha_N,\alpha^-_{\rm BR}}$ indicates that the last term exists only when one of the Bethe roots (and by convention the last one) coincides with the boundary root $\alpha^-_{\rm BR}$.

Hence, the thermodynamic limit of the boundary magnetization in the ground state is given by

$$\lim_{L\to\infty} \langle\,\sigma^z_1\,\rangle = \langle\,\sigma^z_1\,\rangle_0 + \langle\,\sigma^z_1\,\rangle_{\rm BR}, \tag{9.47}$$

where $\langle\,\sigma^z_1\,\rangle_0$ denotes the contribution given by the dense distribution of real roots, which is

$$\langle\,\sigma^z_1\,\rangle_0 = 1 + \frac{\sinh^2\xi_-}{2}\int_{-\frac{\pi}{2}}^{\frac{\pi}{2}} \frac{\sin(2\alpha)}{\sin^2(\alpha)+\sinh^2(\frac{\zeta}{2}+\xi_-)}\,\rho'(\alpha)\,d\alpha, \tag{9.48}$$

whereas $\langle\,\sigma^z_1\,\rangle_{\rm BR}$ denotes the possible contribution from the boundary root $\alpha^-_{\rm BR}$ given

by

$$\langle\, \sigma_1^z \,\rangle_{\rm BR} = \mathtt{H}(h_-, h_+)\, \frac{2\pi i\, \sinh^2 \xi_-}{1+\delta_{\xi_-,\xi_+}}\, \rho'(-i(\zeta/2+\xi_-)). \tag{9.49}$$

Here we have introduced the function $\mathtt{H}(h_-, h_+)$ which is 1 when the boundary root $\alpha_{\rm BR}^-$ belongs to the set of Bethe roots parametrizing the ground state, and 0 otherwise. Note that the presence of the boundary root $\alpha_{\rm BR}^+$ does not play a direct role here, since it does not correspond to a divergence in the form factor. However, we have seen in the previous chapter that the presence of the boundary root $\alpha_{\rm BR}^-$ in the set of roots for the ground state depends in fact on the value of *both* boundary magnetic fields, so that the value of the boundary magnetization depends also indirectly on the boundary field h_+ at infinity in the thermodynamic limit through the function $\mathtt{H}(h_-, h_+)$ (see Fig. 9.2 for few specific evaluations and for a comparison with numerical data).

For instance, if $|h_+| < h_{\rm cr}^{(1)}$, then $\mathtt{H}(h_-, h_+) = 0$ if $h_- < h_+$ or if $h_- \in [h_{\rm cr}^{(1)}, h_{\rm cr}^{(2)}]$, and $\mathtt{H}(h_-, h_+) = 1$ otherwise. Hence the thermodynamic limit of the boundary magnetization presents, at $h_- = h_+$, a discontinuity corresponding to the boundary root contribution (9.49):

$$\begin{aligned}
\lim_{h_- - h_+ \to 0^-} \lim_{L\to\infty} \langle\, \sigma_1^z \,\rangle - \lim_{h_- - h_+ \to 0^+} \lim_{L\to\infty} \langle\, \sigma_1^z \,\rangle &= - \lim_{h_- - h_+ \to 0^+} \langle\, \sigma_1^z \,\rangle_{\rm BR} \\
&= -2 \langle\, \sigma_1^z \,\rangle_{\rm BR} \Big|_{h_-=h_+} \\
&= -2i\pi\, \sinh^2 \xi_-\, \rho'(-i(\zeta/2+\xi_-)) \\
&= 2 \prod_{n=1}^{\infty} \frac{\left(1-q^{2n}\right)^4 \left(1-e^{4\tilde{\xi}_-} q^{2(2n-1)}\right) \left(1-e^{-4\tilde{\xi}_-} q^{2(2n-1)}\right)}{\left(1-q^{2(2n-1)}\right)^2 \left(1+e^{2\tilde{\xi}_-} q^{2n}\right)^2 \left(1+e^{-2\tilde{\xi}_-} q^{2n}\right)^2},
\end{aligned} \tag{9.50}$$

which vanishes in the limit $h_+ \to \pm h_{\rm cr}^{(1)}$. We recall that $q = e^{-\zeta}$, and that the boundary fields are parametrized in this regime $|h_\pm| < h_{\rm cr}^{(1)}$ as $h_\pm = \sinh\zeta\, \tanh\tilde{\xi}_\pm$. Note that the difference between taking the limit of equal field and evaluating at exactly the same field is given by the factor $1+\delta_{\xi_-,\xi_+}$ in the contribution (9.49) from the boundary root. In our convention we indeed have

$$\lim_{h_- - h_+ \to 0} \frac{1}{1+\delta_{\xi_-,\xi_+}} = 1, \qquad \frac{1}{1+\delta_{\xi_-,\xi_+}}\Big|_{h_-=h_+} = \frac{1}{2}. \tag{9.51}$$

If instead $h_+ < -h_{\rm cr}^{(1)}$, then $\mathtt{H}(h_-, h_+) = 0$ for $h_- < 0$ or $h_- \in [h_{\rm cr}^{(1)}, h_{\rm cr}^{(2)}]$, and $\mathtt{H}(h_-, h_+) = 1$ otherwise. In that case the thermodynamic limit of the boundary magnetization is continuous at $h_- = h_+$. By symmetry of the model under the reversal of all spins and change of sign of the boundary fields, this is also the case when $h_+ > h_{\rm cr}^{(1)}$. In the latter case, we can more precisely use the symmetry relation:

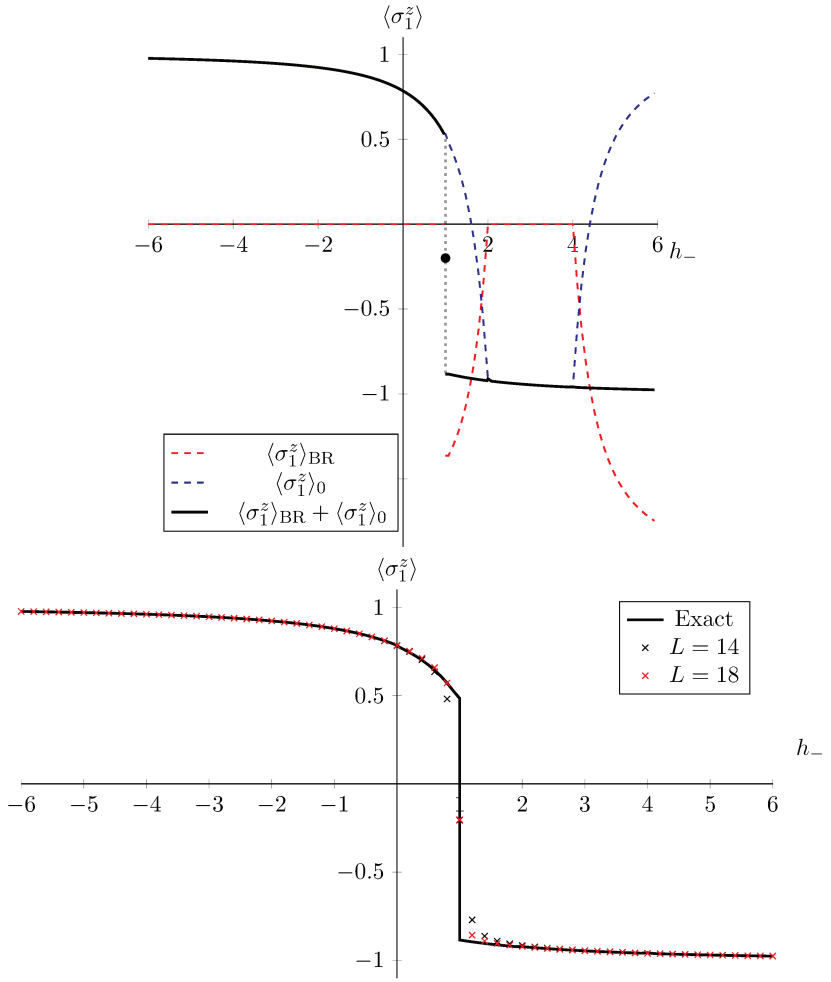

Figure 9.2 – Contribution of the boundary root to the boundary magnetization for L even. *Above:* Mechanism by which the boundary root acts in the boundary magnetization, for the case $\Delta = 3$ and $h_+ = 1$. The blue line shows the contributions of the real roots to this quantity, as a density of roots (9.48). The red line shows the contribution of the boundary root (9.49), which for the example only belongs to the ground state for $h_- \geq 1$, and $h_- \notin [h_{\mathrm{cr}}^{(1)}, h_{\mathrm{cr}}^{(2)}]$. *Below:* Comparison of numerical exact diagonalization to the analytical results obtained for the boundary magnetization. Notice how the thermodynamic limit preserves the information about the field at the h_+ boundary as a jump in the magnetization at the opposite boundary.

$$\langle\,\sigma_1^z\,\rangle\Big|_{h_-,h_+} = -\langle\,\sigma_1^z\,\rangle\Big|_{-h_-,-h_+}, \tag{9.52}$$

in particular when the ground state has negative magnetization.

The integral in (9.48) can be computed by closing the integration contour on the lower half-plane and evaluating the corresponding residues. It gives

$$\begin{aligned}\langle\,\sigma_1^z\,\rangle_0 = -i\pi\,\sinh^2\xi_-\,\rho'\big(-i|\zeta/2-\tilde{\xi}_-|+\delta_-\pi/2\big)\\ +\sinh^2\xi_-\sum_{n=1}^{+\infty}(-1)^n\left[\frac{1}{\sinh^2(n\zeta+\xi_-)}-\frac{1}{\sinh^2(n\zeta-\xi_-)}\right].\end{aligned} \tag{9.53}$$

It follows in particular from (9.53) that

$$\begin{aligned}\langle\,\sigma_1^z\,\rangle_0\Big|_{h_-}+\langle\,\sigma_1^z\,\rangle_0\Big|_{-h_-} = -i\pi\,\sinh^2\xi_-\,\Big[\rho'(-i|\zeta/2-\tilde{\xi}_-|+\delta_-\pi/2)\\ +\rho'(-i|\zeta/2+\tilde{\xi}_-|+\delta_-\pi/2)\Big],\end{aligned} \tag{9.54}$$

so that the expression (9.47)–(9.49) can in fact be written in the following more compact form, which is valid for all values of the boundary magnetic fields $h_\pm$ (including cases for which the ground state has magnetization -1):

$$\lim_{L\to\infty}\langle\,\sigma_1^z\,\rangle = \langle\,\sigma_1^z\,\rangle_0 + \Theta_{h_-,h_+}\,2\pi i\,\sinh^2\xi_-\,\rho'(-i(\zeta/2+\xi_-)), \tag{9.55}$$

where

$$\Theta_{h_-,h_+} = \begin{cases} 1 & \text{if}\quad \max(-h_{\rm cr}^{(1)},h_+) < h_- < h_{\rm cr}^{(1)} \quad\text{or}\quad h_{\rm cr}^{(2)} < h_-,\\ \frac{1}{2} & \text{if}\quad h_- = h_+ \quad\text{and}\quad |h_\pm| < h_{\rm cr}^{(1)},\\ 0 & \text{otherwise.}\end{cases} \tag{9.56}$$

Notice that, at $h_- = h_+ = 0$ (i.e., for $\xi_+ = \xi_- = i\pi/2$), we have

$$\langle\,\sigma_1^z\,\rangle_0\Big|_{h_-=h_+=0} = -\langle\,\sigma_1^z\,\rangle_{\rm BR}\Big|_{h_-=h_+=0}, \tag{9.57}$$

so that

$$\lim_{L\to\infty}\langle\,\sigma_1^z\,\rangle\Big|_{h_-=h_+=0} = 0, \tag{9.58}$$

as it should be. Moreover, due to the factor δ_{ξ_-,ξ_+} in the contribution (9.49) of the

boundary root, we have the relation

$$\lim_{h_-\to 0^\pm}\lim_{h_+\to 0}\lim_{L\to\infty}\langle\,\sigma_1^z\,\rangle = \pm\langle\,\sigma_1^z\,\rangle_{\rm BR}\Big|_{h_-=h_+=0}$$
$$= \mp i\pi\,\rho'(-i\zeta/2+\pi/2) = \mp\prod_{n=1}^{+\infty}\left(\frac{1-q^{2n}}{1+q^{2n}}\right)^4, \qquad (9.59)$$

which corresponds (up to the sign) to the square of the bulk magnetization [144], as already noticed in [138], and as studied also in [142, 143] for the finite-temperature case in the framework of the Quantum Transfer Matrix method. Note that the study of this section is general for $T=0$, namely, we consider any value of the two boundary fields.

9.2.2 The form factor between the two states of lowest energy for $|h_\pm| < h_{\rm cr}^{(1)}$

We now consider the form factor of the σ_1^z operator between the two states of lowest energy in the regime $|h_\pm| < h_{\rm cr}^{(1)}$, which is relevant for the computation of the boundary autocorrelation function. Since in this regime these two states are separated by a gap from the (continuum of the) other excited states in the thermodynamic limit, this form factor gives the only possible non-zero contribution to the large-time limit of the connected boundary autocorrelation function $\langle\,\sigma_1^z(t)\,\sigma_1^z\,\rangle^c_{T=0}$.

The case $h_- = h_+$

We here work directly in the regime $h_- = h_+ = h$ (namely $\xi_- = \xi_+ = \xi$) and we write the form factor between the two quasi-degenerate ground states as

$$\langle\,{\rm GS}_1, h\,|\,\sigma_1^z\,|\,{\rm GS}_2, h\,\rangle = \frac{\langle\,\boldsymbol{\alpha}^+\,|\,\sigma_1^z\,|\,\boldsymbol{\alpha}^-\,\rangle}{\langle\,\boldsymbol{\alpha}^+\,|\,\boldsymbol{\alpha}^+\,\rangle^{1/2}\,\langle\,\boldsymbol{\alpha}^-\,|\,\boldsymbol{\alpha}^-\,\rangle^{1/2}},$$
$$= \left(\frac{\langle\,\boldsymbol{\alpha}^+\,|\,\boldsymbol{\alpha}^+\,\rangle}{\langle\,\boldsymbol{\alpha}^-\,|\,\boldsymbol{\alpha}^-\,\rangle}\right)^{1/2}\frac{\langle\,\boldsymbol{\alpha}^+\,|\,\sigma_1^z\,|\,\boldsymbol{\alpha}^-\,\rangle}{\langle\,\boldsymbol{\alpha}^+\,|\,\boldsymbol{\alpha}^+\,\rangle}, \qquad (9.60)$$

which can be expressed by means of (9.27) and (9.14). In (9.60), $\boldsymbol{\alpha}_+$ and $\boldsymbol{\alpha}_-$ denote the two sets of Bethe roots associated with the two quasi-degenerate ground states identified in the previous section.

Let us first consider the first ratio. We recall that the Bethe roots of the two states only differ by exponentially small corrections in L,

$$\alpha_j^+ - \alpha_j^- = O(L^{-\infty}), \qquad 1\le j\le N, \qquad (9.61)$$

so that most of the prefactors in (9.14) simplify up to exponentially small corrections in L:

$$\frac{\langle\, \boldsymbol{\alpha}^+ \,|\, \boldsymbol{\alpha}^+ \,\rangle}{\langle\, \boldsymbol{\alpha}^- \,|\, \boldsymbol{\alpha}^- \,\rangle} = \frac{\sin(\alpha_N^+ + i\xi + i\frac{\zeta}{2})}{\sin(\alpha_N^- + i\xi + i\frac{\zeta}{2})} \frac{\mathsf{Det}_N\big[\mathcal{M}(\boldsymbol{\alpha}^+, \boldsymbol{\alpha}^+)\big]}{\mathsf{Det}_N\big[\mathcal{M}(\boldsymbol{\alpha}^-, \boldsymbol{\alpha}^-)\big]} + O(L^{-\infty}),$$
$$= -\frac{\mathsf{Det}_N\big[\mathcal{M}(\boldsymbol{\alpha}^+, \boldsymbol{\alpha}^+)\big]}{\mathsf{Det}_N\big[\mathcal{M}(\boldsymbol{\alpha}^-, \boldsymbol{\alpha}^-)\big]} + O(L^{-\infty}). \tag{9.62}$$

Here we have explicitly used that the two boundary complex roots $\alpha_N^\pm \equiv \alpha_{\mathrm{BR}}^\pm$ are of the form

$$\alpha_N^\pm = -i(\zeta/2 + \xi + \epsilon_\pm) \qquad \text{with} \quad \epsilon_\pm = \pm\epsilon\,(1 + O(L^{-\infty})), \tag{9.63}$$

see (8.62). Moreover, it follows from (9.33) that

$$\big[\mathcal{M}(\boldsymbol{\alpha}^+, \boldsymbol{\alpha}^+)\big]_{jk} = \big[\mathcal{M}(\boldsymbol{\alpha}^-, \boldsymbol{\alpha}^-)\big]_{jk} + O(L^{-\infty}), \tag{9.64}$$

for each row such that $\alpha_j^\pm$ are real roots, i.e., for $1 \le j \le N-1$. The N-th row has to be treated separately since in that case the complex root $\alpha_N^\pm$ approaches, with an exponentially small deviation $\epsilon_\pm \sim \pm\epsilon$, the double pole of the function g' (8.11) so that the corresponding diagonal coefficient is exponentially diverging with L, see (9.45), and we have

$$\big[\mathcal{M}(\boldsymbol{\alpha}^+, \boldsymbol{\alpha}^+)\big]_{NN} = -\big[\mathcal{M}(\boldsymbol{\alpha}^-, \boldsymbol{\alpha}^-)\big]_{NN} \big(1 + O(L^{-\infty})\big), \tag{9.65}$$

whereas the off-diagonal coefficients $\big[\mathcal{M}(\boldsymbol{\alpha}^\pm, \boldsymbol{\alpha}^\pm)\big]_{Nk}$ with $k \neq N$ remain finite (and therefore are exponentially subleading with respect to (9.65)). Finally, we obtain from (9.62), (9.64) and (9.65) that

$$\frac{\langle\, \boldsymbol{\alpha}^+ \,|\, \boldsymbol{\alpha}^+ \,\rangle}{\langle\, \boldsymbol{\alpha}^- \,|\, \boldsymbol{\alpha}^- \,\rangle} = 1 + O(L^{-\infty}). \tag{9.66}$$

Let us now consider the second ratio in (9.60). Using again (9.61) to simplify the prefactors, and the identity (9.21) to decompose the determinant in the numerator, we obtain that

$$\frac{\langle\, \boldsymbol{\alpha}^+ \,|\, \sigma_1^z \,|\, \boldsymbol{\alpha}^- \,\rangle}{\langle\, \boldsymbol{\alpha}^+ \,|\, \boldsymbol{\alpha}^+ \,\rangle} = \frac{\mathsf{Det}_N\big[\mathcal{M}(\boldsymbol{\alpha}^+, \boldsymbol{\alpha}^-) - 2\mathcal{P}(\boldsymbol{\alpha}^+, \boldsymbol{\alpha}^-)\big]}{\mathsf{Det}_N\big[\mathcal{M}(\boldsymbol{\alpha}^+, \boldsymbol{\alpha}^+)\big]} + O(L^{-\infty})$$
$$= \frac{\mathsf{Det}_N\big[\mathcal{M}(\boldsymbol{\alpha}^+, \boldsymbol{\alpha}^-)\big]}{\mathsf{Det}_N\big[\mathcal{M}(\boldsymbol{\alpha}^+, \boldsymbol{\alpha}^+)\big]} - 2\sum_{\ell=1}^{N} \frac{\mathsf{Det}_N\big[\widetilde{\mathcal{M}}^{(\ell)}(\boldsymbol{\alpha}^+, \boldsymbol{\alpha}^-)\big]}{\mathsf{Det}_N\big[\mathcal{M}(\boldsymbol{\alpha}^+, \boldsymbol{\alpha}^+)\big]}$$
$$+ O(L^{-\infty}), \tag{9.67}$$

where

$$\big[\widetilde{\mathcal{M}}^{(\ell)}(\boldsymbol{\alpha}^+,\boldsymbol{\alpha}^-)\big]_{jk} = \big[\mathcal{M}(\boldsymbol{\alpha}^+,\boldsymbol{\alpha}^-)\big]_{jk} \quad \text{if} \quad k\neq\ell, \tag{9.68}$$

$$\big[\widetilde{\mathcal{M}}^{(\ell)}(\boldsymbol{\alpha}^+,\boldsymbol{\alpha}^-)\big]_{j\ell} = \big[\mathcal{P}(\boldsymbol{\alpha}^+,\boldsymbol{\alpha}^-)\big]_{j\ell}. \tag{9.69}$$

Note that, from the orthogonality property of two different Bethe states, the first term in (9.67) should in fact vanish. For the rest of terms we rewrite the numerators, using (9.61) and the definitions (9.31) and (9.32). The case $k=\ell$ gives:

$$\begin{aligned}\big[\mathcal{P}(\boldsymbol{\alpha}^+,\boldsymbol{\alpha}^-)\big]_{j\ell} &= \big[\mathcal{P}(\boldsymbol{\alpha}^-,\boldsymbol{\alpha}^-)\big]_{j\ell}\big(1+O(L^{-\infty})\\ &= p''(\alpha_j^+)\,\mathfrak{v}(\alpha_\ell^-)\,\big(1+O(L^{-\infty})\big),\end{aligned} \tag{9.70}$$

whereas $k\neq\ell$ gives:

$$\begin{aligned}\big[\mathcal{M}(\boldsymbol{\alpha}^+,\boldsymbol{\alpha}^-)\big]_{jk} = i\,\delta_{jk}\,\frac{\mathfrak{a}(\alpha_j^-|\boldsymbol{\alpha}^+)-\mathfrak{a}(\alpha_j^+|\boldsymbol{\alpha}^+)}{\alpha_j^- - \alpha_j^+}\big(1+O(L^{-\infty})\big)\\ -2\pi\big[K(\alpha_j^- - \alpha_k^-) - K(\alpha_j^- + \alpha_k^-)\big].\end{aligned} \tag{9.71}$$

Now, if $\alpha_j^\pm$ are real roots ($j<N$), we obtain that

$$\begin{aligned}\big[\mathcal{M}(\boldsymbol{\alpha}^+,\boldsymbol{\alpha}^-)\big]_{jk} &= i\,\delta_{jk}\,\mathfrak{a}'(\alpha_j^+|\boldsymbol{\alpha}^+)\big(1+O(L^{-\infty})\big)\\ &\qquad -2\pi\big[K(\alpha_j^- - \alpha_k^-) - K(\alpha_j^- + \alpha_k^-)\big]\\ &= \big[\mathcal{M}(\boldsymbol{\alpha}^+,\boldsymbol{\alpha}^+)\big]_{jk} + O(L^{-\infty}),\end{aligned} \tag{9.72}$$

so that we recover for the first $N-1$ rows the elements of the Gaudin matrix (9.33) up to exponentially small corrections in L. The row $j=N$ has to be treated separately since the two complex roots $\alpha_N^\pm$ are, in the leading order, symmetrically distributed around a zero of the function $\mathfrak{a}$ (see (9.63)). We write only the result, referring to [141] for full details about how it is obtained:

$$\begin{aligned}\big[\mathcal{M}(\boldsymbol{\alpha}^+,\boldsymbol{\alpha}^-)\big]_{Nk} = -\delta_{Nk}\Big\{&2Lp'(\alpha_N^-) + \widetilde{g}'(\alpha_N^-) - 2\theta'(2\alpha_N^-)\\ &+\sum_{k=1}^{N}\big[\theta'(\alpha_N^- - \alpha_k^-) + \theta'(\alpha_N^- + \alpha_k^-)\big]\Big\}\big(1+O(L^{-\infty})\big)\\ &-2\pi\big[K(\alpha_N^- - \alpha_k^-) - K(\alpha_N^- + \alpha_k^-)\big],\end{aligned} \tag{9.73}$$

in which we have defined

$$\widetilde{g}'(\alpha) = 2i\,\frac{\cos(\alpha - i\xi - i\zeta/2)}{\sin(\alpha - i\xi - i\zeta/2)}. \tag{9.74}$$

Notice that, contrary to what happens for the Gaudin matrix $\mathcal{M}(\boldsymbol{\alpha}^+, \boldsymbol{\alpha}^+)$ in the denominator of (9.67) (see (9.45)), there is no singularity in this last row associated with the complex root. Hence, in (9.67), all terms but the one with $\ell = N$ vanish as ϵ (i.e., exponentially fast with L) in the large L limit due to the fact that $\mathsf{Det}_N\big[\mathcal{M}(\boldsymbol{\alpha}^+, \boldsymbol{\alpha}^+)\big]$ diverges as $1/\epsilon$. The only term in the sum (9.67) which does not vanish is the term with $\ell = N$, since the corresponding matrix elements of $\mathcal{P}(\boldsymbol{\alpha}^+, \boldsymbol{\alpha}^-)$ themselves diverge as $1/\epsilon$. Therefore

$$\begin{aligned}
\frac{\langle\, \boldsymbol{\alpha}^+ \,|\, \sigma_1^z \,|\, \boldsymbol{\alpha}^- \,\rangle}{\langle\, \boldsymbol{\alpha}^+ \,|\, \boldsymbol{\alpha}^+ \,\rangle} &= -2\mathsf{Det}_N\big[\mathcal{M}(\boldsymbol{\alpha}^+, \boldsymbol{\alpha}^+)^{-1} \cdot \widetilde{\mathcal{M}}^{(N)}(\boldsymbol{\alpha}^+, \boldsymbol{\alpha}^-)\big] + O(L^{-\infty}) \\
&= -2\sum_{k=1}^{N} \big[\mathcal{M}(\boldsymbol{\alpha}^+, \boldsymbol{\alpha}^+)^{-1}\big]_{Nk} \big[\mathcal{P}(\boldsymbol{\alpha}^+, \boldsymbol{\alpha}^-)\big]_{kN} + O(L^{-\infty}) \\
&= -2\sum_{k=1}^{N} \big[\mathcal{M}(\boldsymbol{\alpha}^+, \boldsymbol{\alpha}^+)^{-1}\big]_{Nk} p''(\alpha_k^+)\, \mathsf{v}(\alpha_N^-) + O(L^{-\infty}) \\
&= -2\,\mathsf{u}(\alpha_N^+)\,\mathsf{v}(\alpha_N^-) + O(L^{-\infty}),
\end{aligned} \tag{9.75}$$

in which

$$\mathsf{u}(\alpha_N^+) \underset{L\to+\infty}{\sim} -\frac{\epsilon\,\pi}{2}\,\rho'(-i\zeta/2 - i\xi), \tag{9.76}$$

$$\mathsf{v}(\alpha_N^-) \underset{L\to+\infty}{\sim} -i\frac{\sinh^2\xi}{\epsilon}, \tag{9.77}$$

so that

$$\frac{\langle\, \boldsymbol{\alpha}^+ \,|\, \sigma_1^z \,|\, \boldsymbol{\alpha}^- \,\rangle}{\langle\, \boldsymbol{\alpha}^+ \,|\, \boldsymbol{\alpha}^+ \,\rangle} \underset{L\to+\infty}{\sim} -\pi\, i \sinh^2\xi\ \rho'(-i\zeta/2 - i\xi). \tag{9.78}$$

Note that this is equal (up to the sign) to the contribution $\langle\, \sigma_1^z \,\rangle_{\mathrm{BR}}$ to the boundary magnetization from the boundary root when $\xi_- = \xi_+ = \xi$, see eq. (9.49).

Finally,

$$\begin{aligned}
\lim_{L\to\infty} \langle\, \mathrm{GS}_1, h \,|\, \sigma_1^z \,|\, \mathrm{GS}_2, h \,\rangle &= -\pi\, i \sinh^2\xi\ \rho'(-i\zeta/2 - i\xi) = -\langle\, \sigma_1^z \,\rangle_{\mathrm{BR}}\Big|_{\xi_+=\xi_-=\xi} \\
&= \prod_{n=1}^{\infty} \frac{\big(1-q^{2n}\big)^4 \big(1 - e^{4\tilde{\xi}_-} q^{2(2n-1)}\big)\big(1 - e^{-4\tilde{\xi}_-} q^{2(2n-1)}\big)}{\big(1-q^{2(2n-1)}\big)^2 \big(1 + e^{2\tilde{\xi}_-} q^{2n}\big)^2 \big(1 + e^{-2\tilde{\xi}_-} q^{2n}\big)^2},
\end{aligned} \tag{9.79}$$

which is exactly half of the discontinuity of the boundary magnetization at $h_+ = h_-$, see (9.50).

The case $h_- \neq h_+$

As soon as the two boundary fields are different, the degeneracy of the ground state is broken and the two states with $\frac{L}{2}-1$ real roots and one boundary root have different energy (see previous chapter). We show here that the form factor between these two states decays exponentially with the system size L, so that the thermodynamic limit of the boundary autocorrelation function effectively vanishes in the large time limit.

It is more convenient to consider the square of the form factor,

$$\frac{\langle\, \boldsymbol{\alpha}^+ \,|\, \sigma_1^z \,|\, \boldsymbol{\alpha}^- \,\rangle \langle\, \boldsymbol{\alpha}^- \,|\, \sigma_1^z \,|\, \boldsymbol{\alpha}^+ \,\rangle}{\langle\, \boldsymbol{\alpha}^- \,|\, \boldsymbol{\alpha}^- \,\rangle \langle\, \boldsymbol{\alpha}^+ \,|\, \boldsymbol{\alpha}^+ \,\rangle} = \frac{\mathsf{Det}_N\big[\mathcal{M}(\boldsymbol{\alpha}^+,\boldsymbol{\alpha}^-) - 2\mathcal{P}(\boldsymbol{\alpha}^+,\boldsymbol{\alpha}^-)\big]}{\mathsf{Det}_N\big[\mathcal{M}(\boldsymbol{\alpha}^-,\boldsymbol{\alpha}^-)\big]} \times \frac{\mathsf{Det}_N\big[\mathcal{M}(\boldsymbol{\alpha}^-,\boldsymbol{\alpha}^+) - 2\mathcal{P}(\boldsymbol{\alpha}^-,\boldsymbol{\alpha}^+)\big]}{\mathsf{Det}_N\big[\mathcal{M}(\boldsymbol{\alpha}^+,\boldsymbol{\alpha}^+)\big]}, \quad (9.80)$$

which enters the expression for the spin auto-correlation function. As previously, we use the fact that $\mathcal{P}(\boldsymbol{\alpha}^{-\sigma},\boldsymbol{\alpha}^{\sigma})$ for $\sigma \in \{+,-\}$ is a rank-one matrix to write

$$\frac{\mathsf{Det}_N\big[\mathcal{M}(\boldsymbol{\alpha}^{-\sigma},\boldsymbol{\alpha}^{\sigma}) - 2\mathcal{P}(\boldsymbol{\alpha}^{-\sigma},\boldsymbol{\alpha}^{\sigma})\big]}{\mathsf{Det}_N\big[\mathcal{M}(\boldsymbol{\alpha}^{\sigma},\boldsymbol{\alpha}^{\sigma})\big]} = \frac{\mathsf{Det}_N\big[\mathcal{M}(\boldsymbol{\alpha}^{-\sigma},\boldsymbol{\alpha}^{\sigma})\big]}{\mathsf{Det}_N\big[\mathcal{M}(\boldsymbol{\alpha}^{\sigma},\boldsymbol{\alpha}^{\sigma})\big]} - 2\sum_{\ell=1}^{N} \frac{\mathsf{Det}_N\big[\widetilde{\mathcal{M}}^{(\ell)}(\boldsymbol{\alpha}^{-\sigma},\boldsymbol{\alpha}^{\sigma})\big]}{\mathsf{Det}_N\big[\mathcal{M}(\boldsymbol{\alpha}^{\sigma},\boldsymbol{\alpha}^{\sigma})\big]}, \quad (9.81)$$

where

$$\big[\widetilde{\mathcal{M}}^{(\ell)}(\boldsymbol{\alpha}^{-\sigma},\boldsymbol{\alpha}^{\sigma})\big]_{jk} = \big[\mathcal{M}(\boldsymbol{\alpha}^{-\sigma},\boldsymbol{\alpha}^{\sigma})\big]_{jk} \quad \text{if} \quad k \neq \ell, \quad (9.82)$$

$$\big[\widetilde{\mathcal{M}}^{(\ell)}(\boldsymbol{\alpha}^{-\sigma},\boldsymbol{\alpha}^{\sigma})\big]_{j\ell} = \big[\mathcal{P}(\boldsymbol{\alpha}^{-\sigma},\boldsymbol{\alpha}^{\sigma})\big]_{j\ell}, \quad (9.83)$$

with the first term in the sum (9.81) vanishing due to the orthogonality property of two different Bethe states.

We need to evaluate the order of the different determinants appearing in (9.81). We begin by using the counting functions $\mathfrak{Z}_\pm$ defined above (8.63) and the Gaudin matrix (9.33):

$$[\mathcal{M}(\boldsymbol{\alpha}^{\sigma},\boldsymbol{\alpha}^{\sigma})]_{jk} = -2L\,\mathfrak{Z}'_\sigma(\alpha_j^\sigma)\left\{\delta_{jk} + \frac{\pi}{L}\,\frac{K(\alpha_j^\sigma-\alpha_k^\sigma) - K(\alpha_j^\sigma+\alpha_k^\sigma)}{\mathfrak{Z}'_\sigma(\alpha_j^\sigma)}\right\} + O(L^{-\infty}), \qquad j \neq N, \quad (9.84)$$

$$[\mathcal{M}(\boldsymbol{\alpha}^{\sigma},\boldsymbol{\alpha}^{\sigma})]_{Nk} = -\frac{1}{\epsilon_\sigma}\left[(1+\delta_{\xi_-,\xi_+})\,\delta_{Nk} + O(\epsilon_\sigma)\right], \quad (9.85)$$

so that the determinant of $\mathcal{M}(\boldsymbol{\alpha}^{\sigma},\boldsymbol{\alpha}^{\sigma})$ is of order $\frac{L^{N-1}}{\epsilon_\sigma}$ in the large L limit.

The behavior of the matrix elements of $\mathcal{M}(\boldsymbol{\alpha}^{-\sigma}, \boldsymbol{\alpha}^{\sigma})$, which is given by the expression (9.31), is also of order L except for $j = N$ for which it remains finite (a detailed explanation can be found in our paper [141]). Finally, it is also easy to see that the matrix elements $\left[\mathcal{P}(\boldsymbol{\alpha}^{-\sigma}, \boldsymbol{\alpha}^{\sigma})\right]_{jk}$ all remain finite, except for $\sigma = -$ and $k = N$ since $\left[\mathcal{P}(\boldsymbol{\alpha}^{+}, \boldsymbol{\alpha}^{-})\right]_{jN}$ diverges as $1/\epsilon_{-}$.

Therefore, all terms with $\ell < N$ in the sum (9.81) vanish exponentially fast with L in the large L limit, due to the extra divergence in $1/\epsilon_{\sigma}$ of the Gaudin determinant $\mathsf{Det}_N\left[\mathcal{M}(\boldsymbol{\alpha}^{\sigma}, \boldsymbol{\alpha}^{\sigma})\right]$ in the denominator with respect to the numerator $\mathsf{Det}_N\left[\widetilde{\mathcal{M}}^{(\ell)}(\boldsymbol{\alpha}^{-\sigma}, \boldsymbol{\alpha}^{\sigma})\right]$. The only term that does not vanish is the one with $\ell = N$ and for $\sigma = -$, since the corresponding matrix elements of $\mathcal{P}(\boldsymbol{\alpha}^{+}, \boldsymbol{\alpha}^{-})$ also diverges as $1/\epsilon_{-}$, which compensates the divergence in the denominator. However, if $\sigma = +$, the extra divergence in $1/\epsilon_{+}$ in the denominator is not compensated even in the last term of (9.81), so that the product (9.80) vanishes as ϵ_{+}, i.e., exponentially fast with L.

Conclusion: boundary autocorrelation in the even-length case

We have therefore shown here that, in the regime $|h_{\pm}| < h_{\mathrm{cr}}^{(1)}$, the thermodynamic limit of the connected boundary autocorrelation function decays to zero for $h_{-} \neq h_{+}$:

$$\lim_{t\to\infty} \lim_{L\to\infty} \langle \sigma_1^z(t)\sigma_1^z \rangle^c \big|_{T=0,\, h_{-}\neq h_{+}} = 0. \tag{9.86}$$

This is due to the vanishing of the boundary form factor of the σ_1^z operator between the ground state and the first excited state in the thermodynamic limit. Indeed, these two states, being separated from the continuum of the other states by a gap in the thermodynamic limit, provide the only possible non-zero contribution to (9.86).

On the contrary, when we are exactly at $h_{-} = h_{+}$ (still in the regime $|h_{\pm}| < h_{\mathrm{cr}}^{(1)}$), the thermodynamic limit of the connected boundary autocorrelation function no longer decays to zero. We have shown that it is directly related to the discontinuity of the boundary magnetization at this point or, in other terms, to the boundary root contribution to the boundary magnetization:

$$\begin{aligned} \lim_{t\to\infty} \lim_{L\to\infty} \langle \sigma_1^z(t)\sigma_1^z \rangle^c \big|_{T=0,\, h_{-}=h_{+}} &= \left| \langle \sigma_1^z \rangle_{\mathrm{BR}} \big|_{\xi_{+}=\xi_{-}=\xi} \right|^2, \\ &= \pi^2 \, \sinh^4 \xi \, |\rho'(-i\zeta/2 - i\xi)|^2. \end{aligned} \tag{9.87}$$

This is due to the non-vanishing contribution, in the thermodynamic limit, of the boundary form factor of the σ_1^z operator between the ground state and the first excited state (which in that case is quasi-degenerate with the ground state), these two states being separated from the continuum of the other states by a gap in the

thermodynamic limit.

9.3 Form factors in the thermodynamic limit: the odd-length open chain

Let us now consider the computation of the boundary magnetization and boundary autocorrelation in the odd length case.

As we have seen in the previous chapter, the description of the ground state and its degeneracies are very different in the odd length case compared to the even length case. The Bethe eigenstates (and therefore the ground state(s)) of a chain of odd length L always have a finite magnetization. Moreover, we no longer have quasi-degenerate ground states for $h_+ = h_- \neq 0$; instead, due to the spin-flip symmetry, there exists an *exact* degeneracy of the whole spectrum at $h_+ = -h_-$, but the two ground states are in this case in different magnetization sectors $m = +1/2$ and $m = -1/2$. Hence, the change of parity of the length of the chain has some drastic effect on the microscopic description of the spectrum. We can nevertheless expect to observe a similar behavior in the thermodynamic limit for the chain with L odd and antiparallel boundary fields and for the chain with L even and parallel boundary fields.

9.3.1 Boundary magnetization in the ground state

If $h_+ + h_- < 0$, i.e., $h_- < -h_+$, the boundary magnetization in the ground state is

$$\langle\, \sigma_1^z \,\rangle = \langle\, \mathrm{GS}_+ \,|\, \sigma_1^z \,|\, \mathrm{GS}_+ \,\rangle, \tag{9.88}$$

where $|\, \mathrm{GS}_+ \,\rangle$ is the normalized ground state with magnetization $+1/2$ which is described in subsection 8.2.2. The boundary magnetization is therefore in this case still given in the thermodynamic limit by the formulas (9.47), (9.48) and (9.49), the only difference being in the value of the factor H_{h_-,h_+}, i.e., in the dependance of the presence of the boundary root α_{BR}^- in the set of Bethe roots for the ground state with respect to the boundary fields $h_\pm$. In the present case, $H_{h_-,h_+} = 1$ only if $h_- > h_{\mathrm{cr}}^{(2)}$, which may happen only if $h_+ < -h_{\mathrm{cr}}^{(2)}$ (so that the condition $h_+ + h_- < 0$ is still satisfied).

One can obtain the value of the boundary magnetization in the case $h_- > -h_+$,

by symmetry from the previous case by means of formula (9.52):

$$\begin{aligned}\langle\,\sigma_1^z\,\rangle\Big|_{\substack{h_-,h_+\\ h_->-h_+}} &= \langle\,\mathrm{GS}_-\,|\,\sigma_1^z\,|\,\mathrm{GS}_-\,\rangle\Big|_{h_-,h_+}\\ &= -\langle\,\mathrm{GS}_+\,|\,\sigma_1^z\,|\,\mathrm{GS}_+\,\rangle\Big|_{-h_-,-h_+}\end{aligned}\tag{9.89}$$

where $|\,\mathrm{GS}_-\,\rangle$ is the normalized state of magnetization $-1/2$ which is the ground state if $h_- + h_+ > 0$. We can therefore expect to have, even for finite odd L, a discontinuity of the boundary magnetization at $h_- = -h_+$ which is given by:

$$\begin{aligned}&\lim_{\substack{h_-\to-h_+\\ h_-<-h_+}}\langle\,\sigma_1^z\,\rangle - \lim_{\substack{h_-\to-h_+\\ h_->-h_+}}\langle\,\sigma_1^z\,\rangle\\ &\quad= \langle\,\mathrm{GS}_+\,|\,\sigma_1^z\,|\,\mathrm{GS}_+\,\rangle\Big|_{h_-=-h_+,h_+} - \langle\,\mathrm{GS}_-\,|\,\sigma_1^z\,|\,\mathrm{GS}_-\,\rangle\Big|_{h_-=-h_+,h_+}\\ &\quad= \langle\,\mathrm{GS}_+\,|\,\sigma_1^z\,|\,\mathrm{GS}_+\,\rangle\Big|_{h_-=-h_+,h_+} + \langle\,\mathrm{GS}_+\,|\,\sigma_1^z\,|\,\mathrm{GS}_+\,\rangle\Big|_{-h_-=h_+,-h_+},\end{aligned}\tag{9.90}$$

in which we have used (9.89). This discontinuity can be evaluated in the thermodynamic limit by means of (9.53). It is easy to check that it vanishes if $|h_+| > h_{\mathrm{cr}}^{(1)}$, whereas, if $|h_+| < h_{\mathrm{cr}}^{(1)}$, it gives

$$\begin{aligned}&\lim_{\substack{h_-\to-h_+\\ h_-<-h_+}}\lim_{L\to\infty}\langle\,\sigma_1^z\,\rangle - \lim_{\substack{h_-\to-h_+\\ h_->-h_+}}\lim_{L\to\infty}\langle\,\sigma_1^z\,\rangle = \langle\,\sigma_1^z\,\rangle_0\Big|_{h_-} + \langle\,\sigma_1^z\,\rangle_0\Big|_{-h_-}\\ &\quad= -i\pi\,\sinh^2\xi_-\left[\rho'(-i|\zeta/2-\tilde{\xi}_-|+\pi/2)+\rho'(-i|\zeta/2+\tilde{\xi}_-|+\pi/2)\right]\\ &\quad= -2i\pi\,\sinh^2\xi_-\,\rho'(-i(\zeta/2+\xi_-)),\end{aligned}\tag{9.91}$$

and we recover the value of the discontinuity (9.50) that we had obtained for the thermodynamic limit of the boundary magnetization for even length L at $h_- = h_+$.

Hence, as expected, it follows from the previous study that the thermodynamic behavior of the boundary magnetization coincides for even and odd L (see fomula (9.55)), *provided we change the sign of the boundary field* h_+ *at infinity*. In other words, the quantity h which should be kept fixed when considering the thermodynamic limit is the combination $h \equiv (-1)^L h_+$. The only possible discrepancy is when we are exactly at $h_- = -h_+$ for L odd with respect to the case $h_- = h_+$ for L even. Whereas we did not have an exact degeneracy at this point in the even L case, so that the ground states can be defined without ambiguity from the consideration of the finite size corrections, this not the case for L odd: even for finite size we have a two-dimensional eigenspace generated by the two degenerate normalized Bethe states $|\,\mathrm{GS}_+\,\rangle$ and $|\,\mathrm{GS}_-\,\rangle$. We see that, in that case, to recover the factor $1/2$ that we had obtained at this point from the consideration of the boundary root in the

even L case (see (9.49) and (9.55)), we have to consider the mean value of σ_1^z in a superposition

$$|\,\widetilde{\mathrm{GS}}_\pm\,\rangle = \frac{|\,\mathrm{GS}_+\,\rangle \pm |\,\mathrm{GS}_-\,\rangle}{\sqrt{2}} \tag{9.92}$$

of these two ground Bethe states of different magnetization. Note that (9.92) corresponds to the two ground states which are also eigenstates of the spin-flip operator $\mathcal{F} = \otimes_{n=1}^{L}\sigma_n^x$: $\mathcal{F}\,|\,\widetilde{\mathrm{GS}}_\pm\,\rangle = \pm|\,\widetilde{\mathrm{GS}}_\pm\,\rangle$.

9.3.2 The spin-spin autocorrelation function at $h_- = -h_+$

It is clear that the large L limit of the connected autocorrelation function computed in the ground Bethe state $|\,\mathrm{GS}_\pm\,\rangle$ always vanishes at large time for L odd, even in the case of a degeneracy of the ground state when $h_- = -h_+$:

$$\lim_{t\to\infty}\lim_{L\to\infty}\langle\,\mathrm{GS}_\pm\,|\,\sigma_1^z(t)\,\sigma_1^z\,|\,\mathrm{GS}_\pm\,\rangle^c = 0. \tag{9.93}$$

Indeed, in the latter case, the two ground Bethe states have different magnetization, and therefore cannot contribute to the form-factor series of the autocorrelation function since the matrix elements of the operator σ_1^z between states of different magnetization always vanish. On the other hand, if at $h_- = -h_+$ one considers as above the mean value in a superposition $|\,\widetilde{\mathrm{GS}}_\pm\,\rangle$ (9.92) of these two ground states which corresponds to an eigenstate of the spin-flip operator, one obtains

$$\lim_{t\to\infty}\lim_{L\to\infty}\langle\,\widetilde{\mathrm{GS}}_\pm\,|\,\sigma_1^z(t)\,\sigma_1^z\,|\,\widetilde{\mathrm{GS}}_\pm\,\rangle^c = \lim_{L\to\infty}\Big|\langle\,\widetilde{\mathrm{GS}}_\pm\,|\,\sigma_1^z\,|\,\widetilde{\mathrm{GS}}_\mp\,\rangle\Big|^2, \tag{9.94}$$

where the contributing form factor,

$$\langle\,\widetilde{\mathrm{GS}}_\pm\,|\,\sigma_1^z\,|\,\widetilde{\mathrm{GS}}_\mp\,\rangle = \frac{1}{2}\big(\langle\,\mathrm{GS}_+\,|\,\sigma_1^z\,|\,\mathrm{GS}_+\,\rangle - \langle\,\mathrm{GS}_-\,|\,\sigma_1^z\,|\,\mathrm{GS}_-\,\rangle\big), \tag{9.95}$$

is effectively given by half of the discontinuity of the boundary magnetization (9.90).

The fact that we have to consider the superposition of Bethe states (9.92) is somehow the counterpart of the fact that, for even L at the point $h_- = h_+$, the boundary root in the ground state is delocalized between the two edges and contributes only with a factor $1/2$ to the boundary magnetization: it can therefore be seen as a "superposition" of the two boundary roots which characterize the ground state for $h_- > h_+$ or $h_- < h_+$ respectively.

Chapter 10

Conclusion and perspectives

In our study of the open-boundary XXZ chain, we have arrived at the following results:

(i) The ground state description in terms of Bethe roots is highly dependent on the boundary parameters of the chain, as well as on the parity of the length of the chain. Unlike in the periodic chain, the set of Bethe roots describing the ground state may include some isolated complex solutions, related to the boundary factors appearing in the Bethe equations. We have determined the range of values of the boundary fields for which these boundary roots are present for the ground state –for even and odd number of spins– as well as compared the energy of the lowest energy states. For the even-length chain, we have found that, when the boundary fields are in the interval $\big(-(\Delta-1), \Delta-1\big)$ and that they coincide, the spectrum is gapped and there are two quasi-degenerate ground states in the large L limit.

(ii) We have recalculated the boundary magnetization in the half-infinite chain limit. Although there exist previous results on this quantity, they were only for a null boundary field at infinity $h_+ = 0$. Thanks to our study of the ground state, we are capable to calculate this quantity in the more general case $h_+ \neq 0$. We see that the boundary magnetization of the half-infinite chain still depends on the boundary field h_+ at infinity, in that, when one varies h_-, there exists a discontinuity of this quantity at $h_- = h_+$ in the even length case. This is due to the fact that the description of the ground state in terms of the boundary root is different when $h_- < h_+$ (the boundary root is localized in the right edge and does not contribute to the value of magnetization) and when $h_- > h_+$ (the boundary root is localized in the left edge and contributes to the value of magnetization). In the odd length case, the discontinuity is at $h_- = -h_+$ and is due to the fact that the ground state is not in the same magnetization

sector when $h_- < -h_+$ and when $h_- > -h_+$.

(iii) We have obtained the long-time limit of the autocorrelation function of the σ_1^z operator, for L even. The later is non-zero only at $h_+ = h_-$, due to the quasi-degeneracy of the ground state, and is related to the aforementioned discontinuity of the boundary magnetization.

Let us conclude by a discussion and some perspectives and open questions.

A first remark is that our result for the boundary magnetization, which takes into account the contribution of the boundary root in the ground state depending on *both* boundary fields, can be directly extended to the more complicated zero-temperature correlation functions computed in [135, 137]: from our study of the ground state, we know how to modify and adjust the multiple integral representations obtained in [135, 137] so as to take into account a non-zero boundary field h_+ at infinity, namely, how to change the contour to integrate the boundary root when it is present in the ground state.

It would also be interesting to consider the effect of more general boundary fields along the three axes $(\sigma^x, \sigma^y, \sigma^z)$. As already mentioned, the spin chain is in that case still exactly solvable, but there is no reference state that can be used to apply the Algebraic Bethe Ansatz. One can use the quantum version of the *Separation of Variables* to construct the eigenstates of the transfer matrix. The recent results about the computation of the corresponding scalar products [127, 128] in this framework may enable a generalization of our results to this more general case.

The boundary root, which is crucial in the quantities calculated for the L even case, becomes less so in the odd case, since in that case the ground state only includes it in a gapless region and accompanied by a hole. However, the odd case does reveal hints about the emergence of the complex roots: as we mentioned above, our analysis was suited for studying non-positive magnetization states, the others being "beyond the equator" of Bethe states. One can nevertheless push the analysis and notice that the complementary degenerate ground state "beyond the equator" for L odd would be given by $(L-1)/2$ real roots and complemented by *two* complex roots. If these two states are related to the pair of lowest energy states with an isolated boundary root of the L even case, then there must exist a mechanism by which the passage from even to odd (thus changing the reflection symmetry of the Hamiltonian) "breaks" the complex pair and distributes it into the two quasi-degenerate states.

The fact that physical observables should coincide at the thermodynamic limit at even and odd sizes provides more context about the emergence of this isolated complex root. As we mentioned, the breaking of reflection symmetry suggests that the quasi-degeneracy is a residual effect at finite size. Indeed, the results of [88]

concerning the effects of the *strong zero modes* are for an even chain in the zero-magnetization sector. A look at the higher energy levels (still fixing $h_+ = h_-$) shows that many of the states at zero-magnetization may also present quasi-degeneracies. Thus, one possibility is that the mechanism that we have found for the ground state is also present in the entire spectrum. An Algebraic Bethe Ansatz analysis of even and odd state is within reach and will surely shed light on this question.

From a different perspective, it would be interesting to study the boundary correlation functions for non-zero temperature through the QTM approach. This approach has been shown to be rigorous at high temperature [145]. However, it is less clear how one can recover our result through this approach by taking the low temperature limit. In fact, the order in which limits are taken does matter here: we started from the finite chain, calculated the boundary magnetization with respect to the ground state (so at the $T \to 0$ limit), and then took the large L limit. If we interchange limits as in the QTM prescription, we could lose the memory of the finite-size effect. Indeed, the QTM technique shifts the analysis to that of a periodic chain representing thermal evolution via a discretized inverse temperature β and the $L \to \infty$ limit is taken before the Trotter limit [146]. More research in this direction is desirable.

Finally, recall from the introduction that the physical effect that motivated the calculation of the autocorrelation function was its long-coherence time even at infinite temperature. Therefore, even a Thermodynamic Bethe Ansatz study would be enlightening to figure out what happens in the case of a thermal state of the open-boundary chain. Indeed, the string hypothesis applied to the case of boundary roots (in a similar fashion to [147]) would allow a description of a thermal representative state. The study of boundary conserved charges and the description of non-equilibrium dynamics of the open XXZ chain will without a doubt benefit from the results of this work. We wish that this contribution will push progress into this area of research.

Bibliography

[1] Stauffer D., and Aharony A. (1971). *Introduction to Percolation Theory*. Oxford University Press, New York.

[2] Efros A.L. (1987). *Physics and Geometry of Disorder: Percolation Theory*. Science for Everyone. Mir Publishers. ISBN 0828532915,9780828532914. URL http://gen.lib.rus.ec/book/index.php?md5=092557081B5EBE6A8D9C5E246E939B3C.

[3] Cardy J. (1996). *Scaling and Renormalization in Statistical Physics*. Cambridge Lecture Notes in Physics. Cambridge University Press. doi:10.1017/CBO9781316036440.

[4] Polchinski J. (1988). Scale and conformal invariance in quantum field theory. *Nuclear Physics B*, 303(2):226–236.

[5] Smirnov S. (2001). Critical percolation in the plane: Conformal invariance, Cardy's formula, scaling limits. *Comptes Rendus de l'Académie des Sciences-Series I-Mathematics*, 333(3):239–244.

[6] Chelkak D., and Smirnov S. (2012). Universality in the 2D Ising model and conformal invariance of fermionic observables. *Inventiones mathematicae*, 189(3):515–580.

[7] Wu F.Y. (1982). The Potts model. *Rev Mod Phys*, 54:235–268. doi:10.1103/RevModPhys.54.235. URL http://link.aps.org/doi/10.1103/RevModPhys.54.235.

[8] Picco M., Ribault S., and Santachiara R. (2016). A conformal bootstrap approach to critical percolation in two dimensions. *SciPost Phys*, 1:009. doi:10.21468/SciPostPhys.1.1.009. URL https://scipost.org/10.21468/SciPostPhys.1.1.009.

[9] Jacobsen J.L., and Saleur H. (2019). Bootstrap approach to geometrical four-point functions in the two-dimensional critical Q-state Potts model: a study of the s-channel spectra. *Journal of High Energy Physics*, 2019(1):84.

[10] Picco M., Ribault S., and Santachiara R. (2019). On four-point connectivities in the critical 2d Potts model. *SciPost Phys*, 7:44. doi:10.21468/SciPostPhys.7.4.044. URL https://scipost.org/10.21468/SciPostPhys.7.4.044.

[11] He Y., Jacobsen J.L., and Saleur H. (2020). Geometrical four-point functions in the two-dimensional critical Q-state Potts model: The interchiral conformal bootstrap. *arXiv preprint arXiv:200507258*.

[12] Nivesvivat R., and Ribault S. (2020). Logarithmic CFT at generic central charge: from Liouville theory to the Q-state Potts model. *arXiv preprint arXiv:200704190*.

[13] Grans-Samuelsson L., Liu L., He Y., Jacobsen J.L., and Saleur H. (2020). The action of the Virasoro algebra in the two-dimensional Potts and loop models at generic Q. *arXiv preprint arXiv:200711539*.

[14] Javerzat N., Grijalva S., Rosso A., and Santachiara R. (2020). Topological effects and conformal invariance in long-range correlated random surfaces. *arXiv preprint arXiv:200511830*.

[15] Javerzat N., Picco M., and Santachiara R. (2020). Two-point connectivity of two-dimensional critical Q-Potts random clusters on the torus. *Journal of Statistical Mechanics: Theory and Experiment*, 2020(2):023101.

[16] Prakash S., Havlin S., Schwartz M., and Stanley H.E. (1992). Structural and dynamical properties of long-range correlated percolation. *Phys Rev A*, 46:R1724–R1727. doi:10.1103/PhysRevA.46.R1724. URL https://link.aps.org/doi/10.1103/PhysRevA.46.R1724.

[17] Zierenberg J., Fricke N., Marenz M., Spitzner F.P., Blavatska V., and Janke W. (2017). Percolation thresholds and fractal dimensions for square and cubic lattices with long-range correlated defects. *Physical Review E*, 96(6). doi:10.1103/physreve.96.062125. URL http://dx.doi.org/10.1103/PhysRevE.96.062125.

[18] de Castro C.P., Lukovic M., Andrade R.F.S., and Herrmann H.J. (2017). The influence of statistical properties of Fourier coefficients on random Gaussian surfaces. *Scientific Reports*, 7(1). doi:10.1038/s41598-017-02135-y. URL http://dx.doi.org/10.1038/s41598-017-02135-y.

[19] de Castro C.P., Lukovic M., Pompanin G., Andrade R.F.S., and Herrmann H.J. (2018). Schramm-Loewner evolution and perimeter of percolation clusters of correlated random landscapes. *Scientific Reports*, 8(1). doi:10.1038/s41598-018-23489-x. URL http://dx.doi.org/10.1038/s41598-018-23489-x.

[20] Barnsley M.F., Devaney R.L., Mandelbrot B.B., et al. (1988). *The science of fractal images*. Springer.

[21] Newman M., and Ziff R.M. (2000). Efficient Monte Carlo algorithm and high-precision results for percolation. *Physical Review Letters*, 85(19):4104.

[22] Weinrib A. (1984). Long-range correlated percolation. *Phys Rev B*, 29:387–395. doi:10.1103/PhysRevB.29.387. URL https://link.aps.org/doi/10.1103/PhysRevB.29.387.

[23] Schmittbuhl J., Vilotte J.P., and Roux S. (1993). Percolation through self-affine surfaces. *Journal of Physics A: Mathematical and General*, 26(22):6115–6133. doi:10.1088/0305-4470/26/22/014. URL https://doi.org/10.1088%2F0305-4470%2F26%2F22%2F014.

[24] Saleur H., and Derrida B. (1985). A combination of Monte Carlo and transfer matrix methods to study 2D and 3D percolation.

[25] Binder K. (1981). Finite size scaling analysis of Ising model block distribution functions. *Zeitschrift für Physik B Condensed Matter*, 43(2):119–140.

[26] De Boor C., De Boor C., Mathématicien E.U., De Boor C., and De Boor C. (1978). *A practical guide to splines*, volume 27. springer-verlag New York.

[27] Schrenk K.J., Posé N., Kranz J.J., van Kessenich L.V.M., Araújo N.A.M., and Herrmann H.J. (2013). Percolation with long-range correlated disorder. *Phys Rev E*, 88:052102. doi:10.1103/PhysRevE.88.052102. URL https://link.aps.org/doi/10.1103/PhysRevE.88.052102.

[28] Delfino G., and Viti J. (2011). On three-point connectivity in two-dimensional percolation. *JPhys*, A44:032001. doi:10.1088/1751-8113/44/3/032001.

[29] Delfino G., Picco M., Santachiara R., and Viti J. (2013). Spin clusters and conformal field theory. *Journal of Statistical Mechanics: Theory and Experiment*, 2013(11):P11011. doi:10.1088/1742-5468/2013/11/p11011. URL https://doi.org/10.1088%2F1742-5468%2F2013%2F11%2Fp11011.

[30] Ziff R.M., Simmons J.J.H., and Kleban P. (2011). Factorization of correlations in two-dimensional percolation on the plane and torus. *Journal of Physics A Mathematical General*, 44(6):065002. doi:10.1088/1751-8113/44/6/065002.

[31] Bernard D., Boffetta G., Celani A., and Falkovich G. (2006). Conformal invariance in two-dimensional turbulence. *Nature Physics*, (2):124.

[32] Bogomolny E., and Schmit C. (2007). Random wavefunctions and percolation. *Journal of Physics A Mathematical General*, 40:14033–14043. doi:10.1088/1751-8113/40/47/001.

[33] Heisenberg W. (1928). Zur Theorie der Ferromagnetismus. *Zeitschrift für Physik*, 49:619–636.

[34] Bethe H. (1931). Zür Theorie der Metalle I. Eigenwerte und Eigenfunktionen Atomkete. *Zeitschrift für Physik*, 71:205–226. doi:10.1007/BF01341708. URL https://doi.org/10.1007/BF01341708.

[35] Gaudin M. (1983). *La fonction d'onde de Bethe*. Masson.

[36] Orbach R. (1958). Linear antiferromagnetic chain with anisotropic coupling. *Phys Rev*, 112:309–316.

[37] Hulthén L. (1939). Über das Austauschproblem eines Kristalls. *Ark Mat Astron Fys A*, 26(11):1–106.

[38] Walker L.R. (1959). Antiferromagnetic linear chain. *Phys Rev*, 116:1089–1090.

[39] Yang C.N., and Yang C.P. (1966). One-dimensional chain of anisotropic spin-spin interactions. I. Proof of Bethe's hypothesis for ground state in a finite system. *Phys Rev*, 150(1):321–327.

[40] Yang C.N., and Yang C.P. (1966). One-dimensional chain of anisotropic spin-spin interactions. II. Properties of the ground state energy per lattice site for an infinite system. *Phys Rev*, 150(1):327–339.

[41] Yang C.N., and Yang C.P. (1966). One-dimensional chain of anisotropic spin-spin interactions. III. Applications. *Phys Rev*, 151:258.

[42] Takahashi M. (1971). One-dimensional Heisenberg model at finite temperature. *Prog Theor Phys*, 46:401. URL https://doi.org/10.1143/PTP.46.401.

[43] Gaudin M. (1971). Thermodynamics of the Heisenberg-Ising ring for $\Delta > 1$. *Phys Rev Lett*, 26:1301.

[44] Yang C.N., and Yang C.P. (1969). Thermodynamics of a one-dimensional system of bosons with repulsive delta-function interaction. *J Math Phys*, 10:1115–1122.

[45] Lieb E. (1967). Exact solution of the entropy of two-dimensional ice. *Phys Rev Lett*, 18:692.

[46] Lieb E. (1967). Exact solution of the F-model of an antiferroelectric. *Phys Rev Lett*, 18:1046.

[47] Lieb E. (1967). Exact solution of the two-dimensional Slater KDP model of a ferroelectric. *Phys Rev Lett*, 19:108–110.

[48] McCoy B.M., and Wu T.T. (1968). Hydrogen-bonded crystals and the anisotropic Heisenberg chain. *Il Nuovo Cimento B (1965-1970)*, 56(2):311–315. doi:10.1007/BF02710156. URL https://doi.org/10.1007/BF02710156.

[49] Baxter R.J. (1972). One-dimensional anisotropic Heisenberg chain. *Ann Phys*, 70:323–37.

[50] Baxter R.J. (1982). *Exactly solved models in statistical mechanics*. Academic Press, London. ISBN 0-12-083180-5. URL https://physics.anu.edu.au/theophys/_files/Exactly.pdf.

[51] Faddeev L.D., and Sklyanin E.K. (1978). Quantum-mechanical approach to completely integrable field theory models. *Sov Phys Dokl*, 23:902–904.

[52] Sklyanin E.K., Takhtajan L.A., and Faddeev L.D. (1979). Quantum inverse problem method I. *Theor Math Phys*, 40:688–706. doi:10.1007/BF01018718. URL https://doi.org/10.1007/BF01018718, translated from Teor. Mat. Fiz. 40 (1979) 194-220.

[53] Takhtadzhan L.A., and Faddeev L.D. (1979). The Quantum method of the inverse problem and the Heisenberg XYZ model. *Russ Math Surveys*, 34(5):11–68. doi:10.1070/RM1979v034n05ABEH003909.

[54] Faddeev L.D., and Takhtajan L.A. (1981). Quantum inverse scattering method. *Sov Sci Rev Math*, C 1:107.

[55] Gardner C.S., Greene J.M., Kruskal M.D., and Miura R.M. (1967). Method for solving the Korteweg-de Vries equation. *Phys Rev Lett*, 19:1095–1097.

[56] Faddeev L.D., and Takhtajan L.A. (1987). *Hamiltonian methods in the theory of solitons*. Springer-Verlag.

[57] Babelon O., Bernard D., and Talon M. (2003). *Introduction to Classical Integrable Systems*. Cambridge University Press.

[58] Faddeev L.D. (1996). How algebraic Bethe ansatz works for integrable model.

[59] Jimbo M. (1985). A q-difference analogue of $U(g)$ and the Yang-Baxter equation. *Lett Math Phys*, 10:63–69.

[60] Drinfel'd V.G. (1987). Quantum groups. In *Proc. Internat. Congress of Math., Berkeley, USA, 1986*, pp. 798–820. AMS.

[61] Jimbo M. (1992). Topics from representations of $U_q(g)$. An introductory guide to physicists. In *Nankai Lectures on Mathematical Physics*, pp. 1–61. World Scientific, Singapore.

[62] Jimbo M., Miki K., Miwa T., and Nakayashiki A. (1992). Correlation functions of the XXZ model for $\Delta < -1$. *Phys Lett A*, 168:256–263.

[63] Jimbo M., and Miwa T. (1995). *Algebraic analysis of solvable lattice models*. Number 85 in CBMS Regional Conference Series in Mathematics. AMS, Providence, RI.

[64] Kitanine N., Maillet J.M., and Terras V. (2000). Correlation functions of the XXZ Heisenberg spin-1/2 chain in a magnetic field. *Nucl Phys B*, 567:554–582. doi:10.1016/S0550-3213(99)00619-7. URL https://doi.org/10.1016/S0550-3213(99)00619-7.

[65] Kitanine N., Maillet J.M., and Terras V. (1999). Form factors of the XXZ Heisenberg spin-1/2 finite chain. *Nucl Phys B*, 554:647–678. doi:10.1016/S0550-3213(99)00295-3. URL https://doi.org/10.1016/S0550-3213(99)00295-3.

[66] Caux J.S., Hagemans R., and Maillet J.M. (2005). Computation of dynamical correlation functions of Heisenberg chains: the gapless anisotropic regime. *J Stat Mech*, 2005:P09003. doi:10.1088/1742-5468/2005/09/P09003. URL https://doi.org/10.1088%2F1742-5468%2F2005%2F09%2Fp09003.

[67] Caux J.S., and Maillet J.M. (2005). Computation of dynamical correlation functions of Heisenberg chains in a magnetic field. *Phys Rev Lett*, 95:077201. doi:10.1103/PhysRevLett.95.077201. URL https://doi.org/10.1103/PhysRevLett.95.077201.

[68] Kitanine N., Kozlowski K.K., Maillet J.M., Slavnov N.A., and Terras V. (2009). Algebraic Bethe ansatz approach to the asymptotic behavior of correlation functions. *J Stat Mech*, 2009:P04003. doi:10.1088/1742-5468/2009/04/P04003. URL https://doi.org/10.1088%2F1742-5468%2F2009%2F04%2Fp04003.

[69] Kitanine N., Kozlowski K.K., Maillet J.M., Slavnov N.A., and Terras V. (2009). On the thermodynamic limit of form factors in the massless XXZ Heisenberg chain. *J Math Phys*, 50:095209. doi:10.1063/1.3136683. URL https://doi.org/10.1063/1.3136683.

[70] Kitanine N., Kozlowski K.K., Maillet J.M., Slavnov N.A., and Terras V. (2011). The thermodynamic limit of particle-hole form factors in the massless XXZ Heisenberg chain. *J Stat Mech*, 2011:P05028. doi:10.1088/1742-5468/2011/05/P05028. URL https://doi.org/10.1088%2F1742-5468%2F2011%2F05%2Fp05028.

[71] Kitanine N., Kozlowski K.K., Maillet J.M., Slavnov N.A., and Terras V. (2011). A form factor approach to the asymptotic behavior of correlation functions in critical models. *J Stat Mech*, 2011:P12010. doi:10.1088/1742-5468/2011/12/P12010. URL https://doi.org/10.1088%2F1742-5468%2F2011%2F12%2Fp12010.

[72] Kitanine N., Kozlowski K.K., Maillet J.M., Slavnov N.A., and Terras V. (2012). Form factor approach to dynamical correlation functions in critical models. *J Stat Mech*, 2012:P09001. doi:10.1088/1742-5468/2012/09/P09001. URL https://doi.org/10.1088%2F1742-5468%2F2012%2F09%2Fp09001.

[73] Kitanine N., Kozlowski K.K., Maillet J.M., and Terras V. (2014). Large-distance asymptotic behaviour of multi-point correlation functions in massless quantum models. *J Stat Mech*, 2014:P05011. doi:10.1088/1742-5468/2014/05/P05011. URL https://doi.org/10.1088%2F1742-5468%2F2014%2F05%2Fp05011.

[74] Kozlowski K.K. (2018). On the thermodynamic limit of form factor expansions of dynamical correlation functions in the massless regime of the XXZ spin 1/2 chain. *Journal of Mathematical Physics*, 59(9):091408. doi:10.1063/1.5021892. URL https://doi.org/10.1063/1.5021892.

[75] Göhmann F., Klümper A., and Seel A. (2004). Integral representations for cor-

relation functions of the XXZ chain at finite temperature. *J Phys A*, 37:7625–7652.

[76] Göhmann F., Klümper A., and Seel A. (2005). Integral representation of the density matrix of the XXZ chain at finite temperatures. *J Phys A : Math Gen*, 38:1833–1841.

[77] Dugave M., Göhmann F., and Kozlowski K.K. (2013). Thermal form factors of the XXZ chain and the large-distance asymptotics of its temperature dependent correlation functions. *J Stat Mech*, 2013:P07010.

[78] Dugave M., Göhmann F., Kozlowski K.K., and Suzuki J. (2016). Thermal form factor approach to the ground-state correlation functions of the XXZ chain in the antiferromagnetic massive regime. *Journal of Physics A: Mathematical and Theoretical*, 49(39):394001.

[79] Göhmann F., Karbach M., Klümper A., Kozlowski K.K., and Suzuki J. (2017). Thermal form-factor approach to dynamical correlation functions of integrable lattice models. *Journal of Statistical Mechanics: Theory and Experiment*, 2017(11):113106.

[80] Klumper A. (1992). Free energy and correlation lengths of quantum chains related to restricted solid-on-solid lattice models. *Annalen der Physik*, 504(7):540–553. doi:10.1002/andp.19925040707. URL https://onlinelibrary.wiley.com/doi/abs/10.1002/andp.19925040707.

[81] Klumper A. (1993). Thermodynamics of the anisotropic spin-1/2 Heisenberg chain and related quantum chains. *Zeitschrift fÃŒr Physik B Condensed Matter*, 91:507–519. doi:10.1007/BF01316831. URL https://doi.org/10.1007/BF01316831.

[82] Destri C., and de Vega H.J. (1992). New thermodynamic Bethe ansatz equations without strings. *Phys Rev Lett*, 69:2313–2317. doi:10.1103/PhysRevLett.69.2313. URL https://link.aps.org/doi/10.1103/PhysRevLett.69.2313.

[83] Destri C., and de Vega H.J. (1995). Unified approach to Thermodynamic Bethe Ansatz and finite size corrections for lattice models and field theories. *Nucl Phys B*, 438:413–454.

[84] Alcaraz F., Barber M., Batchelor M., Baxter R., and Quispel G. (1987). Surface Exponents of The Quantum XXZ, Ashkin-Teller and Potts Models. *J Phys A: Math Gen*, 20:6397–6409. doi:10.1088/0305-4470/20/18/

038. URL http://iopscience.iop.org/article/10.1088/0305-4470/20/18/038/meta.

[85] Cherednik I.V. (1984). Factorizing Particles On A Half Line And Root Systems. *Theor Math Phys*, 61:977–983. doi:10.1007/BF01038545. URL http://dx.doi.org/10.1007/BF01038545.

[86] Sklyanin E.K. (1988). Boundary conditions for integrable quantum systems. *J Phys A: Math Gen*, 21(10):2375–2389. doi:10.1088/0305-4470/21/10/015. URL http://stacks.iop.org/0305-4470/21/i=10/a=015.

[87] Sarma S.D., Freedman M., and Nayak C. (2015). Majorana zero modes and topological quantum computation. *npj Quantum Information*, 1(1). doi:10.1038/npjqi.2015.1. URL https://doi.org/10.1038/npjqi.2015.1.

[88] Fendley P. (2016). Strong zero modes and eigenstate phase transitions in the XYZ/interacting Majorana chain. *J Phys A : Math Theor*, 49(30):30LT01. doi:10.1088/1751-8113/49/30/30LT01. URL http://stacks.iop.org/1751-8121/49/i=30/a=30LT01.

[89] Pinto R.A., Haque M., and Flach S. (2009). Edge-localized states in quantum one-dimensional lattices. *Phys Rev A*, 79:052118. doi:10.1103/PhysRevA.79.052118. URL https://link.aps.org/doi/10.1103/PhysRevA.79.052118.

[90] Kemp J., Yao N.Y., Laumann C.R., and Fendley P. (2017). Long coherence times for edge spins. *J Stat Mech*, 2017(6):063105. URL http://stacks.iop.org/1742-5468/2017/i=6/a=063105.

[91] Maceira I.A., and Mila F. (2018). Infinite coherence time of edge spins in finite-length chains. *Phys Rev B*, 97:064424. doi:10.1103/PhysRevB.97.064424. URL https://link.aps.org/doi/10.1103/PhysRevB.97.064424.

[92] Kozlowski K.K. (2018). On condensation properties of Bethe roots associated with the XXZ chain. *Communications in Mathematical Physics*, 357(3):1009–1069.

[93] Babelon O., de Vega H.J., and Viallet C.M. (1983). Analysis of the Bethe Ansatz equations of the XXZ model. *Nucl Phys B*, 220:13–34. doi:10.1016/0550-3213(83)90131-1. URL https://doi.org/10.1016/0550-3213(83)90131-1.

[94] Vladimirov A.A. (1986). Proof of the invariance of the Bethe-Ansatz solution under complex conjugation. *Theor Math Phys*, 66:102–105.

[95] Woynarovich F. (1982). On the eigenstates of a Heisenberg chain with complex wavenumbers not forming strings. *Journal of Physics C: Solid State Physics*, 15(31):6397.

[96] Woynarovich F. (1982). On the Sz= 0 excited states of an anisotropic Heisenberg chain. *Journal of Physics A: Mathematical and General*, 15(9):2985.

[97] Ilakovac A., Kolanovic M., Pallua S., and Prester P. (1999). Violation of the string hypothesis and the Heisenberg XXZ spin chain. *Physical Review B*, 60(10):7271.

[98] Takahashi M., and Suzuki M. (1972). One-dimensional anisotropic Heisenberg model at finite temperature. *Prog Theor Phys*, 48:2187–2209.

[99] Göhmann F. (2019). Statistical mechanics of integrable quantum spin systems. *arXiv preprint arXiv:190909967*.

[100] Maillet J.M., and Terras V. (2000). On the quantum inverse scattering problem. *Nucl Phys B*, 575:627–644. doi:10.1016/S0550-3213(00)00097-3. URL https://doi.org/10.1016/S0550-3213(00)00097-3.

[101] Göhmann F., and Korepin V.E. (2000). Solution of the quantum inverse problem. *J Phys A*, 33:1199–1220. doi:10.1088/0305-4470/33/6/308. URL https://doi.org/10.1088%2F0305-4470%2F33%2F6%2F308.

[102] Slavnov N.A. (1989). Calculation of scalar products of wave functions and form factors in the framework of the algebraic Bethe Ansatz. *Theor Math Phys*, 79:502–508. doi:10.1007/BF01016531. URL https://doi.org/10.1007/BF01016531.

[103] Kitanine N., Maillet J.M., Slavnov N.A., and Terras V. (2002). Spin-spin correlation functions of the XXZ-1/2 Heisenberg chain in a magnetic field. *Nucl Phys B*, 641:487–518. doi:10.1016/S0550-3213(02)00583-7. URL https://doi.org/10.1016/S0550-3213(02)00583-7.

[104] Kitanine N., Maillet J.M., Slavnov N.A., and Terras V. (2005). Master equation for spin-spin correlation functions of the XXZ chain. *Nucl Phys B*, 712:600–622. doi:10.1016/j.nuclphysb.2005.01.050. URL https://doi.org/10.1016/j.nuclphysb.2005.01.050.

[105] Kitanine N., Maillet J.M., Slavnov N.A., and Terras V. (2005). Dynamical correlation functions of the XXZ spin-1/2 chain. *Nucl Phys B*, 729:558–580. doi:10.1016/j.nuclphysb.2005.08.046. URL https://doi.org/10.1016/j.nuclphysb.2005.08.046.

[106] Kozlowski K.K., and Terras V. (2011). Long-time and large-distance asymptotic behavior of the current-current correlators in the non-linear Schrödinger model. *J Stat Mech*, 2011:P09013. doi:10.1088/1742-5468/2011/09/P09013. URL https://doi.org/10.1088/1742-5468/2011/09/P09013.

[107] Kozlowski K.K. (2017). Form factors of bound states in the XXZ chain. *J Phys A: Math Theor*, 50(18):184002. doi:10.1088/1751-8121/aa5757. URL http://stacks.iop.org/1751-8121/50/i=18/a=184002.

[108] Dugave M., Göhmann F., and Kozlowski K.K. (2014). Low-temperature large-distance asymptotics of the transversal two-point functions of the XXZ chain. *J Stat Mech*, 2014:P04012.

[109] Biegel D., Karbach M., and Müller G. (2002). Transition rates via Bethe ansatz for the spin-1/2 Heisenberg chain. *EPL (Europhysics Letters)*, 59(6):882–888. URL http://stacks.iop.org/0295-5075/59/i=6/a=882.

[110] Biegel D., Karbach M., and Müller G. (2003). Transition rates via Bethe ansatz for the spin-1/2 planar XXZ antiferromagnet. *J Phys A: Math Gen*, 36(20):5361–5368. doi:10.1088/0305-4470/36/20/301. URL http://stacks.iop.org/0305-4470/36/i=20/a=301.

[111] Jimbo M., and Miwa T. (1996). Quantum KZ equation with $|q| = 1$ and correlation functions of the XXZ model in the gapless regime. *J Phys A: Math Gen*, 29:2923–2958.

[112] Boos H., Jimbo M., Miwa T., Smirnov F., and Takeyama Y. (2005). A recursion formula for the correlation functions of an inhomogeneous XXX model. *Algebra and Analysis*, 17:115–159.

[113] Boos H., Jimbo M., Miwa T., Smirnov F., and Takeyama Y. (2006). Reduced qKZ equation and correlation functions of the XXZ model. *Comm Math Phys*, pp. 245–276.

[114] Boos H., Jimbo M., Miwa T., Smirnov F., and Takeyama Y. (2006). Density matrix of a finite sub-chain of the Heisenberg anti-ferromagnet. *Lett Math Phys*, 75:201–208.

[115] Boos H., Jimbo M., Miwa T., Smirnov F., and Takeyama Y. (2006). Algebraic representation of correlation functions in integrable spin chains. *Annales Henri Poincaré*, 7:1395–1428.

[116] Boos H., Jimbo M., Miwa T., Smirnov F., and Takeyama Y. (2007). Hidden Grassmann structure in the XXZ model. *Comm Math Phys*, 272:263–281.

[117] Boos H., Jimbo M., Miwa T., Smirnov F., and Takeyama Y. (2009). Hidden Grassmann Structure in the XXZ Model II: Creation Operators. *Comm Math Phys*, 286:875–932.

[118] Jimbo M., Miwa T., and Smirnov F. (2009). Hidden Grassmann structure in the XXZ model III: introducing the Matsubara direction. *J Phys A : Math Gen*, 42:304018.

[119] Boos H., Jimbo M., Miwa T., and Smirnov F. (2010). Hidden Grassmann Structure in the XXZ Model IV: CFT Limit. *Comm Math Phys*, 299:825–866.

[120] Jimbo M., Miwa T., and Smirnov F. (2011). Hidden Grassmann Structure in the XXZ Model V: Sine-Gordon Model. *Lett Math Phys*, 96:325–365.

[121] Skorik S., and Saleur H. (1995). Boundary bound states and boundary bootstrap in the sine-Gordon model with Dirichlet boundary conditions. *J Phys A: Math Gen*, 28(23):6605–6622. doi:0.1088/0305-4470/28/23/014. URL https://doi.org/10.1088/0305-4470/28/23/014.

[122] Kapustin A., and Skorik S. (1996). Surface excitations and surface energy of the antiferromagnetic XXZ chain by the Bethe ansatz approach. *J Phys A: Math Gen*, 29(8):1629–1638. doi:10.1088/0305-4470/29/8/011. URL https://doi.org/10.1088/0305-4470/29/8/011.

[123] Sklyanin E.K. (1990). Functional Bethe Ansatz. In B. Kupershmidt (editor), *Integrable and Superintegrable Systems*, pp. 8–33. World Scientific, Singapore.

[124] Sklyanin E.K. (1992). Quantum inverse scattering method. Selected topics. In M.L. Ge (editor), *Quantum Group and Quantum Integrable Systems*, pp. 63–97. Nankai Lectures in Mathematical Physics, World Scientific.

[125] Niccoli G. (2012). Non-diagonal open spin-1/2 XXZ quantum chains by separation of variables: Complete spectrum and matrix elements of some quasi-local operators. *J Stat Mech*, 2012:P10025. doi:10.1088/1742-5468/2012/10/P10025. URL http://stacks.iop.org/1742-5468/2012/i=10/a=P10025.

[126] Faldella S., Kitanine N., and Niccoli G. (2014). Complete spectrum and scalar products for the open spin-1/2 XXZ quantum chains with non-diagonal boundary terms. *J Stat Mech*, 2014:P01011. doi:10.1088/1742-5468/2014/01/P01011.

[127] Kitanine N., Maillet J., Niccoli G., and Terras V. (2017). The open XXX spin chain in the SoV framework: scalar product of separate states. *Journal of Physics A: Mathematical and Theoretical*, 50(22):224001.

[128] Kitanine N., Maillet J., Niccoli G., and Terras V. (2018). The open XXZ spin chain in the SoV framework: scalar product of separate states. *Journal of Physics A: Mathematical and Theoretical*, 51(48):485201.

[129] Belliard S., and Crampé N. (2013). Heisenberg XXX Model with General Boundaries: Eigenvectors from Algebraic Bethe Ansatz. *SIGMA*, 9:072. doi:10.3842/SIGMA.2013.072. URL https://doi.org/10.3842/SIGMA.2013.072.

[130] Belliard S. (2015). Modified algebraic Bethe ansatz for XXZ chain on the segment - I - Triangular cases. *Nucl Phys B*, 892:1–20. doi:10.1016/j.nuclphysb.2015.01.003. URL https://doi.org/10.1016/j.nuclphysb.2015.01.003.

[131] Belliard S., and Pimenta R.A. (2015). Modified algebraic Bethe ansatz for XXZ chain on the segment - II - general cases. *Nucl Phys B*, 894:527–552. doi:10.1016/j.nuclphysb.2015.03.016. URL https://doi.org/10.1016/j.nuclphysb.2015.03.016.

[132] Avan J., Belliard S., Grosjean N., and Pimenta R. (2015). Modified algebraic Bethe ansatz for XXZ chain on the segment – III – Proof. *Nucl Phys B*, 899:229–246. doi:10.1016/j.nuclphysb.2015.08.006. URL https://doi.org/10.1016/j.nuclphysb.2015.08.006.

[133] Belliard S., and Pimenta R.A. (2016). Slavnov and Gaudin-Korepin formulas for models without U(1) symmetry: the XXX chain on the segment. *J Phys A: Math Theor*, 49:17LT01.

[134] Wang Y.S. (2002). The scalar products and the norm of Bethe eigenstates for the boundary XXX Heisenberg spin-1/2 finite chain. *Nuclear Phys B*, 622:633–649. doi:10.1016/S0550-3213(01)00610-1. URL https://doi.org/10.1016/S0550-3213(01)00610-1.

[135] Kitanine N., Kozlowski K.K., Maillet J.M., Niccoli G., Slavnov N.A., and Terras V. (2007). Correlation functions of the open XXZ chain: I. *J Stat Mech*, 2007:P10009. doi:10.1088/1742-5468/2007/10/P10009. URL http://stacks.iop.org/1742-5468/2007/i=10/a=P10009.

[136] Wang Y.S. (2000). The reconstruction of local quantum operators for the boundary XXZ spin-1/2 Heisenberg chain. *J Phys A: Math Gen*, 33:4009–4014. doi:10.1088/0305-4470/33/22/305. URL https://doi.org/10.1088%2F0305-4470%2F33%2F22%2F305.

[137] Kitanine N., Kozlowski K.K., Maillet J.M., Niccoli G., Slavnov N.A., and Terras V. (2008). Correlation functions of the open XXZ chain: II. *J Stat Mech*, 2008:P07010. doi:10.1088/1742-5468/2008/07/P07010. URL http://stacks.iop.org/1742-5468/2008/i=07/a=P07010.

[138] Jimbo M., Kedem R., Kojima T., Konno H., and Miwa T. (1995). XXZ chain with a boundary. *Nucl Phys B*, 441(3):437–470. doi:10.1016/0550-3213(95)00062-W. URL https://doi.org/10.1016/0550-3213(95)00062-w.

[139] Izergin A.G., Kitanine N., Maillet J.M., and Terras V. (1999). Spontaneous magnetization of the XXZ Heisenberg spin-1/2 chain. *Nucl Phys B*, 554(3):679–696. doi:10.1016/s0550-3213(99)00273-4. URL https://doi.org/10.1016/s0550-3213(99)00273-4.

[140] Gradshteyn I., and Ryzhik I. (1965). *Table of Integrals, Series and Products*. Academic Press.

[141] Grijalva S., De Nardis J., and Terras V. (2019). Open XXZ chain and boundary modes at zero temperature. *SciPost Phys*, 7:023.

[142] Kozlowski K.K., and Pozsgay B. (2012). Surface free energy of the open XXZ spin-1/2 chain. *J Stat Mech Theory Exp*, 2012(05):P05021. URL http://stacks.iop.org/1742-5468/2012/i=05/a=P05021.

[143] Pozsgay B., and Rákos O. (2018). Exact boundary free energy of the open XXZ chain with arbitrary boundary conditions. *J Stat Mech Theory Exp*, 2018(11):113102. doi:10.1088/1742-5468/aae5a5. URL https://doi.org/10.1088/1742-5468/aae5a5.

[144] Baxter R.J. (1973). Spontaneous staggered polarization of the F-model. *J Stat Phys*, 9(2):145–182. doi:10.1007/bf01016845. URL https://doi.org/10.1007/bf01016845.

[145] Göhmann F., Goomanee S., Kozlowski K.K., and Suzuki J. (2020). Thermodynamics of the Spin-1/2 Heisenberg–Ising Chain at High Temperatures: a Rigorous Approach. *Communications in Mathematical Physics*, pp. 1–51.

[146] Göhmann F., Bortz M., and Frahm H. (2005). Surface free energy for systems with integrable boundary conditions. *J Phys A*, 38:10879–10892.

[147] De Nardis J., Krajenbrink A., Le Doussal P., and Thiery T. (2020). Delta-Bose gas on a half-line and the Kardar-Parisi-Zhang equation: boundary bound states and unbinding transitions. *Journal of Statistical Mechanics: Theory and Experiment*, 2020(4):043207. doi:10.1088/1742-5468/ab7751. URL http://dx.doi.org/10.1088/1742-5468/ab7751.

BIBLIOGRAPHY

List of Figures

List of Tables

université PARIS-SACLAY | ÉCOLE DOCTORALE Physique en l'Île-de-France (PIF)

Titre : Effets de bord dans les chaînes de spin quantiques et effets de taille finie dans le modèle toroïdal de percolation corrélé

Mots clés : Intégrabilité Quantique, Chaînes de Spin, Percolation, Corrélations, Systèmes a Basse Dimension, Phénomènes Critiques, Théorie Conforme des Champs

Résumé : Cette thèse est divisée en deux parties : La première présente un modèle statistique en deux dimensions de percolation corrélée sur un réseau toroïdal. Nous présentons un protocole pour construire des surfaces corrélées à longue portée sur la base de surfaces gaussiennes fractionnaires, puis nous relions les ensembles de niveaux à une famille de mod- èles de percolation corrélés. Les clusters émer- gents sont ensuite étudiés numériquement, et nous testons leur symétrie conforme en vérifiant que les corrections de taille finie de connectivité à deux points suivent les prédictions de la théorie des champs conformes. Nous commen- tons également le comportement des fonctions à trois points et fournissons un code numérique pour reproduire les résultats.

La deuxième partie de la thèse étudie la chaîne quantique XXZ integrable de spin-1/2 avec des conditions aux bords ouvertes, pour un nombre pair et impair de sites. Dans le régime antiferromagnétique, nous utilisons l'Ansatz de Bethe Algébrique pour déterminer les configurations possibles en termes des champs aux bords. On retrouve les conditions d'existence d'états fondamentaux quasi dégénérés séparés par un gap au reste du spectre. Nous calculons l'aimantation au bord à température nulle et constatons qu'elle dépend du champ sur le bord opposé même dans la limite de chaîne semi-infinie. Nous calculons enfin la fonction d'autocorrélation temporelle au bord et montrons que dans le cas de taille paire, elle est finie à la limite de temps long à cause de la quasi-dégénérescence.

Title : Boundary effects in Quantum Spin Chains and Finite-Size Effects in the Toroidal Correlated Percolation model

Keywords : Quantum Integrability, Spin Chains, Percolation, Correlations, Low Dimensional Systems, Critical Phenomena, Conformal Field Theory

Abstract : This thesis is divided in two parts: The first one presents a 2D statistical model of correlated percolation on a toroidal lattice. We present a protocol to construct long-range correlated surfaces based on fractional Gaussian sur- faces and then we relate the level sets to a family of correlated percolation models. The emerging clusters are then numericaly studied, and we test their conformal symmetry by verifying that their planar-limit finite-size corrections follow the predictions of Conformal Field Theory. We comment also the behavior of three-point functions and provide a numerical code to reproduce the results.

The second part of the thesis studies the quantum integrable XXZ spin-1/2 chain with open boundary conditions for even and odd number of sites. We concentrate in the antiferromagnetic regime and use the Algebraic Bethe Ansatz to determine the configurations that arise in terms of the boundary fields. We find the conditions of existence of quasi-degenerate ground states separated by a gap to the rest of the spectrum. We calculate the boundary magnetization at zero temperature and find that it depends on the field at the opposite edge even in the semi-infinite chain limit. We finally calculate the time autocorrelation function at the boundary and show that in the even-size case it is finite for the long-time limit as a result of the quasi-degeneracy.

Maison du doctorat de l'Université Paris-Saclay
2ème étage aile ouest, Ecole normale supérieure Paris-Saclay
4 avenue des Sciences,
91190 Gif sur Yvette, France